

***In vivo* immunogenicity of amorphous
aggregates made of misfolded anti-EGFR
single domain antibody (V_{HH})**

MD. GOLAM KIBRIA

Student ID: 18831704

A DISSERTATION

Submitted to

Tokyo University of Agriculture and Technology

In partial fulfillment of the requirements for the degree of

DOCTOR OF PHILOSOPHY

In

Engineering

Department of Biotechnology and Life Sciences

Graduate School of Engineering

Acknowledgments

Throughout the writing of this dissertation, I have received a great deal of support and assistance. I want to take a moment to thank them.

First and foremost, I would like to express my deep sense of thanks and gratitude to my supervisor Dr. Yutaka Kuroda, Professor, Department of Biotechnology and Life Sciences, Tokyo University of Agriculture and Technology (TUAT) for his day to day supervision, invaluable suggestions, constructive criticism and keen interest to carry out this research work. His immense knowledge, plentiful experience and scientific integrity and dedication have been inspiring throughout my graduate study,

Secondly, I would like to sincerely thank Dr. Yoshihisa Hagihara and Mrs. Yoko Akazawa-Ogawa, Biomedical Research Institute, National Institute of Advanced Industrial Science and Technology (AIST), for their valuable suggestions and experimental support. Without their cooperation, this research work would not have been completed to my satisfaction.

I would like to offer my special thanks to Dr. Nafsoon Rahman and Mrs. Subbaian Brindha for their valuable contribution during my entire course. I gratefully acknowledge the generous support of Mrs. Patricia McGahan for her editorial guidance and insightful discussion on manuscript preparation. I would like to extend my sincere thanks to Mrs. Keiko Takahashi and Mrs. Satoko Nishisaka for their assistance with the administrative and laboratory management tasks.

Special thanks go to Dr. Punitha Velmurugan and Dr. Manjiri Kulkarni, Dr. Tomonori Saotome for their helpful suggestions, experimental teachings, and informative discussion on my research work. I sincerely appreciate the friendly support from Mr. Matsuzawa, Ms. Yukari Shiwaku, Ms. Onchaiya Ms. Akari Fukutani, and Ms. Okawa Mami throughout my long journey.

I am profoundly indebted to my family members, for their love, encouragement and motivation during the time. I especially thank my loving wife Tanzina Tanu for helping me over the years. Without her support and encouragement, it would be very hard to complete my work. I would also like to thank my beloved elder brother Sabbir Ahammed, lieutenant commander, Bangladesh NAVY, and younger brother Mr. Jakir Hossen for handling all the responsibilities that I might have faced in Bangladesh.

My studentship was funded by the Ministry of Education, Culture, Sports, Science and Technology, Japan, I would like to express my thanks to all the members within this network for their support and encouragement.

May Allah bless them all.

DECLARATION

I declare that this thesis is my own work, and it has not been previously submitted for any other degree or diploma. To the best of my knowledge and belief, any previously written or published materials used in this thesis by way of background information, are duly acknowledged in the text of the thesis

TABLE OF CONTENTS

Chapter -1

General Introduction

1.1	Therapeutic protein immunogenicity	2
1.2	Factors related to therapeutic protein immunogenicity	3-4
1.3	Immunogenic response to therapeutic protein aggregates	4
1.3.1	Aggregate's structure/conformation and immunogenicity	5
1.3.2	Aggregate's size and immunogenicity	6
1.4	Protein aggregation	7
1.4.1	Factors influencing protein aggregation	7-8
1.4.2	Classification of protein aggregates	8-9
1.5	How the immune system responds against protein aggregates	9
1.5.1	Innate response	9-10
1.5.2	Adaptive response	10-12
1.6	Anti-EGFR single domain antibody (V_{HH})	13-14
1.7	Motivation	14

Chapter 2

The immunogenicity of an anti-EGFR single domain antibody (V_{HH}) is enhanced by misfolded amorphous aggregation but not by heat-induced aggregation

2.1.1	Introduction	24-25
2.1.2	Aim and objective	25
2.2	Methods and Materials	26-30
2.2.1	Protein expression and purification	26
2.2.2	Generation of the aggregates	26-27
2.2.3	Dynamic light scattering (DLS) and static light scattering (SLS)	28
2.2.4	High-Performance size exclusion chromatography (HP-SEC)	28
2.2.5	Spectroscopic measurements	28-29

2.2.6	Binding activity by surface plasmon resonance (SPR)	29
2.2.7	Mice immunization and measurement of serum IgG level	29-30
2.3	Results	31-33
2.3.1	Structural characterization	31-32
2.3.2	Aggregate size and intermolecular SS bonds	32
2.3.3	Binding activity	33
2.3.4	Effect of aggregate types on immune response	33
2.4	Discussion	34-36
2.5	Conclusions	36

Chapter 3

Immune response with long-term memory triggered by amorphous aggregates of misfolded anti-EGFR V_{HH}-7D12 is directed against the native V_{HH}-7D12 as well as the framework of the analogous V_{HH}-9G8

3.1.1	Introduction	54-55
3.1.2	Aim and objective	55
3.2	Methods and Materials	56-58
3.2.1	Protein expression and purification	56
3.2.2	Generation of misfolded V _{HH} -7D12 aggregates (V _{HH} -Mis)	56
3.2.3	Circular dichroism (cd)	57
3.2.4	Dynamic light scattering (DLS)	57
3.2.5	Mice immunization	57
3.2.6	Enzyme-linked immunosorbent assay (ELISA)	57-58
3.2.7	Cell surface CD marker analysis by flow cytometry	58
3.3	Results	59-61
3.3.1	Structural and biophysical assessment	59
3.3.2	A strong immune response generated by the aggregated V _{HH} - Mis	59-60
3.3.3	Nature of the long term immune response against the native V _{HHS}	60-61

3.3.4	Immunization with V _{HH} -Mis established T-cell effector and central memory	61
3.4	Discussion	62-63
3.5	Conclusion	64
Chapter 4	Conclusions	83-84
Chapter 5	References	86-94

LIST OF FIGURES

Chapter 1

General Introduction

1.1	Factors that may influence the protein's immunogenicity	15
1.2	Schematic representation of the proposed two-wave mechanism of antigen presentation following subcutaneous injection of protein	16
1.3	Protein aggregation pathway	17
1.4	Aggregated protein antigen uptake by antigen-presenting cells (APCs)	18
1.5	T-cell dependent B-cell activation pathway	19
1.6	T-cell independent B-cell activation pathway	20
1.7	Generation of Single Domain Antibody	21

Chapter 2

The immunogenicity of an anti-EGFR single domain antibody (V_{HH}) is enhanced by misfolded amorphous aggregation but not by heat-induced aggregation

2.1	Molecular weight by MALDI-TOF	37
2.2	Schematics and gel analysis of the V_{HH} preparation	38
2.3	Secondary structure content V_{HH} formulations	39
2.4	Circular dichroism (CD) spectra of native and misfolded V_{HH}	40
2.5	Characterization of the tertiary structures by tryptophan fluorescence	41
2.6	Characterization of the tertiary structures by ANS	42
2.7	Aggregate's sizes by Dynamic Light Scattering (DLS)	43
2.8	Degree of aggregation by Static Light Scattering (SLS)	44
2.9	High-performance size exclusion chromatography (HP-SEC) analysis of the oligomerization state	45

2.10	Binding activity to EGFR by Surface Plasmon Resonance (SPR)	46
2.11	Anti-V _{HH} antibody (IgG) titer assayed by ELISA	47
2.12	Long-term IgG response and immunological memory	48
2.13	Microscopic images of V _{HH} formulations	49
2.14	HP-SEC analysis of the oligomerization state	50

Chapter 3

Immune response with long-term memory triggered by amorphous aggregates of misfolded anti-EGFR V_{HH}-7D12 is directed against the native V_{HH}-7D12 as well as the framework of the analogous V_{HH}-9G8

3.1	Determination of molecular weight of purified V _{HHS}	65
3.2	Structure of anti-EGFR V _{HH} -7D12 and V _{HH} -9G8 antibodies and schematic representation of immunization	66
3.3	Secondary and tertiary structural properties of anti-EGFR V _{HH}	67
3.4	Aggregates size measurement by DLS and SLS	68
3.5	Anti-V _{HH} IgG titer by ELISA	69
3.6	Specificity of V _{HH} -Mis anti-sera against native V _{HH} -7D12 and V _{HH} -9G8 assayed by ELISA	70
3.7	Re-immunization of Group-1 mice with native V _{HH} -9G8 (Scheme-2)	71
3.8	Re-immunization of Group-1 mice with native V _{HH} -7D12 (Scheme-2)	72
3.9	Re-immunization of Group-2 mice with native V _{HH} -9G8 (Scheme-2)	73
3.10	Re-immunization of Group-2 mice with native V _{HH} -7D12 (Scheme-2)	74
3.11	Flow-cytometry analysis of cell surface CD (cluster of differentiation) markers (T-helper cells)	75
3.12	Flow-cytometry analysis of cell surface CD (cluster of differentiation) markers (T-cytolytic cells)	76
3.13	Characterization of effector and central T-cell memory by flow cytometry	77
3.14	Determination of IgG sub-class by ELISA	78
3.15	Binding activity measurement by surface plasmon resonance (SPR)	79

LIST OF TABLES

Chapter 1

Introduction

1.1	Classification of protein aggregates	22
-----	--------------------------------------	----

Chapter 2

The immunogenicity of an anti-EGFR single domain antibody (V_{HH}) is enhanced by misfolded amorphous aggregation but not by heat-induced aggregation

2.1	Secondary structure content by BestSel	51
2.2	Tryptophan and ANS fluorescence intensities	51
2.3	Aggregate's sizes by DLS and SLS	52

Chapter 3

Immune response with long-term memory triggered by amorphous aggregates of misfolded anti-EGFR V_{HH} -7D12 is directed against the native V_{HH} -7D12 as well as the framework of the analogous V_{HH} -9G8

3.1	Aggregate's size by DLS and SLS	80
3.2	Serum IgG titer of V_{HH} -Mis immunized mice against native V_{HH} -7D12 and V_{HH} -9G8	81

LIST OF ABBREVIATIONS

EGFR	:	Epidermal Growth Factor Receptor
V _{HH}	:	Variable Heavy Chain only Antibody
CDRs	:	Complementarity Determining Regions
HP-SEC	:	High-Performance Size Exclusion Chromatography
CD	:	Cluster of Differentiation
DLS	:	Dynamic Light Scattering
SLS	:	Static Light Scattering
cd	:	Circular Dichroism
SPR	:	Surface Plasmon Resonance
ELISA	:	Enzyme Linked Immunosorbent Assay
ThT	:	Thioflavin T
ANS	:	8-anilino-1-naphthalene-sulfonic acid

Dissertation Summary

The generation of anti-drug antibodies (ADAs) is a major concern in biotherapeutic drug development. It is now well acknowledged that therapeutic protein aggregation is intimately connected with the host immune response which affects the drug effectiveness. All protein aggregates, however, are not equally immunogenic and what kind of biophysical and biochemical nature makes an aggregate more immunogenic than others is yet well understood. In this research dissertation, I focused on understanding the conformational and biochemical nature of amorphous aggregates related to immune responses and the long-term effects of those immune responses on drug safety measurements. I divided this dissertation into four chapters.

In chapter 1, I reviewed some of the intrinsic and extrinsic factors connected with the immunogenic aspects of a therapeutic protein with particular focus on therapeutic protein aggregation and oligomerization. Additionally, I discussed the immunological mechanisms that are related to protein aggregates and generating anti-drug antibodies (ADAs). Amorphous aggregates, unlike amyloids, possess distinct morphology with diverse biochemical and biophysical nature, and are further classified based on their size, reversibility, chemical modifications and so on. Several clinical studies showed that therapeutic protein aggregates are responsible for unwanted immunogenicity, however, very little is known about the aggregate's nature that is related to clinical immunogenicity. Therefore, I summarized some of the *in vivo* experimental studies that are aimed to connect the biophysical and biochemical parameters of the protein aggregates with immunogenicity. Aggregates can potentially generate the immune response (B-cells activation) with the help of T-cell, so-called T-cell dependent pathways, or without any help of T-cells.

In chapter 2, I examined the immunogenicity of an anti-EGFR V_{HH} (V_{HH} -7D12), a potential anti-cancer drug, and four different aggregates state. Firstly, I produced two heat-induced V_{HH} aggregates, incubated at 65 °C for 45 min (V_{HH} -65) and 95 °C for 110 min (V_{HH} -95). Additionally, I isolated a low-soluble misfolded V_{HH} species from an *E.coli* lysate during refolding of the V_{HH} protein (V_{HH} -Ins). To mimic the V_{HH} -Ins, I also deliberately generated a misfolded V_{HH} species from HPLC purified native V_{HH} -7D12 (V_{HH} -Mis). All biophysical and

immunological experiments were carried out at a protein concentration of 0.3 mg/mL in phosphate saline buffer (PBS, pH 7.4). Circular dichroism (CD) measurements indicated that the secondary structural content of the native V_{HH}-7D12 was typical of a β -sheeted protein. The secondary structure of V_{HH}-Ins and V_{HH}-Mis was completely different from native V_{HH}-7D12. Similarly, tryptophan and ANS (8-Anilino-naphthalene-1-sulfonic acid) fluorescence measurements showed a different tertiary structure content of V_{HH}-Ins and V_{HH}-Mis. On the other hand, V_{HH}-65 showed only a minor change in their secondary and tertiary structures. Surface plasmon resonance (SPR) showed that the native V_{HH}-7D12 binds to EGFR, a target ligand of V_{HH}-7D12, in a concentration-dependent manner. V_{HH}-65 showed slight decreasing activity. The misfolded V_{HH} formulations (V_{HH}-Ins and V_{HH}-Mis) and V_{HH}-95 completely lost their binding activity with EGFR. Further, the size of the V_{HH} aggregates was measured by dynamic light scattering (DLS). The Z-ave hydrodynamic radius of native V_{HH} was 3.5 ± 0.19 nm, as expected for monomeric V_{HH}. V_{HH}-Ins and V_{HH}-Mis in PBS (pH 7.4) formed aggregates larger than 1 μ m (1846.5 ± 409.4 and 1951 ± 373.3 , respectively). V_{HH}-95 formed aggregates that are very similar in size to misfolded V_{HH} (1722 ± 179 nm), whereas V_{HH}-65 produced aggregates smaller than 1 μ m (771.3 ± 26.3 nm). Finally, *in vivo* immunization experiments were performed in mice and the generation of anti-drug antibodies (ADAs), mainly IgG, was determined by ELISA. The results showed that native V_{HH}-7D12 was scarcely immunogenic, as expected for small proteins, while V_{HH}-65 was mildly immunogenic. The misfolded aggregates, V_{HH}-Ins and V_{HH}-Mis, showed higher IgG response. By contrast, the heat-denatured aggregates, V_{HH}-95, having a Z-ave and aggregation propensity similar to that of misfolded V_{HH}s (V_{HH}-Ins and V_{HH}-Mis), was not immunogenic at all. These findings indicate the critical role of biophysical and biochemical attributes of the amorphous aggregates in the generation of an immune response against a protein rather than just their size.

In chapter 3, I reported the immunogenic nature, especially the specificity of the immune response induced by V_{HH}-Mis (misfolded V_{HH}-7D12) and their long-term anti-therapeutic effects. To do so, I used an analogous anti-EGFR V_{HH} (V_{HH}-9G8), along with V_{HH}-7D12, which have 77% sequence similarity. Both of the V_{HH}s share a very similar framework region

but distinct complementary determining regions (CDRs), the functional part of the V_{HH} antibody. The anti-sera raised against the V_{HH} -Mis was further analyzed by ELISA using native V_{HH} -7D12 and native V_{HH} -9G8 as coating antigens. This is because we anticipated seeing cross-reactions because of their identical framework regions. As a result, we observed that 60 % of the mice (8 out of 13) immunized with V_{HH} -Mis the IgG titer against native V_{HH} -7D12 was much stronger than against native V_{HH} -9G8 (**Group-1**), indicating that IgG was directed against the regions that are specific for V_{HH} -7D12, eg V_{HH} -7D12's CDRs. The remaining 40 % of mice (5 out of 13) showed a very similar IgG titer against the native V_{HH} -7D12 and native V_{HH} -9G8 (**Group-2**). We rationalized these results by hypothesizing that the IgG was mostly generated against the V_{HH} 's frameworks that are common for both V_{HHS} . The long-term immunological experiments showed that the pattern of IgG specificity against native V_{HH} -7D12 and V_{HH} -9G8 was essentially unchanged over 17 weeks. After 17 weeks without injection, both groups of mice (**Group-1 and Group-2**) were re-immunized with native V_{HH} -7D12 and V_{HH} -9G8 (boost injection). As a result, we observed that **Group-1** mice increased the IgG titer sharply when re-immunized with native V_{HH} -7D12 but not with native V_{HH} -9G8, indicating that the immunological memory was generated against V_{HH} -7D12, particularly against the V_{HH} -7D12's CDRs. On the other hand, the IgG titer of the **Group-2** mice increased by re-immunizing both of the V_{HHS} , indicating that immunological memory was generated against the framework regions. Finally, the flow-cytometric analysis showed that V_{HH} -Mis immunized mice generated a higher number of effector and central T-cell memory. Overall these observations indicate that the amorphous aggregates of misfolded V_{HH} can induce serum IgG and immunological memory against the native self and with a null to moderate immune response against natively folded V_{HH} analogs. Our findings indeed suggest that by determining the ADAs specificity one might avoid ADAs' appearance by switching the therapeutic antibody to an analogous one that targets the same EGFR and would thus allow the same therapeutic strategy.

In chapter 4, I concluded the overall observations of chapter 2 and chapter 3 and discussed the future aspect of this research. The above studies clearly suggested that native monomeric V_{HH} proteins barely affect immunogenicity. The aggregated species definitely increase the immunogenicity but solely depending on the nature of the aggregates. So far, many of the experimental studies have focused on examining the sizes of amorphous aggregates that

generate ADAs, but counter-examples have led to some controversy. Our observations provided sound evidence that the biophysical and biochemical nature of the aggregates plays a major role rather than just their size. Moreover, the aggregates made of misfolded V_{HHS} can carry the higher risk of immunogenicity with CDRs (active-site of an antibody drug) specific ADAs and carry the long term-immunogenicity risk. I believe that this research will have a further impact on future protein chemistry research and biopharmaceutical safety assessments.

Chapter-1
Introduction

1.1 Therapeutic protein immunogenicity

Immunogenicity of therapeutic protein indicates the host immune responses that unwantedly generated against drug molecules, resulting in anti-drug antibodies (ADAs) [1]. The ADAs response unexpectedly reduces the therapeutic effectiveness of a protein drug, and thereby, worsening the existing disease conditions. For instance, the recombinant factor VIII resulted in ADAs generation of approximately 30 % of haemophilia A patients, which significantly inhibit the hemostatic efficiency of factor VIII [2]. Likewise, ADAs development against interferon (IFN)- β , a relapsing-remitting multiple sclerosis (MS) drug, can inhibit IFN- β binding to its receptor, reducing drug efficacy and accelerating disease progressions [3]. Moreover, even though rarely, ADAs may have strong cross-reactivity with host endogenous proteins, as observed for the recombinant EPO and thrombopoietins [4-6]. ADAs may have drug function neutralizing capacity when the epitope is located at the active-site of the drug molecules, while non-neutralizing ADAs recognize regions other than the active-sites [7]. However, in both cases, either neutralizing or non-neutralizing, ADAs negatively affect the pharmacokinetics and pharmacodynamics of the drug by accelerating the clearance from the body [7].

Therapeutic monoclonal antibodies (mAbs), one of the fast-growing classes of biopharmaceutical products, often provoke ADAs, either in a form of neutralizing or non-neutralizing/binding [8]. The first mouse monoclonal antibody, muromonab-CD3, approved by the FDA induced ADAs in 50% of the patients [9]. Similarly, another murine antibody, edrecolomab, showed undesired immune responses in all (100%) of the patients [10]. Even though antibody humanization technology can significantly reduce the fate of immunogenicity, still many of the antibody therapeutics show immune response, in a form of ADAs. For example, adalimumab, the first fully-humanized monoclonal antibody (mAb) showed immunogenicity in 5% of adult patients with rheumatoid arthritis [11]. In the next section, I will discuss the related factors that influence therapeutic protein immunogenicity.

1.2 Factors related to therapeutic protein immunogenicity

Several intertwined factors are connected with the immune responses against a protein-based therapeutic drug, which are broadly classified into three key categories: (1) treatment-related factors (2) patient-related factors and (3) product-related factors (**Figure 1.1**) [12]. Treatment-related factors, which include duration and frequency of the treatment and eventually the route of drugs administration, have an influential effect on immunogenicity. Generally, long-term therapy is more likely to induce immunogenicity than short-term therapy. One of the well-known examples is the formation of ADAs against various IFN- β products that required different amounts of time [13]. On the other hand, when considering the route of administration, it is evidenced that subcutaneous (SC) injection is more susceptible to increase the immunogenicity other than intravenous (IV) or intramuscular (IM) injection [14]. The higher immunogenic nature of this route is described by their two-wave antigen presentations (**Figure 1.2**) [15]. Nevertheless, subcutaneous injection is most desirable due to patient comfort and compliance. Moreover, this route of administration increases the drugs serum half-life. Intramuscular (IM) administration is also likely to elicit an immune response, but to a lesser extent, when compared with intravenous (IV) administration [15].

Beyond the treatment-related factors, genetic background of the patients, like the inherent polymorphism of human proteins, can often influence immunogenicity. A well-established clinical example with haemophilia patients showed that the genetic defect of the factor VIII gene determines whether an individual will or will not produce ADAs [16, 17]. Another study, conducted by Scharrer et al. showed that race can be a risk factor for generating antibodies [18].

Protein sequence, a critical product-related factor, can cause unwanted immune responses. Usually, non-humanized proteins are highly immunogenic, as a human immune system identifying those molecules as foreign and respond accordingly. As observed for the monoclonal antibodies derived from the murine system, which showed higher immunogenicity in human. For example, muromonab-CD3, the first mouse monoclonal antibody approved by the FDA, showed binding antibodies in 50% of the patients [9]. Similarly, a murine antibody, edrecolomab, showed undesired immune response in all of patients [10]. Factors relating to the downstream processing of a protein product can also

influence its immunogenicity. Such a phenomenon has been reported for factor VIII, where ADAs generation was related to their pasteurization stage in the manufacturing process. It has also been reported that the product impurities and contaminants are associated with antibody development, as shown for insulin and growth hormone products [19]. Experimental studies with ovalbumin showed that trace amounts of impurities are sufficient enough to break the immune tolerance against ovalbumin [20]. However, this problem is now decreasing as the purity of products improves.

Among other product-related factors, protein aggregation is identified as the most critical. One of the earlier clinical evidence showed that human growth hormone (hGH) reduced its undesired immunogenicity by removing the accidental aggregates from the formulations [21, 22]. Some of the other examples regarding aggregates initiated immunogenicity are comprised of erythropoietin (EPO), factor VIII. Therefore, several drug regulatory agencies have paid attention to their guideline to control therapeutic protein aggregation. European Medical Agency (EMA) considered visible and sub-visible aggregates as risk factor and stating, “The formation of aggregates, sub-visible and visible particulates in the drug product is important and should be investigated and closely monitored on the batch release and during stability study” (REF). Food and Drug Administration (FDA) state that “Assessment should be made of the range and level of sub-visible particle (2-10 μm) present in the therapeutic protein product initially and over the course of the shelf life”.

1.3 Immunogenic response to therapeutic protein aggregates

From early clinical studies in the 1960s to more recent examples, it has been found that aggregated therapeutic proteins can adversely affect the host immune response, resulting in ADAs formation [23, 24]. One of the first studies has been reported by Christian [25, 26] in early 1960, where aggregates of human gamma globulin (hGG) induced by heat showed immunogenicity in human volunteers as well as guinea pigs and rats. In the later stage, Ellis and Henney showed strong evidence of aggregate initiated immune response [27]. They separated the monomer and aggregated hGG from three commercially available hGG formulations and injected intradermally. As a result, hGG in monomeric form did not cause any immunogenic reaction in the intradermal skin. On the other hand, the aggregated hGG

showed a strong sensitivity reaction (flares-and-wheals). Similarly, clinical studies with human growth hormones (hGH) showed that removing aggregated particles from drug formulations significantly reduced the antibody formation against hGH [22]. The neutralizing ADAs generation was observed against recombinant human erythropoietin (EPO) when drug formulation and administration schemes were changed [5]. Several hypotheses, even though controversial, indicated the role of micelles formation. Besides several clinical observations, where detection and characterization of aggregates are rarely performed, to date, many experimental studies have reported the possible contribution of aggregates in ADAs generation. However, it is becoming increasingly clear that all aggregate types do not induce equal immune responses in the host. Many intertwined factors are thought to be related to the immune response to protein aggregates, including aggregates biophysical and biochemical nature such as the structural/folding properties, size, availability and frequency of neo-epitopes, amount of aggregates and so on are influential and are still under investigation [28, 29].

1.3.1 Aggregate's structure/conformation and immunogenicity

A natively functional protein has a complex three-dimensional structure. Any physical instability, such as unfolding or misfolding can result in protein aggregation, which further increases immunogenicity. In clinical studies, where the aggregates nature is not accurately monitored and characterized, several experimental studies show a relationship between the aggregate's structure/biophysical properties and immunogenicity. Aggregates containing native-like structures are proposed to be more immunogenic [30, 31]. A well-known example is the immunogenicity of factor VIII, which readily formed both native-like or non-native aggregates depending on the way they are generated [32-34]. Immunization experiments using transgenic mice showed that native-like aggregates were more immunogenic than native monomeric factor VIII and non-native aggregates of factor VIII. In another study, Fathallah et al. showed that native-like monoclonal antibody aggregates were more immunogenic than denatured aggregates [35]. Recent studies have demonstrated that non-native aggregates may induce potent antibody responses, but due to their non-native structure, it is expected that they may not produce a large population of inhibitory antibodies [23, 36].

1.3.2 Aggregate's size and immunogenicity

Size is one of the important factors used to classify the protein aggregates. Fathallah et al. [35] have documented the immunogenicity based on the aggregate size. Small oligomers (<100 nm) and non-native micron size aggregates were generated using heat stress and protein unfolding models. They revealed that a small oligomeric protein was much more immunogenic than a non-native micron size aggregate. To explore more on the aggregate size based immunogenicity, Kijanka et al. [37] conducted their study using a monoclonal antibody in which the antibody was subjected to heat stress to generate different sizes of aggregates. The aggregates were fractionated using low-speed centrifugation and size exclusion chromatography and further classified into a soluble oligomer, sub-micron size and micron size aggregates. Immunization experiments with Balb/c mice revealed that submicron size (0.1-1 μm) formulation was more immunogenic than micron size (1-100 μm) and soluble oligomer enriched fractions. These findings are partly contradict by Fathallah et al., where less than 100 nm size oligomers were reported to be highly immunogenic but both research groups documented the non-immunogenic properties of micron size aggregates. Likewise, micron size aggregates of single chain variable fragment (ScFv) did not show any increase immunogenicity than native monomeric ScFv [38]. In another study, Boll et al. [39] attempted to address the immunological effect of chemical modification along with aggregate size. The sample formulation contained the same size aggregate (15 μm) but with a different level of chemical modification. Immunization experimentation in the mice model showed that extreme chemical modification was required to break the immune tolerance of the micron size aggregates. Suggesting that biochemical properties of aggregates are important in addition to size in breaking immune tolerance. In recent study, using bovine pancreatic trypsin inhibitor (BPTI) protein Rahman et al. showed that a few nanometer size protein aggregates can break the immune tolerance [40]. Overall, there is no solid consensus regarding the relationship between the aggregates size and immunogenicity, suggesting that other aggregates nature might be connected with aggregates immunogenicity.

1.4 Protein aggregation

Protein aggregation is one of the most common routes of protein instability, making the protein product unfit for basic academic research to clinical application. Protein aggregation is generally defined as the abnormal intermolecular interaction of protein molecules, having its natively folded, partially unfolded, misfolded or even completely denatured state (**Figure 1.3**) [41, 42]. Depending on the pathway and the environment, the structurally altered protein may initially form a small dimer, trimer and/or tetramer and in thermodynamically favourable conditions further progress toward sub-visible to visible sizes [43]. Despite numerous attempts to shed light on the pathway of aggregate formation and their associated factors over 60 years, still, there is no solid consensus regarding the protein aggregation pathway and its systematic control [44]. This is because of the diverse types and nature of the aggregates, which are poorly understood due to the difficulties in their specific isolation and detailed experimental characterization.

1.4.1 Factors influencing protein aggregation

Protein aggregation is a multi-factorial as well as multi-step event, where many of the intrinsic and extrinsic factors simultaneously play a major role and result in protein aggregates with different ending states [45-47]. Intrinsic factors which are influential, include amino acid sequences, level of chemical modifications and the physiochemical nature of the protein. For example, a recombinant protein with a higher number of negative charge residues (Asn and Glu) is more soluble than a protein with a higher number of aromatic amino acids (Phe, Tyr, and Trp) expressed in *E.coli* [48]. Chemical modifications, which includes oxidation, deamination in the amino acid side chain and peptide bond cleavage often negatively affects the physical properties such as hydrophobicity, secondary and/or tertiary structure, thermodynamic parameters and thereby changing the protein's solubility profile [49, 50]. Amino acid side chain oxidation, particularly Cys, Met, Trp, and His, is one of the major degradation pathways for proteins [51-53]. The level and specificity of the oxidation mainly depend on the way they are generated [54]. Though amino acid asparagine (Asn) being especially significant for deamination, it has been shown that the Gly in the C-terminal position of a model protein results in the increased deamination of Asn [55].

Extrinsic factors like the composition of buffers, pH, extreme temperatures, freeze-thaw or various mechanical stresses (pumping, shaking, stirring, etc), adsorption to air-liquid and solid-liquid often cause protein aggregation. The anionic condition of the buffer strongly modulates the protein solubility and aggregation. For example, the phosphate ion presents in phosphate buffer may interact with positively charged amino acid residues on the protein surface and diminish their electrostatic repulsive effect, leading to protein aggregation [56]. Solution pH is an important factor regulating protein solubility as well as aggregation. Solution pH determines the net charge of a protein as well as the charge type (positive and negative), thereby affecting the electrostatic interaction between the protein molecules [57]. On the other hand, extreme temperatures or mechanical stresses may cause partial/complete denaturation of protein and result in protein aggregation with undefined biophysical and biochemical properties [58]. This process generally produces irreversible aggregation. Aggregates can even form under the condition which is thermodynamically favoured for a native state, without any external stress [59].

1.4.2 Classification of protein aggregates

From a morphological standpoint, protein aggregates are classified into two major groups: amyloid fibrils and amorphous aggregates. Amyloid fibrils are unique linear assemblies' of aggregates that contain an ordered cross beta-sheet structure and are generally insoluble [60]. Unlike amyloids, amorphous aggregates are randomly formed without any defined ordered intermolecular interaction. Amorphous aggregates can be formed through simple hydrophobic, Van der Waals interaction and/or electrostatic interaction [61]. These aggregates, particularly smaller one are often form reversibly. On the other hand, covalent aggregates that formed through intermolecular disulfide cross-linking, are irreversible in nature. Additionally, most large or insoluble aggregates, even without covalent linkage are irreversible.

Size is perhaps the most common parameter used to classify protein aggregates. Many terms are being used to define the aggregates' size. However, those naming systems are often confusing, because different research groups use different terms to indicate the same size aggregates. In 2012, Narhi et al. proposed quantitative categories, such as >100 μ m (previous term visible particles), 1-100 μ m (previously known as sub-visible particles), 100-1000nm

(sub-micron), and < 100nm or nanometer size aggregates, which were previously defined as oligomers or soluble aggregates (**Table 1.1**) [62].

In aggregates, protein molecules may get associated into their native conformation to unfolded conformation, and anything in between the both. Aggregates conformation includes the properties of secondary and tertiary structure, stability and surface hydrophobicity. Based on these characteristic feature aggregates are classified as “native,” “partially unfolded,” “misfolded,” “inherently disordered,” “unfolded,” or “amyloid [62].

Chemical modification in the protein molecules is one of the critical factors for aggregate formation, thereby aggregates are often characterized based on the chemical modification. Covalent cross-linking is one of the best example that results in irreversible protein aggregation. Aggregates may contain reducible intermolecular or intramolecular disulfide cross-linking. On the other hand, non-reducible chemical crosslinking includes thioether and dityrosine covalent bonds [62].

1.5 How the immune system responds against protein aggregates

The immune system, a complex biological process, responds differently against different aggregate types, therefore, the exact mechanism is yet to be fully understood. The biophysical and biochemical nature of the protein aggregates, including size, morphology, stability and their surface charge properties greatly influences their immunogenicity. It is now becoming increasingly clear that all type of aggregates is not equally immunogenic. However, the defensive mechanism against aggregated proteins, as like other pathogens, is mainly conducted by two different but interconnected subsystems, where innate responses provide the first line defences and adaptive immune responses provide long-term and much stronger defences.

1.5.1 Innate response

The innate immune response protects the organism, when the adaptive response is not stimulated, by preventing the immediate spread of the pathogen throughout the body. The prime component of innate immune response is the phagocytic cells (neutrophils, macrophage), natural killer cells, cytokines, and the member of the complement system. Aggregated proteins may induce local inflammation at the site of administration, as observed

for the deposition of beta-amyloid in Alzheimer patients [63], and activate the innate immune cells embedded in the tissue [64, 65]. It has also been reported that aggregated protein in beta-amyloid plaque increased the production of TNF- α through Toll-like receptor 2 and 4 (TLR2 and TLR4) stimulation [66]. TLRs are a family of transmembrane receptors, which recognize the pathogen-associated molecular patterns (PAMPs), and thereby known as a pattern recognition receptor [67, 68]. Widely known PAMPs is the bacterial lipopolysaccharide (LPS), an outer membrane component of gram-negative bacteria, which initiate the innate immune response by activating the TLR4 [69]. Similarly, the aggregated protein, for example, the monoclonal antibody aggregates, activate the TLR2 and TLR4 and induce the secretion of inflammatory cytokine [70]. Moreover, the antibody aggregates also involved in Fc gamma (Fc γ) receptor-mediated innate immune response. It has been shown that antibody aggregates crosslink the Fc γ receptor on the antigen-presenting cells (APCs) more efficiently than a monomeric counterpart [71]. In another study, using surface plasmon resonance (SPR) showed that the dimer and multimers of IgG1 monoclonal antibody bind more strongly with the Fc γ receptor than that of monomeric IgG1 [71]. The complement system is one of the major defences in innate immune responses, which can be initially activated by any of three pathways (alternative, classical, and lectin) [72]. During the immune response against a foreign antigen, the complement protein binds or fixes with the antigen-antibody complex. Experimental studies reported that the aggregated IgG more efficiently binded and activated the C1 protein (the first binding protein in the classical pathway) than that of monomeric IgG [73]. Similarly, the antivenoms IgG that forms dimers and polymers in the presence of preservatives (thimerosal and/or phenol) induce a higher complement activation [74].

1.5.2 Adaptive response

Unlike the innate immune response, the development of adaptive immunity requires a longer time as this system of response uses an immunological memory to learn about the threat and enhance the immune response accordingly. The adaptive immune response follows a series of sequential intra and extracellular events and ultimately activates antigen-specific antibody-secreting B-cells, either with the help of T-cells or without T-cells involvement.

a) The mechanism of aggregates mediating T-cell dependent B-cell activation

Generation of effective anti-drug antibodies (ADAs) response against a therapeutic protein through the activation of T-cells are termed a thymus-dependent or a T-cell dependent (TD) pathway. This T-cell dependent B-cell activation requires three major signaling pathways:

- I) Activation of T-cells by antigen-presenting cells (APCs)
- II) Interaction of protein antigen with B-cell receptors (BCRs)
- III) Interaction of toll-like receptors of B-cells with foreign protein moieties

I) Activation of T-cells by antigen-presenting cells (APCs): Antigen-presenting cells (APCs) play the master role for T-cell activation. Firstly, antigen processing is induced by professional antigen sensing dendritic cells (DCs) in the periphery [75]. Protein aggregates have a different molecular pattern, thereby APCs, such as DCs, follow distinct uptake pathways (**Figure 1.4**). Protein aggregates may follow a pathogen-associated molecular pattern (PAMP) and be efficiently uptaken by pattern recognition receptors, known as toll-like receptors (TLRs). Alternatively, either small or large aggregates of protein can often mimic the ‘immune complex’, particularly the IgG aggregates, and hence increase the binding with Fc γ R [76]. Finally, aggregated proteins are internalized through receptor-mediated phagocytosis and digested by lysosome and produce small linear peptides, which are then bound with MHC-II molecules and are presented on the cell surface molecules. In addition, the co-stimulatory molecules (CD80 and CD86) are also expressed. After antigen encounters and processing by APCs, systematically they migrate to lymph nodes, particularly in the T-cell zone [77]. Here they perform a thorough scan and find the appropriate T-cells, whose receptors are perfectly fit with antigenic peptides just like in a ‘key-lock’ manner (**Figure 1.5**). Finally, the antigen primed activated T-cells move to follicles, where B-cells reside.

II) Interaction of protein antigen with B-cell receptors (BCRs): The protein antigens first migrate to secondary lymphoid organs, such as lymph nodes through lymphatic vessels, where they are filtered through a draining system and thereby become accessible to B-cells. Next, protein antigens are scanned by B-cells, and the B-cell receptors (BCRs) bind with specific antigens, resulting in the activation of B-cells (**Figure 1.5**). Like APCs, the antigen bind BCRs which are internalized by activated B-cells and finally expressed as MHC-II associated peptides on the B-cell surface. The BCRs antigen clustering provides the **first signal** for B-

cells proliferation and differentiation. But they require a **second signal** which comes from the activated helper T-cells primed with the same antigen (**Figure 1.5**). To do so, after BCR-antigen interaction, B-cells migrate to the border of the B/T-cell zone, where the peptide associated MHC-II of the B-cell interacts with TCRs of the T-cell. At the same time CD40 ligand (CD40L) of the T-cell bind with the CD40 receptor of the B-cells.

III) Interaction of toll-like receptors of B-cells with foreign protein moieties: In addition to those two signals, it has been reported that a third signal is required to finalize the B-cells maturation. This **third signal** is accomplished by the antigenic epitopes of the foreign proteins that bind with toll-like receptors (TLRs), which reside on the B-cell.

b) The mechanism of aggregates mediating T-cell independent B-cell activation

T-cell independent B-cell activation and antibody production strongly requires the B-cell receptors (BCRs) cross-linking. B-cells of the marginal zone of the spleen (MZ B-cells) and B-1 cells play a major role in the TI pathway, as they can generate a rapid response and do not involve affinity maturation. The large protein aggregates consist of at least ten repetitive arrays of monomers can initiate the TI pathway by cross-linking the BCR residing on B-1 or MZ B-cells (**Figure 1.6**) [78]. However, the large protein aggregates often fail to induce TI, this is because of their irregularly and rigidly ordered structure [79]. The B-cells proliferations then require a **second signal** and it is hypothesized that TLR on the B-cell (particularly B-1 cells) provide the **second signal** by binding with PAMP motifs on the aggregates. There are two distinct subgroups of TI antigens, namely, TI-1 and TI-2 antigens. TI-1 antigen, like bacterial lipopolysaccharides, have an intrinsic property to initiate the B-cells proliferation and differentiation without T-cells help and even without any BCRs specificity. In this case, TLRs play a major role. On the other hand, TI-2 antigens are generally differentiated by their highly repetitive epitope structure. For example, the surface polysaccharide on encapsulated bacteria. They can activate the downstream signalling of the B-cell by cross-linking the BCRs. In such a case the immature B-cells are anergized and only mature B-cells can activate. That may explain why children up to 5 years are not capable of producing effective antibodies against polysaccharide antigens, as the majority of their B cell population is immature.

One of the major differences between TD and TI pathways is that the TI pathway predominantly produces low-affinity IgM antibodies. Some isotype switching may also

happen that produces IgG. Most of the TI antigens do not generate immunological memory as TD dependent antigens.

1.6 Anti-EGFR single domain antibody (V_{HH})

Epidermal growth factor receptor (EGFR) is a receptor of the tyrosine kinase family that efficiently regulates cell growth, differentiation and proliferation by binding with natural ligands, called epidermal growth factor (EGF) [80]. However, the over expressed or mutated EGFRs are often been characterized in cancerous cells, such as lung, breast and nail cancer [80]. Monoclonal antibodies (mAbs), such as cetuximab and panitumumab, targeting EGFR have demonstrated their activity against several cancer types [81, 82]. These mAbs bind with the extracellular domain of the EGFR, inhibit the binding of growth factor associated ligands, including epidermal growth factor (EGF) and transforming growth factor- α and subsequently block the downstream signalling cascade. However, their relatively large size often decrease their efficient tumor penetration.

Single domain antibody (V_{HH}), often referred to as a nanobody, is an engineered fragment antibody developed from a unique class of antibodies called heavy chain only antibody (HcAb) [83]. *Camelidae* (camels, llamas and dromedaries) naturally produces HcAb and unlike conventional mammalian IgG antibody, this class of antibody naturally devoid the light chain and CH1 domain, so-called heavy chain only antibody (HcAb) (**Figure 1.7**). As compared to conventional VH/VL antigen-binding interface, a single domain V_{HH} itself holds three complementary determining regions (CDRs) and retain its antigen specificity [83]. CDRs adopt a loop structure, where CDR3 found as a long loop structure (20~30 amino acids) that increase their ability to fit with the antigen surface and resulting in strong binding with the corresponding antigen. Moreover, this extended CDRs loop allows the antibody to bind the protein cleft/pocket, including the enzyme active site, which is not possible for a conventional antibody's binding interface [84-86]. Their minimal size (~15 kDa) provides an efficient tumor penetration rate. Moreover, their cost-effective bacterial expression makes them an ideal antibody drug candidate. To date, three EGFR targeting V_{HH} antibodies have developed: V_{HH} -7D12, V_{HH} -9G8 and V_{HH} -Ega1. These V_{HH} s have different CDRs and thereby bind different EGFR epitopes and regulate the downstream signalling. Among them, V_{HH} -7D12 binds with EGFR extracellular domain III and directly inhibits the EGF, similarly to the

monoclonal antibody cetuximab. On the other hand, V_{HH}-9G8 binds to a region located between the EGFR extracellular domain II and domain III and thereby inhibits the receptor dimerization. However, due to their smaller size, it is expected that V_{HH} antibody will be less immunogenic but yet to be investigated.

1.7 Motivation

It is well acknowledged that protein aggregate causes unwanted immunogenicity. Several recent studies have reported the relationship between the aggregate's properties, particularly the aggregate's size, and the strength of the immune responses. However, some of the conclusions remain a matter of debate. It is now becoming increasingly clear that amorphous aggregates possess distinct biochemical and biophysical nature. In protein chemistry, amorphous aggregates, besides their size, are often characterized based on their conformation (native, misfolded, partially unfolded or completely unfolded), reversibility and also the type of chemical modifications. Therefore, I aimed at exploring the conformational and biochemical nature of the amorphous aggregates and investigated their immunogenic response in mice models, using anti-EGFR V_{HH} antibodies, as a model of therapeutic protein. In addition, I aimed to determine the type of IgG and the T-cell immunological memory generated by anti-EGFR V_{HH} aggregates and their long-term immunogenicity risk against the native anti-EGFR V_{HH} antibodies as well as another analogous V_{HH} antibody drug.

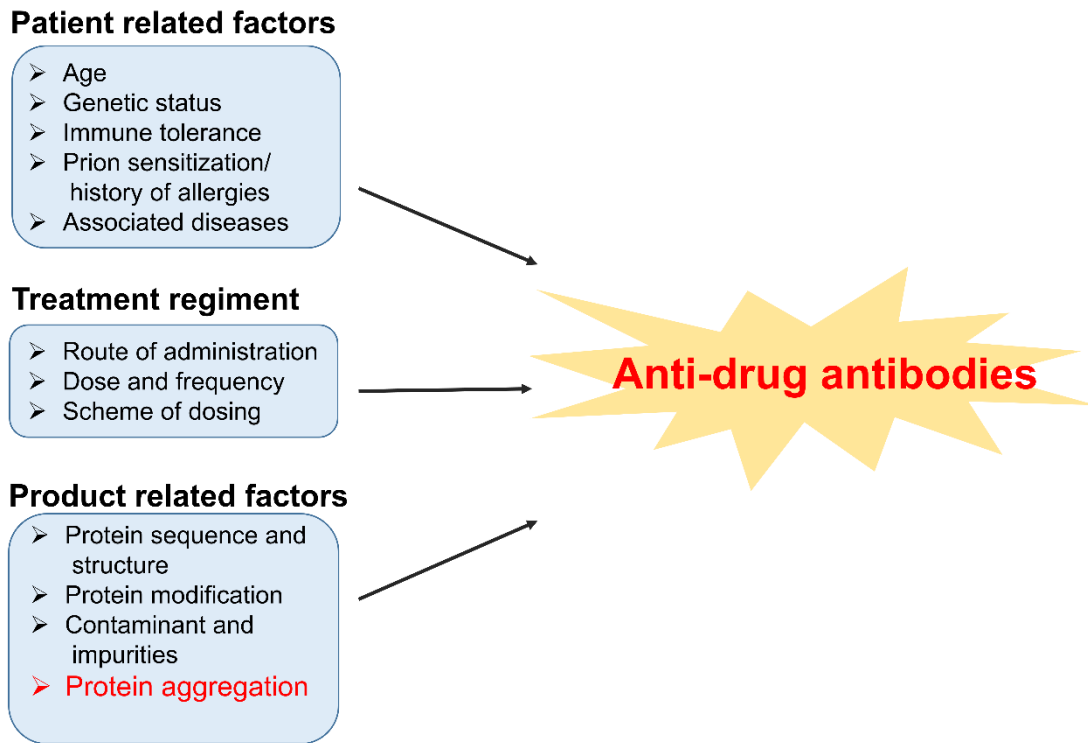


Figure 1.1: Factors that may influence the protein’s immunogenicity. Treatment, product, and patient-related factors that can impact upon the immunogenic potential of a bio-therapeutic. (Figure adopted from Ratanji, K. D. et al., *J. Immunotoxicol.* 2014) [12].

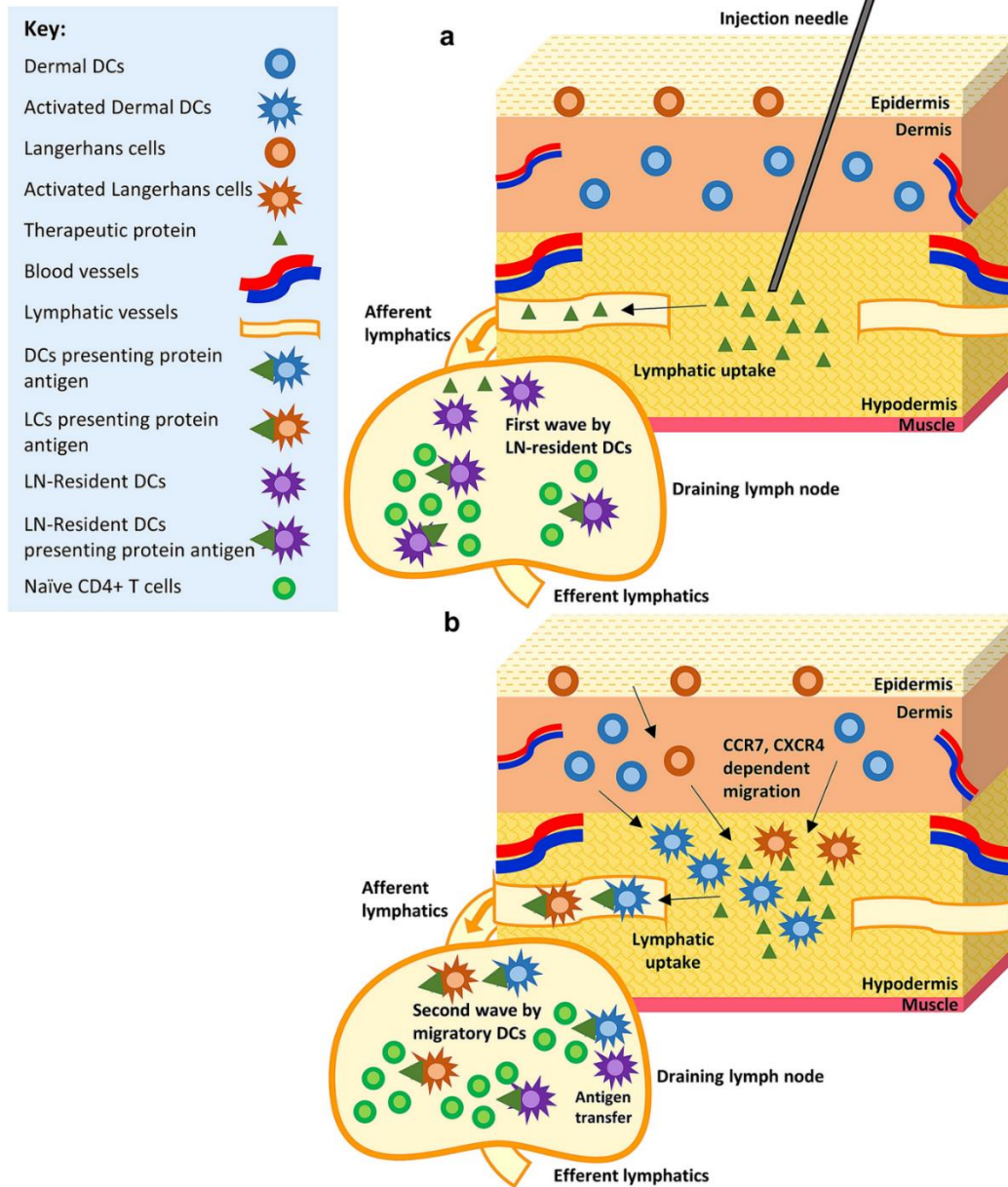


Figure 1.2: Schematic representation of the proposed two-wave mechanism of antigen presentation following subcutaneous injection of protein. (A) Protein antigens migrate to lymph nodes through lymphatic vessels and encountered by LN-resident DC cells, which provides the first wave of antigen presentation. **(B)** Protein antigen uptake by migratory DC and DC-antigen complex migrate to lymph nodes and creates a second wave of antigen presentation. (Figure: Nicole L. Jarvi, Sathy V. Balu-Iyer, *BioDrugs*, 2021) [15].

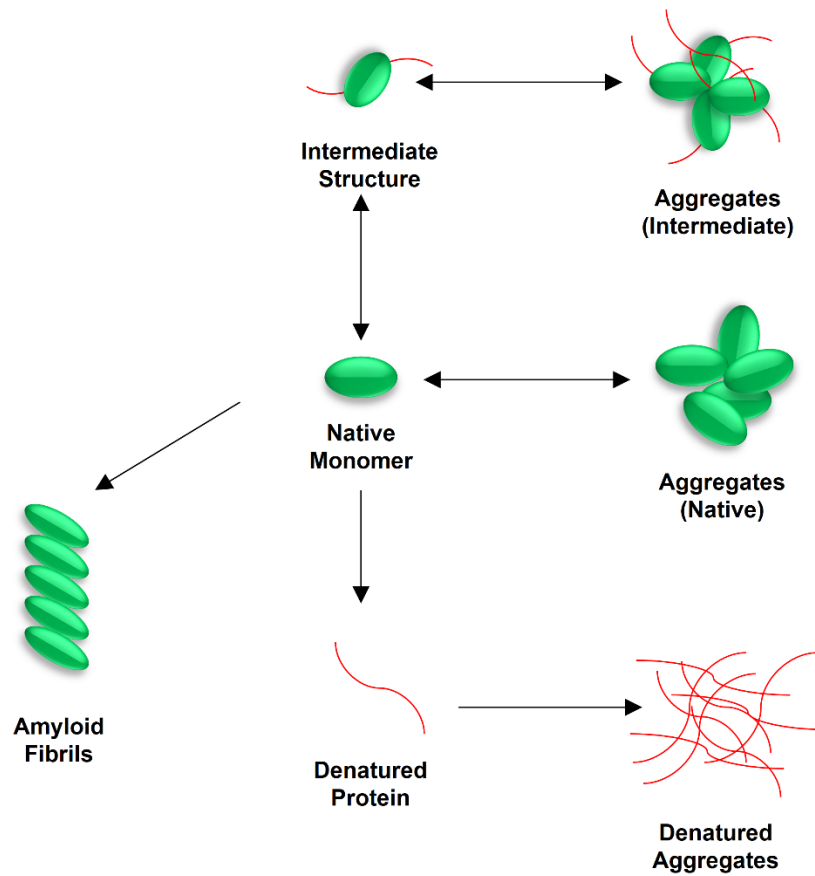


Figure 1.3: Protein aggregation pathway. In aggregates, individual protein molecules **may** get associated with different types and levels of intermolecular interaction. Protein aggregates may be formed with a defined ordered structure, called amyloid fibrils. Aggregates may also be formed under the complete denaturation of the monomeric protein, which are amorphous in nature and generally irreversible. Partial denaturation of protein molecules also influences the formation of the aggregates by increasing the intermolecular hydrophobic interaction. Depending on the solution condition these types of aggregates may reverse back to their initial condition or not.

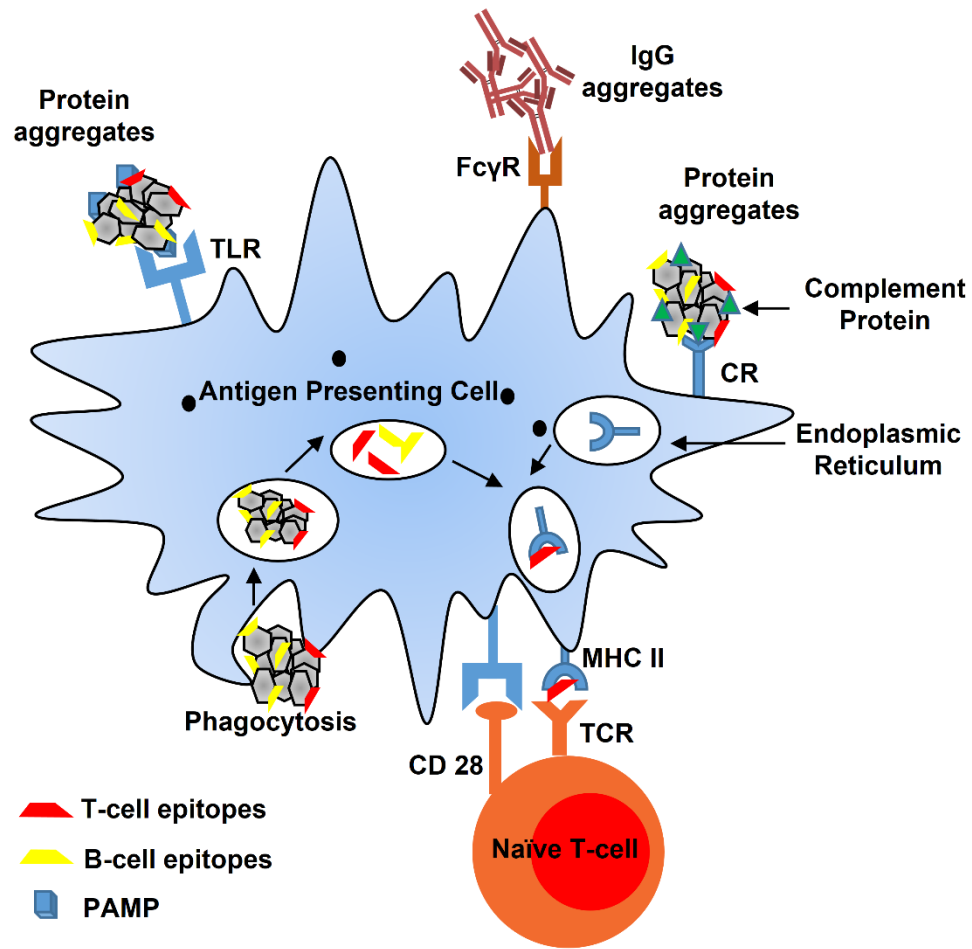


Figure 1.4: Aggregated protein antigen uptake by antigen-presenting cells (APCs). Protein antigen can be taken up by APC through receptor-mediated endocytosis or phagocytosis. Protein aggregates may be taken up by pattern recognition receptors, known as toll-like receptors (TLR). Antibody aggregates may be taken up by Fcγ receptors. (Figure adopted from Moussa et al., *J.Pharm.Sci.*, 2016)

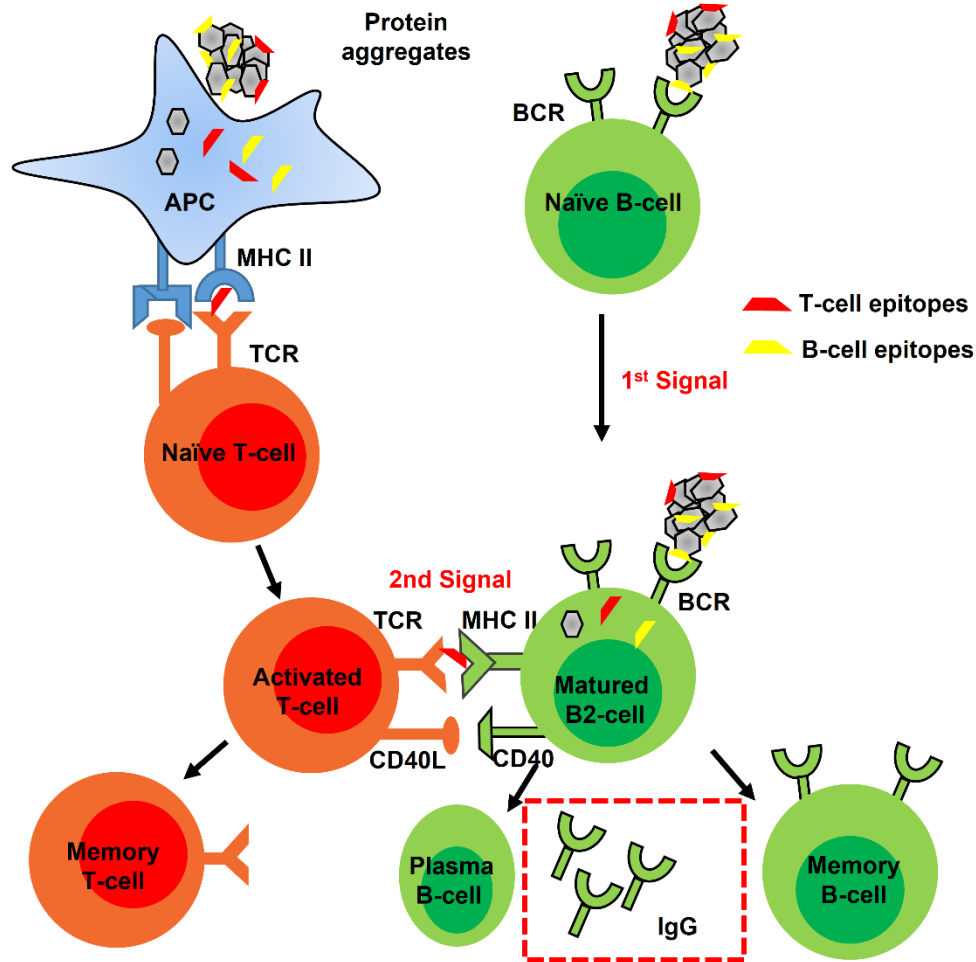


Figure 1.5: T-cell dependent B-cell activation pathway. Recognition of antigen by B-cell receptors (BCRs) provides the first signal for B-cells activation. The second signal comes from the T-cells that are activated by the same antigens. Finally, antigen-binding with TLRs on the B-cells provide the third signal for B-cells activation.

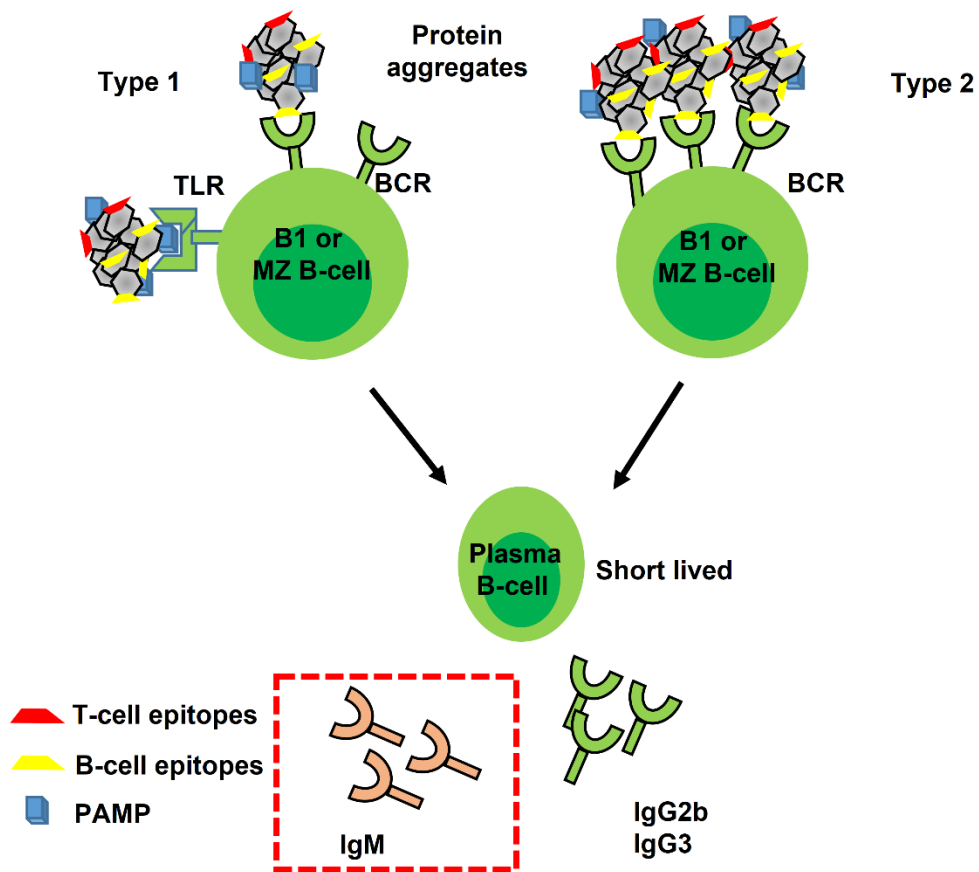


Figure1.6: T-cell independent B-cell activation. In T-cell independent pathway, B-cells are activated by cross-linking of BCRs. Particularly Type 2 antigens activate the B-cells by BCRs cross-linking. Type 1 antigen binds with both the BCRs and TLRs and thereby activates the B-cells without T-cells help, which mainly produces IgM and some class-switching to IgG. (Figure adopted from Moussa et al., *J.Pharm.Sci.*, 2016)

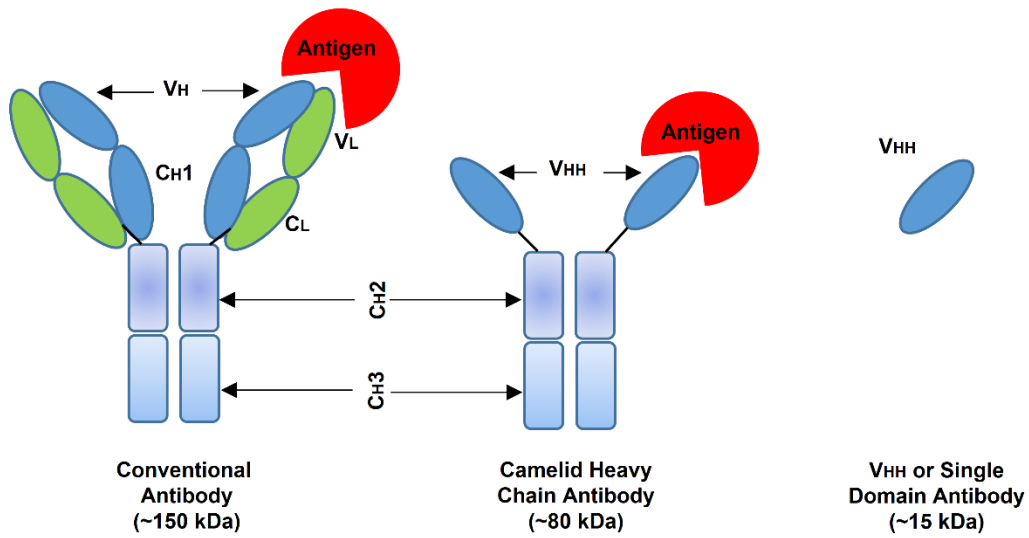


Figure1.7: Generation of Single Domain Antibody. *Camelidae* (camels, llamas and dromedaries) naturally produces heavy chain only antibody (HcAb). Unlike conventional mammalian IgG antibody, this class of antibody naturally devoids the light chain and CH1 domain, so-called heavy chain only antibody (HcAb).

Table 1.1 Classification of protein aggregates (Narhi, L.O., et al., Classification of protein aggregates. Journal of pharmaceutical sciences, 2012. **101**(2): p. 493-8)

Category	Classification
Size	<100 nm, 100–1000 nm (sub-micrometer), 1–100 :m, >100 :m
Reversibility	Reversible, irreversible, dissociable, dissociable under physiological conditions, dissociable under defined (list) conditions
Secondary/tertiary structure	Native, partially unfolded, unfolded, inherently disordered, Amyloid
Covalent modification	Cross-linked, reducible cross-link, nonreducible cross-link, intramolecular modification, oxidation, deamidation, no modification
Morphology	Number of monomeric subunits, aspect ratio, surface roughness, internal morphology, optical properties, translucent, heterogeneous

Chapter-2

The immunogenicity of an anti-EGFR single domain antibody (V_{HH}) is enhanced by misfolded amorphous aggregation but not by heat-induced aggregation

2.1.1 Introduction

Advances in biotechnology have paved the way for the use of recombinant therapeutic proteins [87]. However, protein aggregation may cause unwanted immunogenicity, which not only lessens the efficacy and safety of protein-based drugs [23] but can also hamper the function of endogenous proteins [5, 88]. This phenomenon has been coined ADAs (anti-drug antibodies) [89] and has been invoked in several clinical reports [90, 91]. For example, clinical studies have noticed that the risks of ADAs against human growth hormone (hGH) might be associated with the formation of aggregates [21, 22]. *In vivo* and *in vitro* immunological studies are also suggesting that protein aggregation can cause ADAs, as shown for human interferon-beta (INF- β) [92], factor VIII [93], and monoclonal antibodies (mAbs) [94].

Several studies have reported the relationship between aggregate's structural and biophysical properties and immunogenicity. For example, though native-like structural factor VIII aggregates were immunogenic [93], the aggregates of the fully unfolded factor VIII were less immunogenic [95]. On the other hand, natively functional aggregates (according to dot blotting) of IgG mAbs generated by freeze-thaw or shaking are not immunogenic, but they turn immunogenic upon chemical modification, such as oxidation [96]. Similarly, oxidation of rhIFN-1a aggregates increased its immunogenicity [97].

Recent studies have reported a relationship between the strength of the immune response and the aggregate's size [35, 37, 38] or the concentration [70], but some of the conclusions remain a matter of debate. For instance, *in vivo* mice experiments have shown that aggregates of mAb smaller than 100 nm sizes can generate a robust immune response [35]. Even few nanometers size protein's aggregates have been reported as immunogenic [40]. However, other studies reported that mAbs that formed submicron aggregates between 0.1 and 1 μ m were the most immunogenic [37]. Amorphous aggregates are thus not equally immunogenic, and beside the aggregate's size, other intertwined factors, such as the aggregate's biophysical and biochemical nature, appear to affect a protein's immunogenicity.

The biophysical nature of protein amorphous aggregates has attracted interest from a protein chemistry viewpoint [98]. It is now becoming increasingly clear that amorphous aggregates can display distinctive features besides their size: they can be formed by the association of natively folded, partially-folded, denatured or even misfolded proteins.

Furthermore, amorphous aggregates can be classified according to their sizes but also according to the reversibility of association, the formation of covalent intermolecular bonds, chemical modifications, and possibly morphologies [49, 62, 99]. The biophysical and biochemical nature of the aggregates will depend not only on the protein but also on the way they are generated [100] since aggregation can appear at any stage of the protein's production [101].

In this study, we used an anti-EGFR V_{HH} antibody (7D12) as a model of a therapeutic protein [102]. This is because several mutations in the epidermal growth factor receptor (EGFR) are associated with tumor formation [103], and full-length anti-EGFR mAbs, such as Panitumumab and Cetuximab [104], are being used in anti-cancer therapies. Due to its smaller size, anti-EGFR V_{HH} is expected to overcome factors limiting the action of the full-length anti-EGFR antibodies such as low tumor penetration, and above all, the high production cost [105]. In addition, ADAs has been reported for 1-5 % of patients using the full-length anti-EGFR mAbs [106]. On the other hand, because of its small size (MW < 15 kDa), anti-EGFR V_{HH}'s propensity to initiate an immune response is expected to be low, but this remains to be experimentally confirmed.

2.1.2 Aim and Objective

Here, we investigated the immunogenicity of a recombinant anti-EGFR V_{HH}, with particular emphasis on the relationship between its *in vivo* immunogenicity and the biophysical and biochemical nature of the aggregates in four different aggregated states: two heat-aggregated states incubated at 65 °C and 95 °C, referred to as V_{HH}-65 and V_{HH}-95, respectively, and two misfolded aggregated states, isolated during the refolding / purification process, referred to as V_{HH}-Ins and V_{HH}-Mis. Biophysical and biochemical properties of those V_{HH} aggregates were characterized using CD, DLS, SLS, size-exclusion chromatography and fluorescence spectroscopy. Further, we assessed their antigenic profile using Jcl:ICR mice model by evaluating the serum anti-V_{HH} IgG response using enzyme linked immunosorbent assay (ELISA).

2.2. Materials and Methods

2.2.1 Protein expression and purification

A synthetic gene encoding the anti-EGFR V_{HH} was cloned into a pAED4 vector [107] at the endonuclease *NdeI* and *EcoRI* sites and transformed into *E. coli* BL21 (DE3) pLysS cell line. The cells were grown in Luria Bertani (LB) medium at 37 °C, and protein expression was induced with 1 mM isopropyl β -d-1-thiogalactopyranoside (IPTG) when the optical density (OD) of the culture reached 0.6 at 590 nm. The *E. coli* cells were harvested 6 hours after the addition of IPTG by mild centrifugation. The cells were lysed by sonication, and the cell lysate was centrifuged at 8000 rpm, 4 °C for 20 min. The precipitate was again sonicated twice using a cell lysis wash buffer (50 mM Tris-HCl pH 8.0, 1 % NP-40 (v/v), 0.1 % deoxycholic acid (w/v) and 5 mM EDTA).

Inclusion bodies collected by sonication were dissolved in 6 M Guanidine hydrochloride, 10 mM Tris-HCl, pH 8.5 (hereafter, **buffer A**), containing 10 mM dithiothreitol (DTT). After centrifugation at 8000 rpm, 4 °C for 20 min and filtration through a 0.2 μ m filter, the samples were loaded onto an open Ni-NTA column (Qiagen, Germany). Subsequently, the column was washed thrice with the wash buffer (6 M urea, 10 mM Tris-HCl pH 8.5, 0.5 M NaCl), and V_{HH} proteins were eluted with the elution buffer (6 M urea, 10 mM Tris-HCl pH 8.5, 0.5 M NaCl, 0.5 M imidazole). After 15 hours of oxidation at room temperature, urea was removed by overnight dialysis against 10 mM Tris-HCl (pH 8.5) at 4 °C. The sample was then centrifuged at 8000 rpm, 4 °C for 20 min, and the supernatant was separated from the precipitate. Finally, the native proteins were purified from the supernatant fraction using a cation-exchange chromatography (Gigacap-s-650 M, Tosoh Bioscience, Tokyo, Japan), and the protein identities were confirmed by TOF/TOFTM 5800 (SCIEX, USA) (**Figure 2.1**). The purified native protein dissolved in Milli-Q (MQ) water was stored at -30 °C as a stock solution. The precipitate fraction was further used for the generation of V_{HH} -Ins.

2.2.2 Generation of the aggregates

V_{HH} -Ins: The precipitate fraction was dissolved in **buffer A**, and a second round of overnight dialysis was performed, and the sample was centrifuged in the same way as described above. The precipitate of the second dialysis was collected, dissolved again in **buffer A**, dialyzed, and centrifuged for the third time. Finally, the precipitate of the third dialysis was dissolved

in 6 M guanidine hydrochloride with 10 % acetic acid solution, followed by overnight dialysis against Milli-Q water at 4 °C with a four-time exchange of the external solution. V_{HH} -Ins was soluble in MQ-water and stored at -30 °C and kept as a stock solution. The aggregated samples were prepared just before the experiments by adding MQ-water and 5X PBS to the protein stock solution at a final protein concentration of 0.3 mg/mL in 1X PBS (137 mM NaCl, 2.7 mM KCl, 10 mM Na_2HPO_4 and 1.8 mM KH_2PO_4 , pH 7.4).

V_{HH} -Mis: The native anti-EGFR V_{HH} protein was first dissolved in **buffer A** with 0.5 M DTT. After 2 hours of incubation at room temperature, the sample underwent dialysis overnight against MQ water at 4 °C. Afterward, the sample was centrifuged, and the precipitate was dissolved in **buffer A** and oxidized for 15 hours. After guanidine hydrochloride removal by overnight dialysis against 10 mM Tris-HCl (pH 8.5), the precipitate was collected by centrifugation. The precipitate was again dissolved in **buffer A** and the second round of dialysis and centrifugation was performed, as described above. The precipitate of the second dialysis was collected, followed by a third round of dialysis and centrifugation. Finally, the precipitate of the third dialysis was dissolved in 6 M guanidine hydrochloride with 10 % acetic acid solution, followed by overnight dialysis against MQ water at 4 °C (the external solution was changed four times). The V_{HH} -Mis stock solution dissolved in MQ-water was stored at -30 °C. The aggregates were generated in the same way as for V_{HH} -Ins. A graphical representation of the V_{HH} -Ins and V_{HH} -Mis purification scheme is available as **Figure 2.2**.

V_{HH} -65 and V_{HH} -95: The purified native anti-EGFR V_{HH} protein was diluted to a concentration of 0.3 mg/mL in PBS (immunization buffer) and incubated at 65 °C for 45 min in a static heating block (V_{HH} -65). For generating the fully denatured aggregates, 0.4 mg/mL of proteins in PBS were heated at 95 °C for 110 min as V_{HH} are highly heat stable [108], and the precipitated proteins were collected after mild centrifugation (4000 ×g, 25 °C for 10 min). The supernatant concentration was measured using Nanodrop (Nanodrop-2000, Thermo Fisher Scientific, USA), and the precipitate was resuspended in a fresh PBS at a concentration of 0.3 mg/mL. Finally, the sample was passed through a 26 gauge syringe needle to produce a homogenous solution of aggregates (V_{HH} -95).

2.2.3 Dynamic Light Scattering (DLS) and Static Light Scattering (SLS)

DLS samples were prepared by diluting the protein stock solutions to 0.3 mg/mL in 20 mM Na-acetate buffer (pH 4.7) and PBS (pH 7.4). Afterward, 100 μ L aliquot in a polystyrene cuvette was used for DLS measurement at 37 °C with automatic attenuation, run duration, and scan numbers. Dynamic light scattering (DLS) was measured using a Zetasizer Nano-S system (Malvern, UK). The aggregate's size distributions were determined by computing the mean Z-average (Z_{ave}) of the hydrodynamic radius and polydispersity index (PDI). The hydrodynamic radius (R_h) was obtained from the size distribution using the Stokes-Einstein equation and averaged over three individual measurements.

SLS was measured under the same conditions at a wavelength of 600 nm and 37 °C with an FP-8500 spectrofluorometer (JASCO, Tokyo, Japan) using a micro-cuvette with an optical path length of 3 mm. The final spectra were obtained by subtracting the corresponding buffer spectrum.

2.2.4 High-Performance Size Exclusion Chromatography (HP-SEC)

The formation of intermolecular SS bonds was investigated by high performance size exclusion chromatography (HP-SEC) using a Shimadzu LC-20AD HPLC equipment (SHIMADZU CORP, Japan). All V_{HH} samples were prepared at a concentration of 0.1 mg/mL in PBS (pH 7.4) containing 6 M guanidine hydrochloride. For the reduced state, 0.5 M dithiothreitol (DTT) was used to cleave the disulfide bond. Before analysis, the samples were centrifuged (20,000 \times g, 20 min, 4 °C) and filtered with a 0.2-micron filter. 20 μ L of the sample was loaded onto a TSK Gel 2000 SWXL column (Tosoh Bioscience, Tokyo, Japan) using PBS (pH 7.4) containing 6 M guanidine hydrochloride as a mobile phase at a flow of 0.5 mL/min. The protein was detected by a fluorescence detector (RF-20A, SHIMADZU CORP, Japan) using an excitation wavelength of 295 nm and an emission wavelength of 345 nm for tryptophan. For experiments under the reduced conditions, the mobile phase was supplemented with 10 mM of DTT.

2.2.5 Spectroscopic measurements

Far-UV circular dichroism (CD) spectroscopy measurements were performed on a JASCO J-820 spectropolarimeter (JASCO, Tokyo, Japan). The protein concentrations of all samples

were fixed to 0.3 mg/mL (20 μ M) in 20 mM Na-acetate buffer (pH 4.7) and PBS (pH 7.4). 300 μ L of the protein solution was placed in a 1 mm path-length quartz cuvette, and the spectra were collected in a continuous scanning mode from 260 to 200 nm wavelength. The spectral baseline was measured for each sample and subtracted to obtain the final spectrum. For each sample, the measurement was repeated three times. The secondary structure content was calculated by BeStSel [109].

Samples for tryptophan and 8-anilino-1-naphthalene-sulfonic acid (ANS) fluorescence measurements were prepared in the same way as for the CD measurements at a protein concentration of 0.3 mg/mL. For ANS fluorescence measurements, ANS was added to the solution at a final concentration of 20 μ M and incubated at 25 °C for 5 min in the dark before measurement [110, 111]. The fluorescence measurements were performed on FP-8500 spectrofluorometer (JASCO, Tokyo, Japan) and using a glass cuvette containing 200 μ L of the sample at 37 °C. The tryptophan excitation and emission wavelength were set to, respectively, 295 nm and 345 nm, and the ANS fluorescence was measured with excitation and emission set to 380 nm and 480 nm, respectively.

2.2.6 Binding activity by Surface Plasmon Resonance (SPR)

The binding affinity of the anti-EGFR V_{HH} to the extracellular domain of human EGFR (Abcam, UK) was carried out by surface plasmon resonance (SPR), as previously reported [112, 113]. In short, V_{HH} of different concentrations was passed over a CM5 sensor chip (Biacore 2000, GE Healthcare, USA), where EGFR (20 μ g/mL) was immobilized using amine coupling chemistry according to the manufacturer's guidance. All measurements were performed at a flow rate of 30 μ L/min in 10 mM HBS-EP buffer pH 7.4, (10 mM HEPES, 150 mM NaCl, 3 mM EDTA and 0.005 % surfactant P20) at 20 °C. We used V_{HH} concentrations between 6.0 and 0.046 μ g/mL. Data were fitted using the BIACORE evaluation software version 4.1, based on a 1:1 Langmuir binding model.

2.2.7 Mice immunization and measurement of serum IgG level

Young 4-week old adult female mice (Jcl:ICR; CLEA, Japan) were used in all experiments. The mice were accommodated on sterilized wood bedding at an ambient temperature maintained at 22 ± 0.5 °C and relative humidity around 47 ± 8 % with a natural half-day light-

dark cycle. In total, 30 mice were divided into six groups ($n=5$). Each group was treated with a different protein formulation, and a control group was treated with PBS only. 100 μL of 0.3 mg/mL V_{HH} protein (monomeric or aggregate) in PBS was injected subcutaneously once a week for up to six weeks. For monitoring the ADA (IgG) generation, tail-bleed (TB) samples were collected three days after each round of immunization. All of the experiments were performed in compliance with the Tokyo University of Agriculture and Technology (TUAT) and Japanese governmental regulations on animal experimentation.

The generation of serum IgG antibodies was measured by standard sandwich ELISA method. For all samples, 96-well microtiter plates (TPP techno plastic product, Switzerland) were coated with 100 μL of 2.5 $\mu\text{g}/\text{mL}$ native or misfolded anti-EGFR V_{HH} in PBS (pH 7.4) and incubated at 25 $^{\circ}\text{C}$ overnight. Unbound proteins were removed by washing with PBS, and the plates were blocked with 1 % BSA at 37 $^{\circ}\text{C}$ for 45 min. Afterward, 150 μL of 50 times diluted serum samples were added onto the 1st well and followed by 3-fold serial dilution in subsequent wells containing 0.1 % BSA-PBS. After incubation at 37 $^{\circ}\text{C}$ for 2 hours and washing with PBS-0.05 % tween-20, 100 $\mu\text{L}/\text{well}$ of goat anti-mouse Fc-specific HRP-conjugated antibody (Thermo Fisher Scientific, USA) was added and incubated again at 37 $^{\circ}\text{C}$ for 90 min. Unbound conjugates were removed by thoroughly washing with PBS-0.05 % tween 20, and OPD (o-phenylenediamine dihydrochloride) was added to the plates, which were incubated for 20 min for coloring. The reaction was stopped with 1 N sulfuric acid, and the plates were placed in a microplate reader for measuring the absorbance at 492 nm (SH-9000 Lab, Hitachi High-Tech Science, Japan). Finally, we analyzed the data by a power fitting of OD 492 nm versus the reciprocal dilution of the antisera and used a cutoff of OD 492 nm = 0.1 above the background value to calculate the antibody titers. A previously developed anti-3ED3 (Dengue 3 domain 3) anti-sera was used in all ELISA experiments as a positive control.

2.3. Results

2.3.1 Structural characterization

We measured the biophysical properties of V_{HH} in two buffers (Na-acetate buffer, pH 4.7 and PBS, pH 7.4) because the misfolded V_{HHS} (V_{HH} -Ins and V_{HH} -Mis) were insoluble in PBS and soluble only at acidic pH, which enabled spectroscopic measurements. The final samples used in all of the experiments were prepared by adding MQ-water and 1M Na-acetate or 5X PBS stock buffer to the protein stock solution at a final protein concentration of 0.3 mg/mL in either 20 mM Na-acetate buffer (pH 4.7) or 1X PBS (pH 7.4). The immunization experiments were all carried out using proteins in 1X PBS.

Secondary structure: The secondary structure content was determined by far-UV CD (200–260 nm). Both at pHs 4.7 and 7.4, the secondary structure content of the native V_{HH} was typical of a β -sheeted protein in line with the X-ray crystal structure (PDB: 4KRL) (**Figure 2.3 A, B** and **Table 2.1**). In addition, the thermal denaturation of V_{HH} was cooperative and fully reversible, indicating a well-packed natively folded structure as reported previously [112] (**Figure 2.4**). By contrast, both the misfolded (V_{HH} -Ins and V_{HH} -Mis) and the 95 °C-incubated V_{HH} -95 were aggregated at pH 7.4, and CD could not be measured. At pH 4.7, where V_{HH} -Ins and V_{HH} -Mis could be solubilized, their spectra indicated a high helical content (**Figure 2.3 A** and **Table 2.1**), but no thermal denaturation was observed (**Figure 2.4**). Finally, the CD spectrum of V_{HH} -65 at pH 7.4 was essentially the same as that of the native V_{HH} .

Tertiary structure: We assessed the tertiary structure of the V_{HHS} using tryptophan and ANS fluorescence. The tryptophan fluorescence of the natively folded V_{HH} showed strong intensity with an emission maximum at 345 nm, whereas the V_{HH} -Ins and V_{HH} -Mis emission was twice and thrice weaker than that of the native V_{HH} , and with a blue shift of 4 nm, possibly reflecting a more hydrophobic environment resulting from the aggregation (**Figure 2.5** and **Table 2.2**). This suggested that the tertiary structure of the two misfolded V_{HH} formulations were non-native, in line with the above far-UV CD results. The emission spectrum of V_{HH} -65 at pH 7.4 was slightly weaker than that of the native V_{HH} (no blue shift), whereas that of V_{HH} -95 was significantly weaker with a 4 nm-blue shift as observed for V_{HH} -Ins and V_{HH} -Mis.

Next, we used ANS, which binds to exposed hydrophobic pockets and gives a strong fluorescence signal, to probe the nature of the tertiary structure [110]. The ANS fluorescence intensity of V_{HH} -Ins and V_{HH} -Mis was significantly stronger than that of the native V_{HH} (**Figure 2.6** and **Table 2.2**), suggesting that the proteins associated in a loosely-packed oligomer similar to a molten-globule [114] but with secondary structures distinct from the native one (**Table 2.1**). V_{HH} -65 showed a marginal intensity increase, whereas V_{HH} -95's intensity was stronger than that of the native V_{HH} but markedly weaker than the misfolded V_{HH} . Altogether, the tryptophan and ANS fluorescence intensity (at PBS, pH 7.4) ranked, respectively, as follows: native V_{HH} > V_{HH} -65 > misfolded (V_{HH} -Ins and V_{HH} -Mis) > V_{HH} -95, and misfolded (V_{HH} -Ins and V_{HH} -Mis) > V_{HH} -95 > V_{HH} -65 > native V_{HH} .

2.3.2 Aggregate sizes and intermolecular SS bonds

We measured the sizes of the aggregates and the degree of aggregation by dynamic and static light scattering (DLS and SLS), respectively. The Zave hydrodynamic radius of the native V_{HH} at pH 4.7 and 7.4 were, respectively, 2.07 ± 0.49 nm (PDI: 0.24 ± 0.06) and 3.54 ± 0.19 nm (PDI: 0.22 ± 0.07) as expected for a monomeric V_{HH} (**Figure 2.7** and **Table 2.3**). In contrast, the Zave of V_{HH} -Ins and V_{HH} -Mis was above 1 μ m at pH 7.4. The Zave of V_{HH} -95 at pH 7.4 was 1722 ± 179 nm (PDI: 0.49 ± 0.09), and that of V_{HH} -65 was slightly smaller at 771.3 ± 26.30 nm (PDI: 0.15 ± 0.06). These aggregation trends were confirmed by static light scattering, which increases along with the particle size [115]. The scattering intensity of the native V_{HH} was minimal, that of V_{HH} -65 was marginally stronger and, those of the misfolded samples (V_{HH} -Ins and V_{HH} -Mis) and that of V_{HH} -95 were the strongest (**Figure 2.8** and **Table 2.3**).

The presence of intermolecular SS bonds was assessed by running the HP-SEC under denaturing conditions with and without reducing agent, dithiothreitol (DTT). Under both conditions, the native V_{HH} and heat aggregated V_{HHS} (V_{HH} -65 and V_{HH} -95) showed a single peak at around 15 min, corresponding to the molecular weight of the monomeric V_{HH} (~15 kDa) (**Figure 2.9 A and B**). On the other hand, the non-reduced V_{HH} -Ins and V_{HH} -Mis showed high molecular weight peaks, which essentially disappeared under the reducing conditions indicating the presence of intermolecular disulfide bonds in the unreduced V_{HH} -Ins and V_{HH} -Mis samples (**Figure 2.9 A and B**).

2.3.3 Binding activity

The binding activities of the V_{HH} to EGFR were measured using surface plasmon resonance (SPR). In line with previous reports [102], the native V_{HH} bound to EGFR in a concentration-dependent manner, further confirming the natively folded nature of our native V_{HH} (**Figure 2.10 A**). The 65 °C incubated V_{HH-65} was weakly active, suggesting that a fraction of the V_{HH-65} are natively folded as suggested by CD (**Figure 2.10 B**) (A rough estimate based on anti-parallel beta-sheet content suggests that over 90 % of V_{HH-65} is folded; (**Table 2.1**)). Contrastingly, the V_{HH-Ins} , V_{HH-Mis} and V_{HH-95} had no binding activity confirming that they are fully unfolded or misfolded (**Figure 2.10 C, D and E**).

2.3.4 Effect of aggregate types on immune response

The level of serum's anti- V_{HH} IgG (after 6 weeks of injection) measured by ELISA using the native V_{HH} as the coating antigen (**Figure 2.11 A**) showed that the native V_{HH} was scarcely immunogenic. The heat 65 °C incubated V_{HH-65} induced a moderate response (for three mice out of five mice). No immune response was observed for V_{HH-95} , even after six injections (for four mice out of five mice). However, we observed that the misfolded V_{HHS} were strongly immunogenic, even though the aggregates formed by the misfolded V_{HHS} (V_{HH-Ins} and V_{HH-Mis}) as well as the heat-induced V_{HH-95} had $R_h > 1$ micron according to DLS. Indeed, all of the five mice injected with V_{HH-Mis} responded unambiguously and in V_{HH-Ins} three out of five mice showed a strong anti- V_{HH} IgG titer.

2.4. Discussion

There are growing concerns and evidence that the amorphous aggregation of therapeutic proteins can cause unwanted immunogenicity [57, 116, 117]. Amorphous aggregates can exhibit, besides their sizes, various biophysical attributes: the characteristics of the aggregates such as conformation, level of chemical modifications, molecular orientation, and possibly morphology, which can affect the immunogenicity of a protein [118].

We thus sought to investigate the biophysical nature of the amorphous aggregates that increase the immunogenicity of the therapeutic protein. To this end, we characterized the biophysical properties and assessed the immunogenicity of V_{HH} in four types of amorphous aggregates: V_{HH} expressed in the inclusion body (V_{HH} -Ins); a misfolded aggregate produced by miss-shuffling the SS bonds of the HPLC-purified native V_{HH} (V_{HH} -Mis), which was used for mimicking the inclusion body fraction in a purified formulation; and two aggregates produced by heat denaturation at 65 and 95 °C and maintaining the native intramolecular SS bonds (V_{HH} -65 and V_{HH} -95, respectively).

The native V_{HH} in a monomeric and active form was barely immunogenic, even after six injections. By contrast, V_{HH} -Ins and V_{HH} -Mis, which formed intermolecular SS bonds and had secondary structure contents clearly distinct from that of the native V_{HH} (**Figure 2.3 A and B**), were highly immunogenic. Tryptophan and ANS fluorescence suggested that V_{HH} -Ins and V_{HH} -Mis formed a loosely-packed, hydrophobic, globular aggregates (**Figure 2.5, 2.6 and Table 2.2**) [110, 119]. Their aggregates were soluble at acidic pH (pH 4.7) but formed large aggregates in PBS buffer (pH 7.4) (**Table 2.3**). The high immunogenicity of V_{HH} -Ins and V_{HH} -Mis appears to be related to the scrambling of disulfide bonds. However, other factors such as side-chain oxidation [120] and the particle's size distribution may influence their immunogenicity. In particular, aggregate's size has been reported as an important factor contributing to the immunogenicity of a protein [118] but here we can only provide a qualitative description of such effect based on the samples' photographs (**Figure 2.13**).

Despite the presence of large aggregates and an aggregation propensity similar to that of misfolded V_{HH} , strikingly, V_{HH} -95 was not able to induce any antibody response. V_{HH} -95 was fully unfolded as assessed by CD, fluorescence, and SPR, and it is possible that the epitopes

were fully denatured. Finally, the higher PDI value of the V_{HH}-95 formulation indicated the heterogeneous nature of the aggregates' sizes (**Table 2.3**).

The heat 65 °C aggregates (V_{HH}-65) retained a native-like secondary and tertiary structure according to CD and fluorescence in line with the high (80 %) retention of its binding activity to EGFR (**Figure 2.10 B**), and it showed a higher immune response than the native V_{HH} and the heat-denatured aggregates (V_{HH}-95). In addition, let us note that V_{HH}-65 contains aggregates with $R_h \sim 770$ nm according to DLS and 80% of the proteins are monomer according to HP-SEC (**Figure 2.14** and **Table 2.3**). These results suggest that native-like aggregates having the same secondary structure content as the native V_{HH}, are responsible for increasing its immunogenicity. Such observation would agree with native-like aggregates of recombinant factor VIII being immunogenic [93] or with our previous experiments with proteins oligomerized into partially denatured aggregates using Isoleucine tag [40, 121].

Interestingly, ELISA experiments, in which we used the misfolded V_{HH} (V_{HH}-Ins) as a coating antigen indicated results similar to those obtained using the native V_{HH} as a coating antigen (**Figure 2.11 B**). This observation is not well explained from a protein structural viewpoint, because the conformation of the misfolded sample is quite different from the native one [122-125], as corroborated by the low content of anti-parallel β -sheets in the misfolded V_{HH}S, which turned into parallel β -sheets, α -helices, and loops as assessed by CD and BeStSel (**Table 2.1**). Though speculative, one rationale for our observation would be that the misfolded protein conserves a native-like epitope structure. A second hypothesis would be that the native V_{HH} denatures when plated on the ELISA plates. To this regard, the long term immunological experiments where the misfolded V_{HH} produced a long term memory (i.e. IgG as well) against the native V_{HH} (**Figure 2.12**) suggests that antibodies were generated against natively structured epitopes supporting the first hypothesis.

Finally, for the purpose of discussion, let us recall some possible molecular mechanisms that might stand behind the immunogenicity increase through the aggregation of a protein. It is now widely recognized that aggregation mediated immune response may occur either through a T cell-dependent or independent pathway [116, 126]. T cell-independent activation of B cells requires a high concentration of antigens leading to B cell receptor (BCR) cross-linkage that activates the B cells but without generating immunological memory [116]. Similarly, in

a T cell-dependent pathway, which is most likely in our case because of the long term immunological memory (**Figure 2.12**), aggregates will also induce a BCR cross-linkage, which will provide the first signal for activating the B cells, the second one being T Cell recognition [116, 127]. Additionally, it has recently been shown that aggregated antibodies may activate dendritic cells, which in turn induces a T cell-dependent activation of B cells [94], such scheme may provide a further rationale for the production of IgG and of the long term immunological memory. To date, we note that the generation of long term memory by aggregated proteins may not occur in transgenic mice tolerant for the antigen protein, as reported for rhINF- β [128].

2.5. Conclusions

Accidental aggregation of therapeutic proteins is the focus of much attention by drug regulatory agencies and biopharmaceutical companies as it may cause severe side effects in the form of undesired immunogenicity and the generation of ADAs. Here, we systematically showed that immunogenicity of a protein's aggregate with hydrodynamic radii of $\sim 2 \mu\text{m}$ (according to DLS) will exhibit different immunogenicities depending on their biochemical (intermolecular SS bonds) and biophysical nature (folded/unfolded). As such, this study is expected to pave the way toward a deeper understanding of the mechanisms underlying the immunogenic response associated with the aggregation of therapeutic proteins.

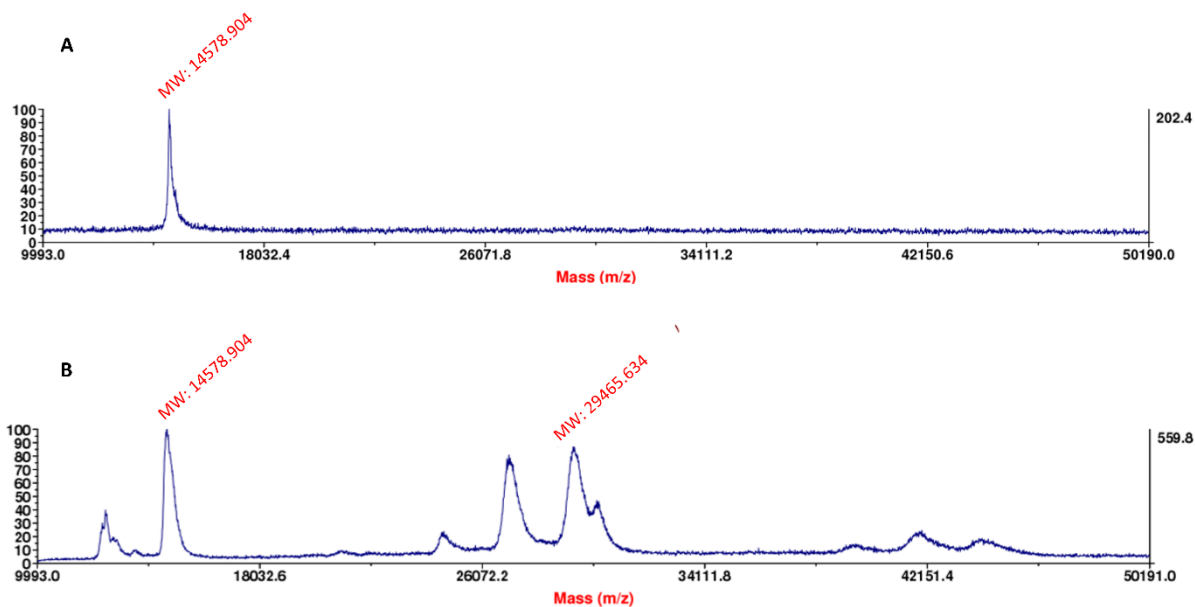


Figure 2.1: Molecular weight by MALDI-TOF. Protein identities were confirmed by MALDI-TOF mass spectroscopy using a TOF/TOFTM 5800 machine (SCIEX) **(A)** Native V_{HH} and **(B)** V_{HH} -Ins. V_{HH} -65, V_{HH} -95, and V_{HH} -Mis were derived from the native V_{HH} .

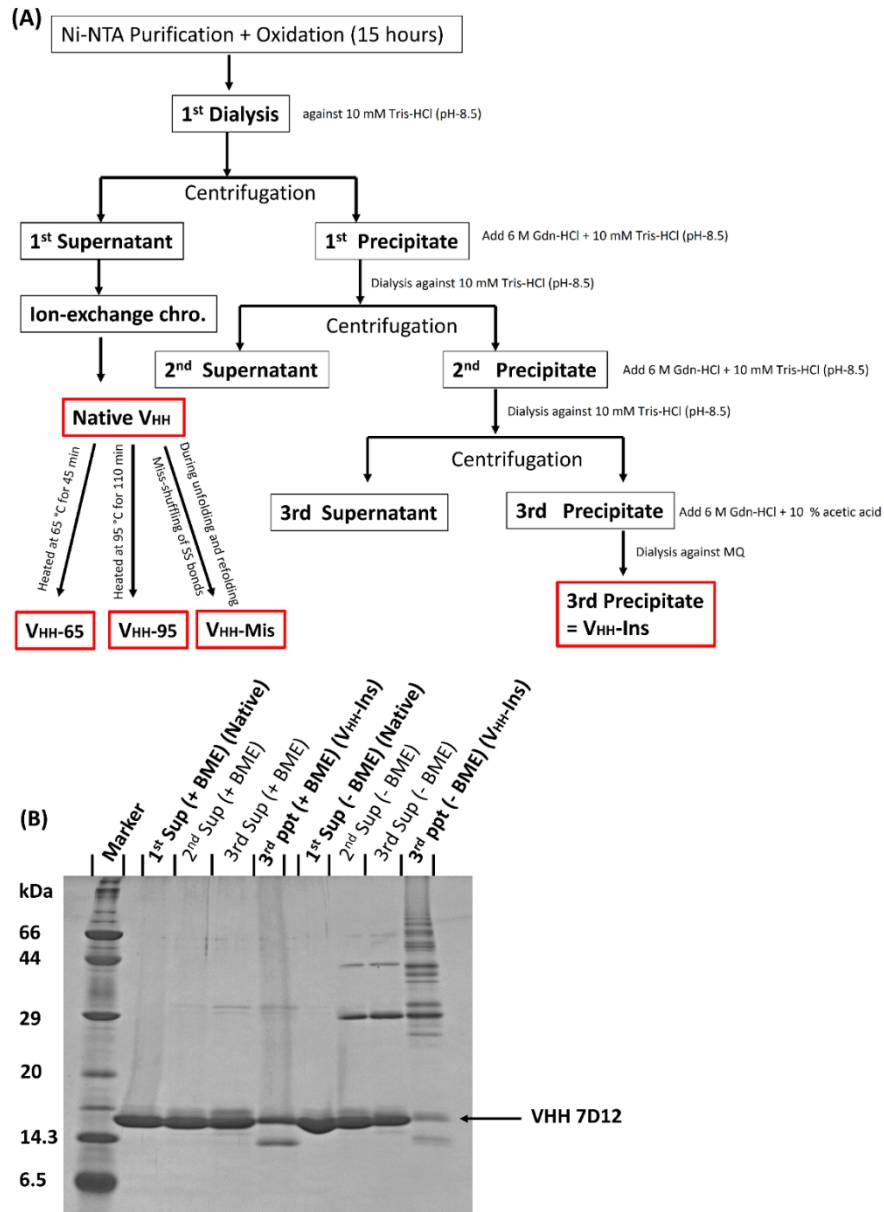


Figure 2.2: Schematics and gel analysis of the V_{HH} preparation. (A) Schematic of the V_{HH} fractions. The V_{HH} fractions used in the experiments are boxed in red. As in previous reports, the native V_{HH} was isolated from the 1st supernatant and purified by ion-exchange chromatography. V_{HH}-Ins is the precipitate obtained after three rounds of precipitation. (B) Sodium dodecyl sulfate-polyacrylamide gel electrophoresis (SDS-PAGE) of the fractions. +BME and -BME indicate, respectively, the presence (reducing condition) and absence (non-reducing condition) of beta-mercaptoethanol in the loading buffer.

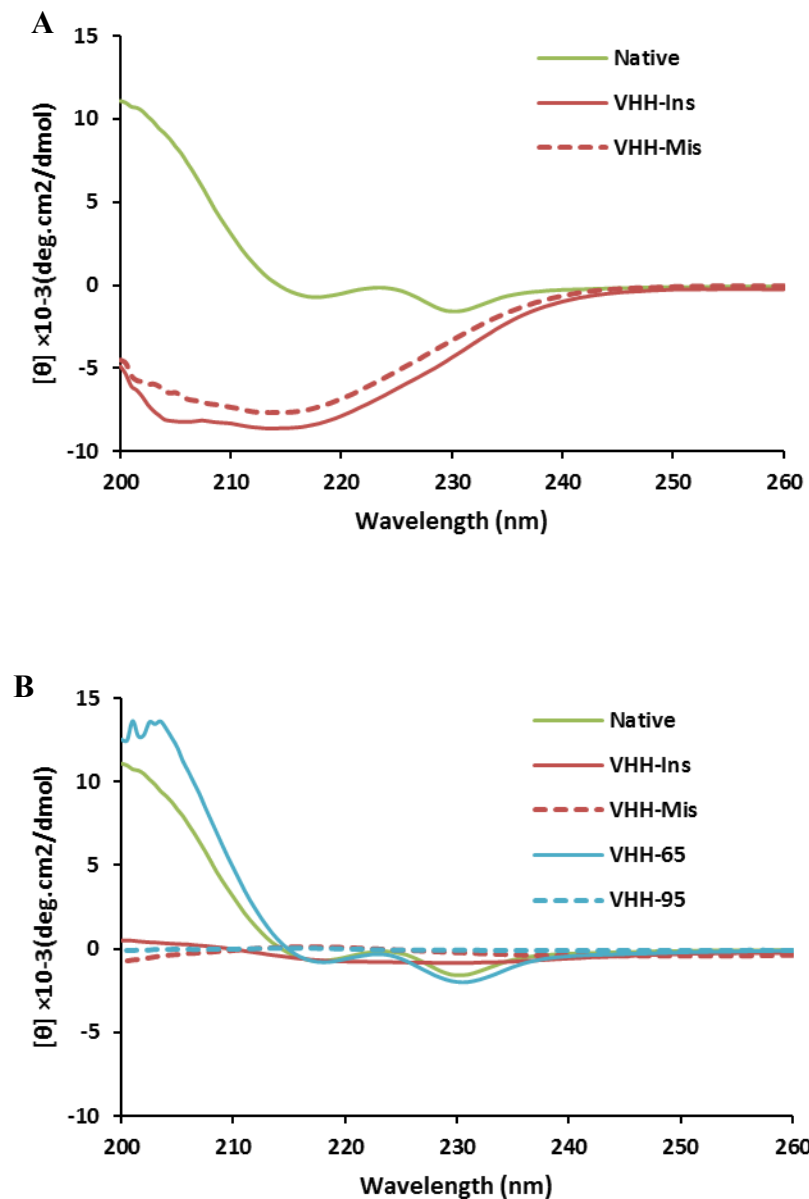


Figure 2.3: Secondary structure content V_{HH} formulations: The secondary structures were analyzed using far-UV CD region (200–260 nm) at a protein concentration of 0.3 mg/mL at 37 °C in 20 mM Na-acetate buffer, pH 4.7 (**A**), and in PBS, pH 7.4 (**B**). Three accumulations were taken for each measurement and the final spectra were obtained by subtracting the corresponding buffer spectrum. Line symbols are explained within the panels.

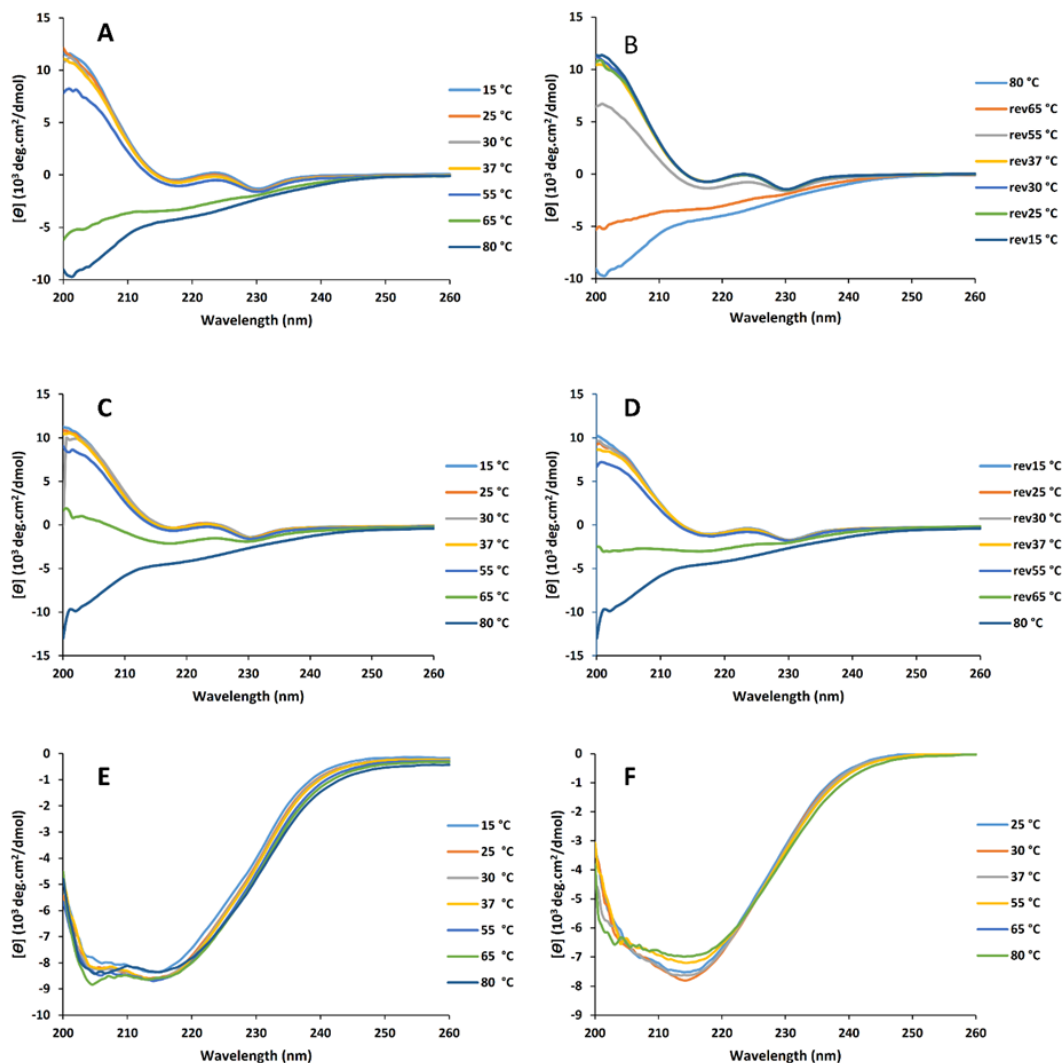


Figure 2.4: Circular dichroism (CD) spectra of native and misfolded V_{HH} . Protein samples were prepared at a concentration of 0.3 mg/mL in 20 mM Na-acetate buffer (pH 4.7) and PBS (pH 7.4). CD spectrum of the native protein (A) in acetate buffer at temperatures from 15 °C to 80 °C (B) reversibility measurement by cooling from 80 °C to 15 °C in acetate buffer (C) in PBS, from 15 °C to 80 °C and (D) reversibility by cooling from 80 °C back to 15 °C, measured in PBS. CD spectrum (E) of V_{HH} -Ins in acetate buffer measured at temperatures from 15 °C to 80 °C (F) V_{HH} -Mis in acetate buffer from 15 °C to 80 °C. Line symbols are explained within the panels. At both buffers, the thermal denaturation of native V_{HH} was cooperative and fully reversible, up to 80 °C as measured, indicating a well-packed natively folded structure. No thermal denaturation was observed for misfolded V_{HH} (V_{HH} -Ins and V_{HH} -Mis) according to CD at 222.

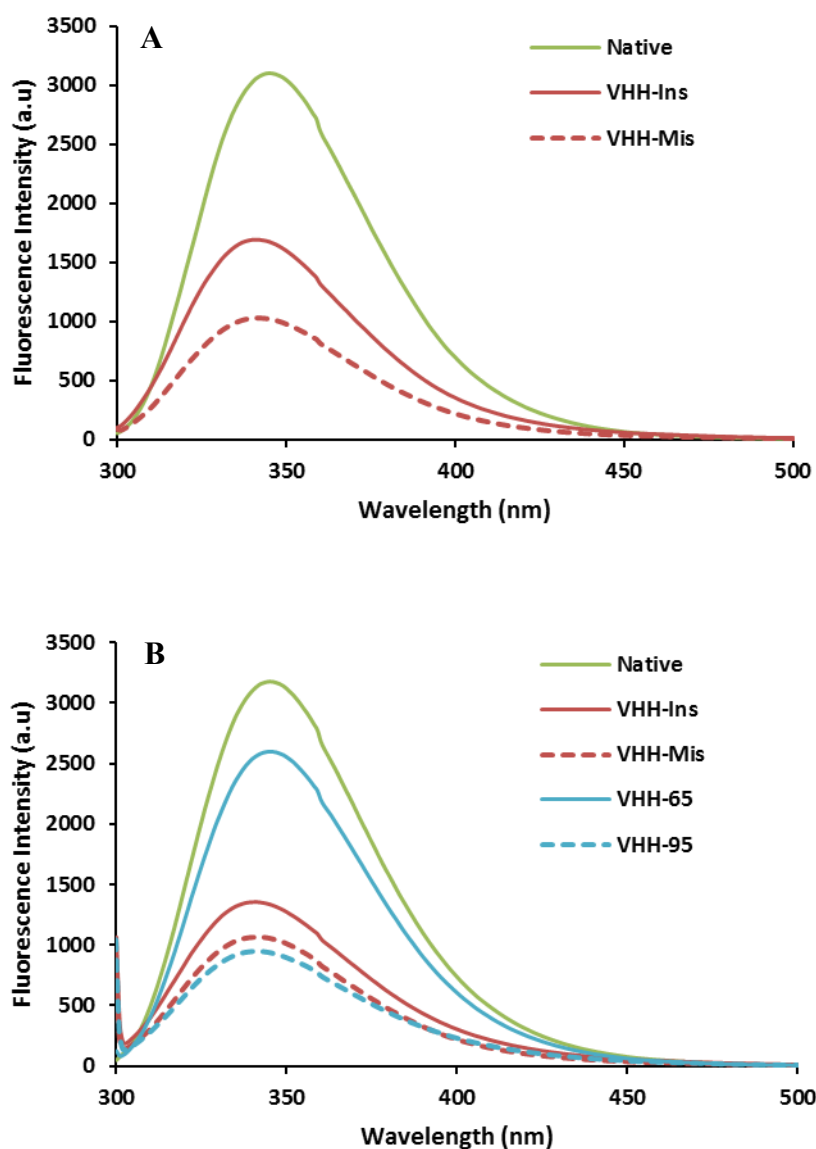


Figure 2.5 Characterization of the tertiary structures by tryptophan. Tryptophan fluorescence intensity were measured at a protein concentration of 0.3 mg/mL at 37 °C. Tryptophan fluorescence intensity spectra **(A)** in 20 mM Na-acetate buffer, pH 4.7, **(B)** in PBS, pH 7.4. Three accumulations were taken for each measurement and the final spectra were obtained by subtracting the corresponding buffer spectrum. Line symbols are explained within the panels.

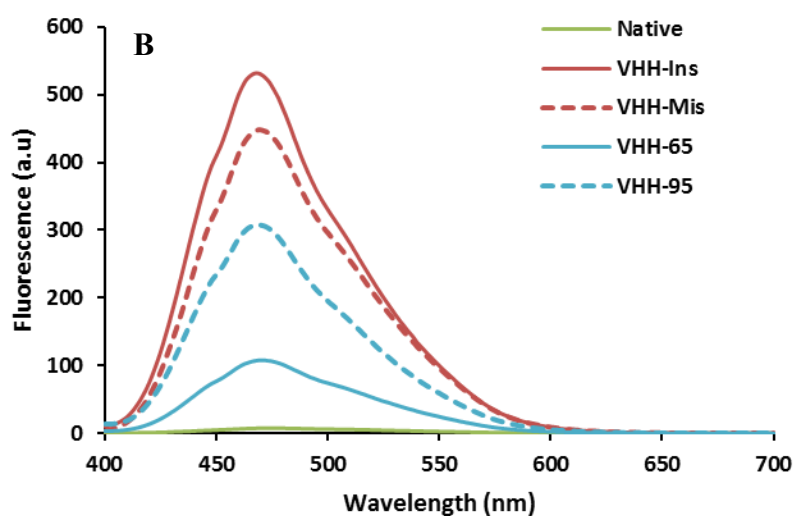
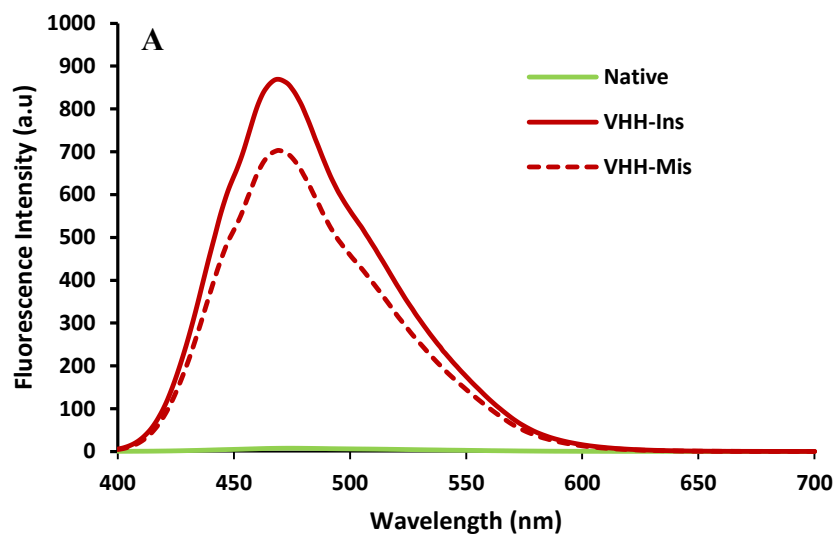


Figure 2.6: Characterization of the tertiary structures by ANS. 8-anilino-1-naphthalene-sulfonic acid (ANS) fluorescence intensity were measured at a protein concentration of 0.3 mg/mL at 37 °C. ANS fluorescence intensity spectra **(A)** in 20 mM Na-acetate buffer, pH 4.7, **(B)** in PBS, pH 7.4. Three accumulations were taken for each measurement and the final spectra were obtained by subtracting the corresponding buffer spectrum. Line symbols are explained within the panels.

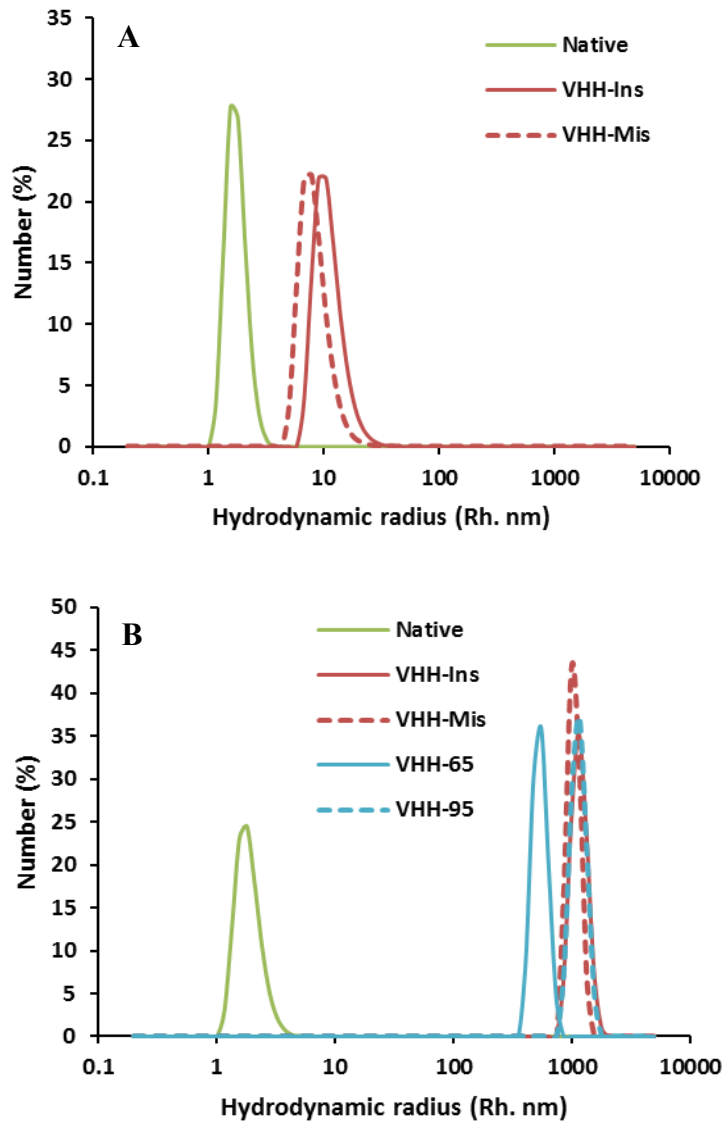


Figure 2.7 Aggregate's sizes by Dynamic Light Scattering (DLS). DLS measurements were performed at a protein concentration of 0.3 mg/mL at 37 °C. DLS spectra of the size distribution number (%) (A) in 20 mM Na-acetate buffer, pH 4.7 and (B) in PBS, pH 7.4. Line symbols are explained within the panels.

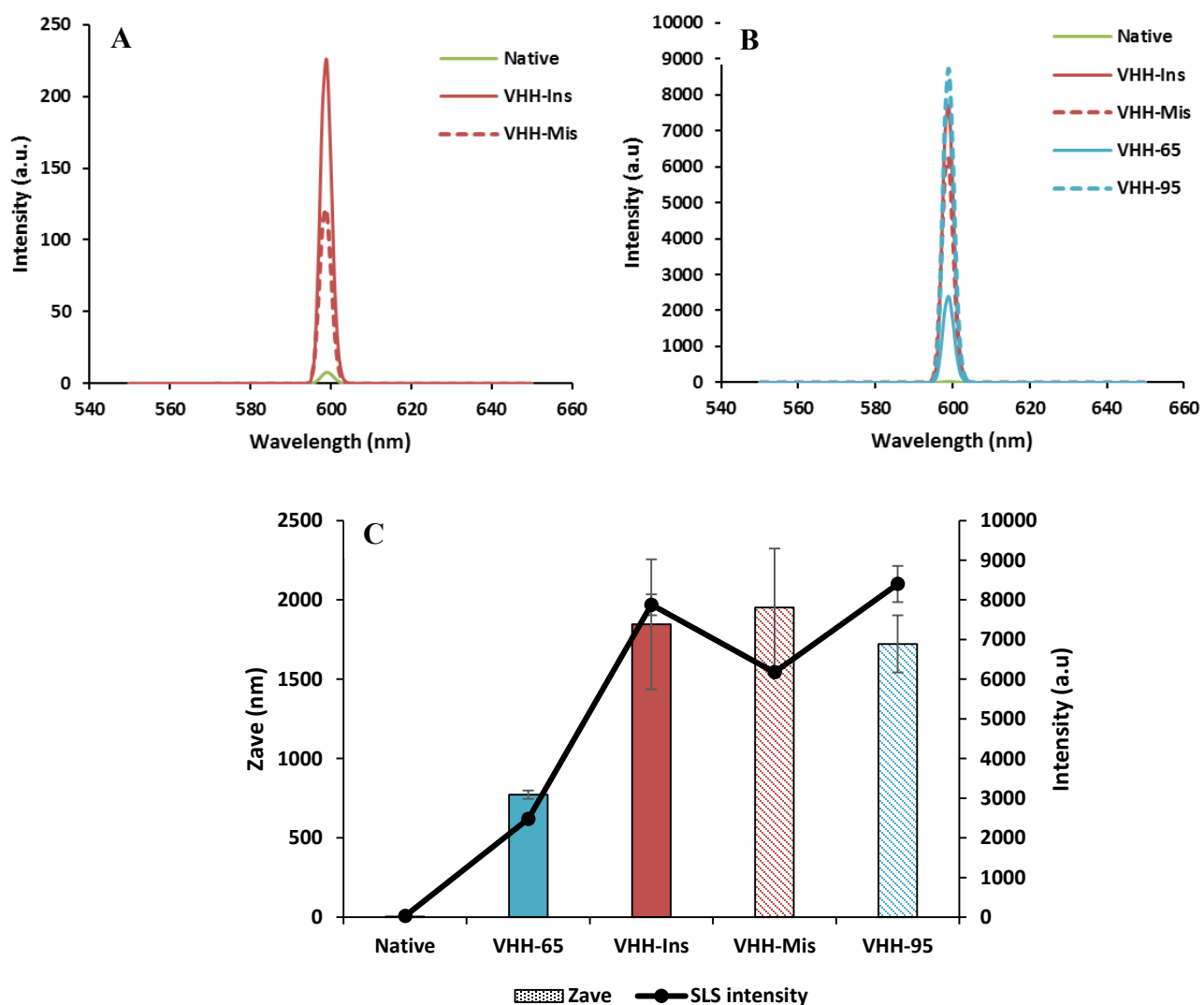


Figure 2.8: Degree of aggregation by Static Light Scattering (SLS). The intensity-based aggregate size was measured at 600 nm by SLS at a protein concentration of 0.3 mg/mL at 37 °C (A) in 20 mM Na-acetate buffer, pH 4.7 and (B) in PBS, pH 7.4. (C) Comparative analysis of SLS intensity (a.u) and DLS Zave (nm) of the different aggregate formulation of anti-EGFR V_{HH} in PBS. Three accumulations were taken for each measurement. Line symbols are explained within the panels.

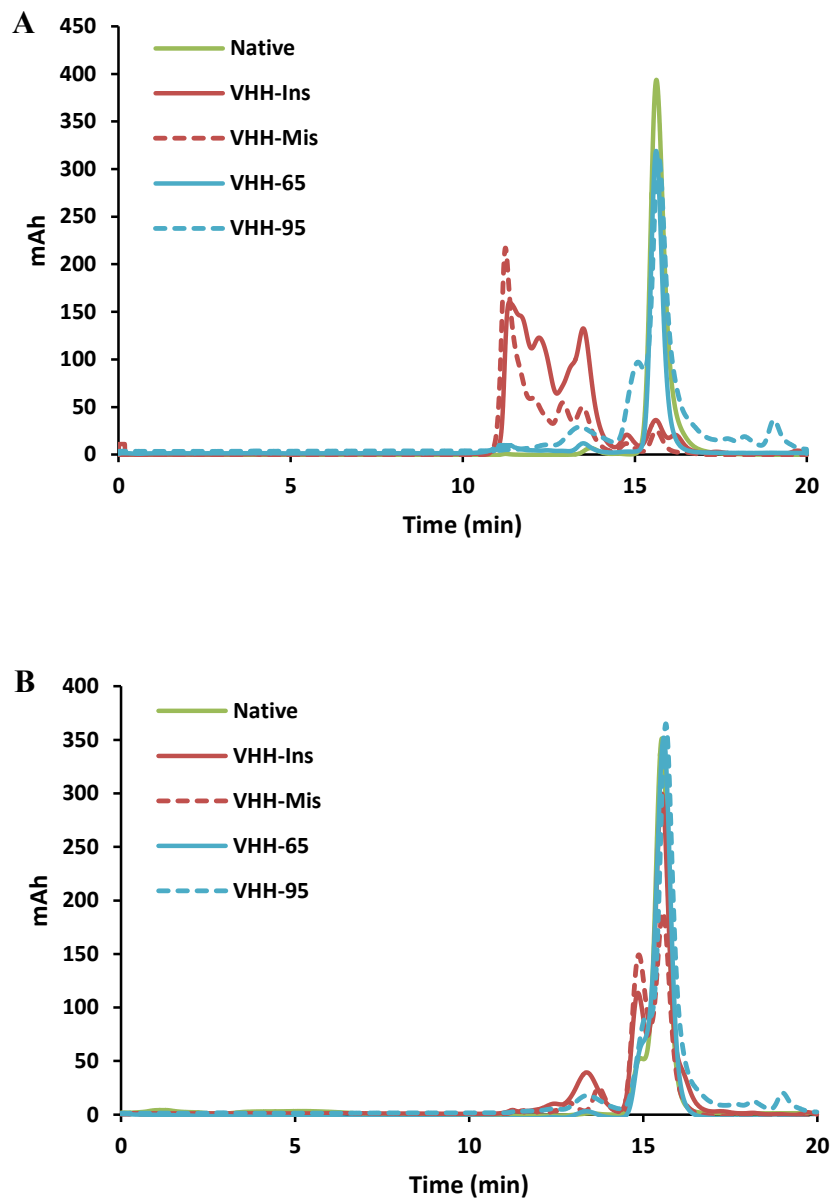


Figure 2.9: High-performance size exclusion chromatography (HP-SEC) analysis of the oligomerization state. Samples for size-exclusion chromatography in a denatured condition were prepared at a protein concentration of 0.1 mg/mL in PBS (pH 7.4) supplemented with 6 M guanidine hydrochloride. 20 μ L of the sample was used for the HP-SEC analysis in a non-reducing (**A**) and a reducing (**B**) condition. Gray, black, and dark black triangles indicate the trimer, dimer, and monomer, respectively. Line symbols are explained within the panels.

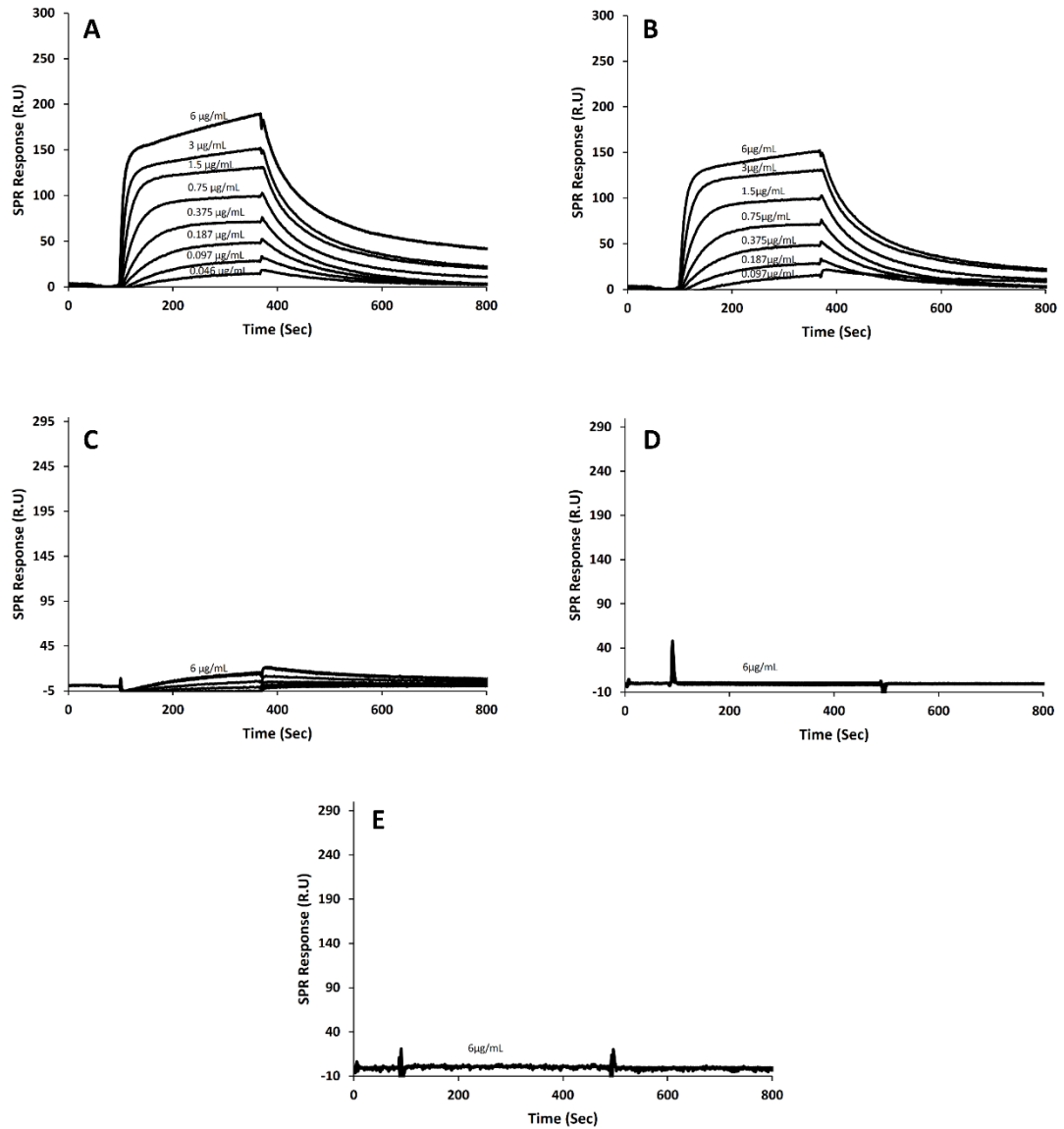


Figure 2.10. Binding activity to EGFR by Surface Plasmon Resonance (SPR). Epidermal Growth Factor Receptor (EGFR) extracellular domain (20 µg/mL) was immobilized on a CM5 sensor chip. Binding activity of anti-EGFR V_{HHS} in (A) native (B) V_{HH-65} (C) V_{HH-Ins} (D) V_{HH-Mis} and (E) V_{HH-95} conditions were analyzed at concentrations between 6 µg/mL and 0.046 µg/mL in HBS-EP buffer.

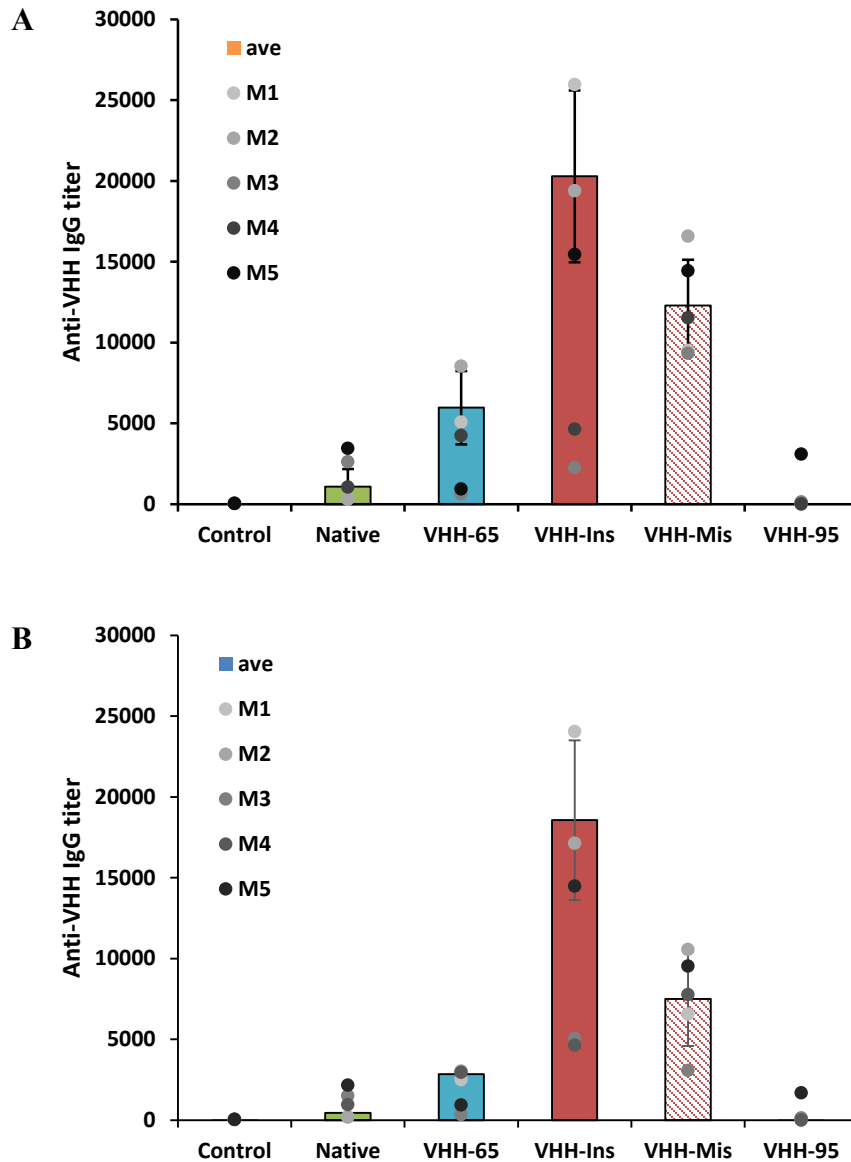


Figure 2.11: Anti-V_{HH} antibody (IgG) titer assayed by ELISA. IgG detection by ELISA was performed using the tail bleeding (TB) sera, after six doses of subcutaneous injection. Each circle indicates the individual mice titer (total of five mice in each group) and the bars show the average titer calculated by excluding the outliers. The number of mice in each group, as well as those used to calculate the average, is mentioned in parenthesis. IgG titer measured using the native anti-EGFR V_{HH} as the coating antigen (**A**), and V_{HH}-Ins as the coating antigen (**B**).

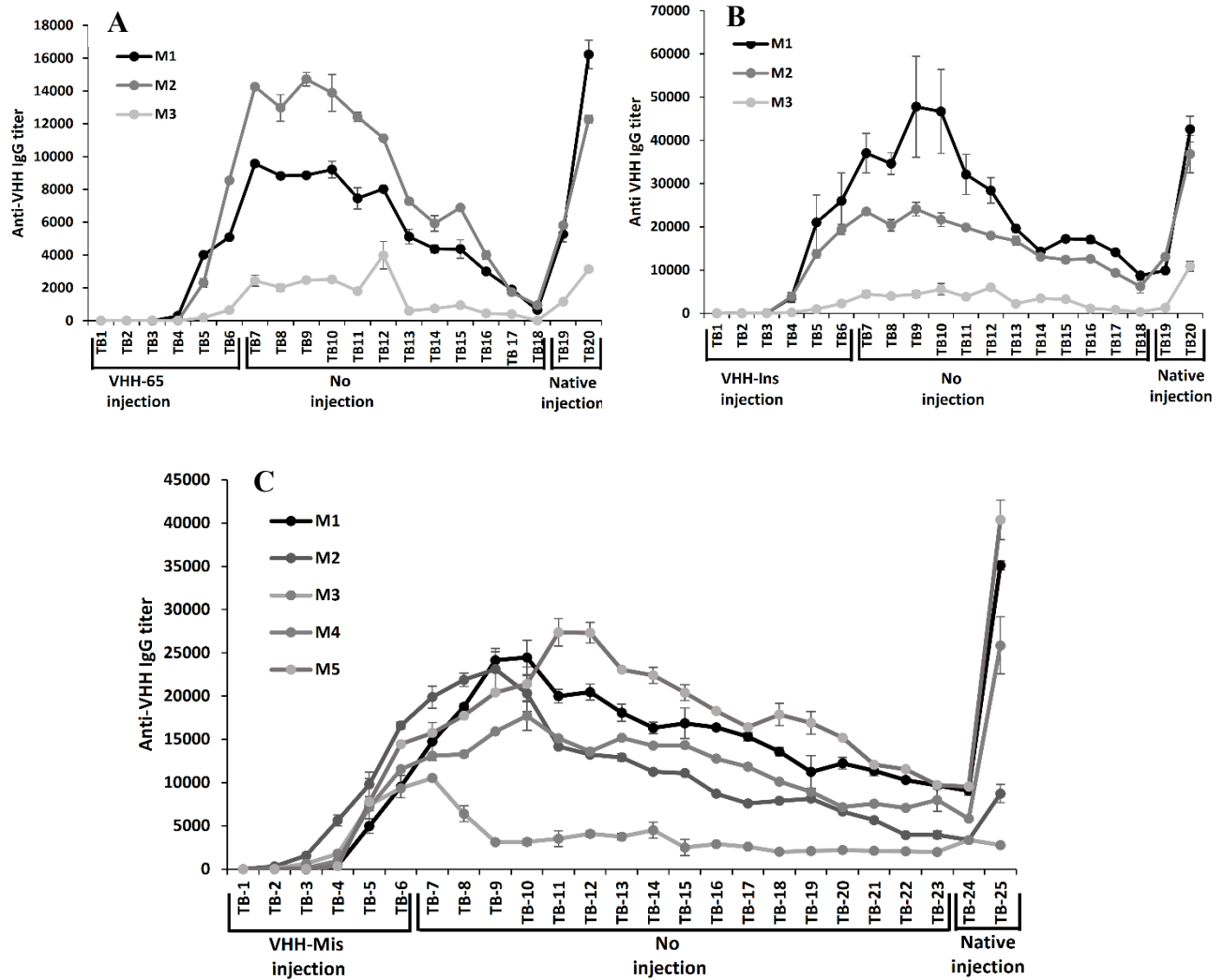


Figure 2.12: Long-term IgG response and immunological memory. (A) Long-term serum IgG and immunological memory of V_{HH}-65 immunized mice **(B)** Long-term serum IgG and immunological memory of V_{HH}-Ins immunized mice and **(C)** Long-term serum IgG and immunological memory of V_{HH}-Mis immunized mice.

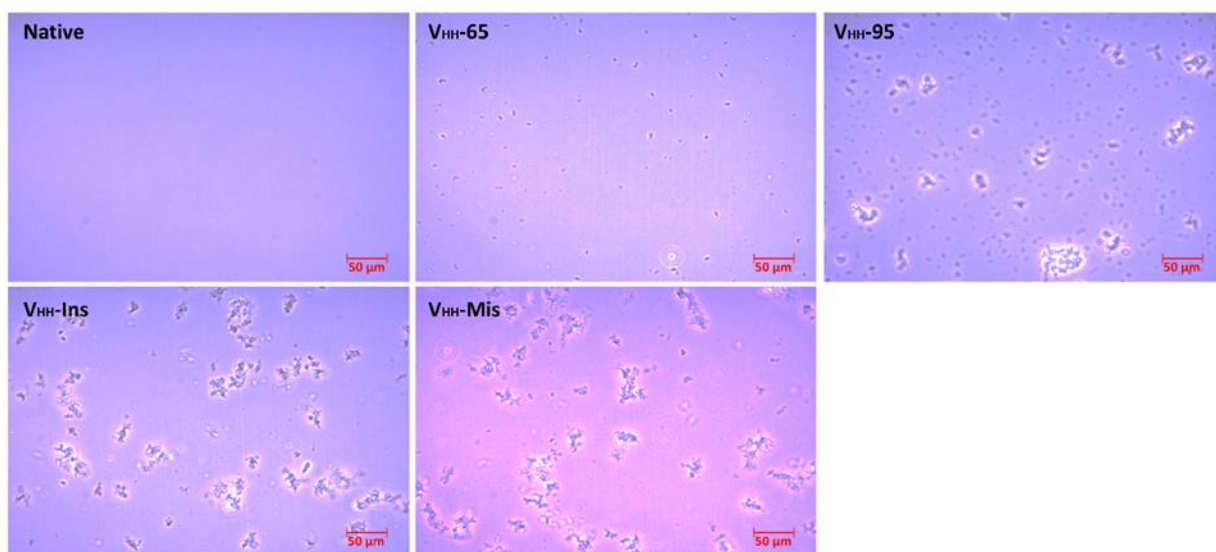


Figure 2.13: Microscopic images of V_{HH} formulations. Representative microscopic images of native V_{HH}, V_{HH}-65, V_{HH}-95, V_{HH}-Ins and V_{HH}-Mis that were used for immunization. The images were taken by an inverted microscope (ECLIPSE Ts2-FL, Nikon, Tokyo, Japan) using a 40x magnification. Note that the size of the aggregates presented here may not be of comparable sizes measured with those of DLS, which cannot measure aggregates >1 μm.

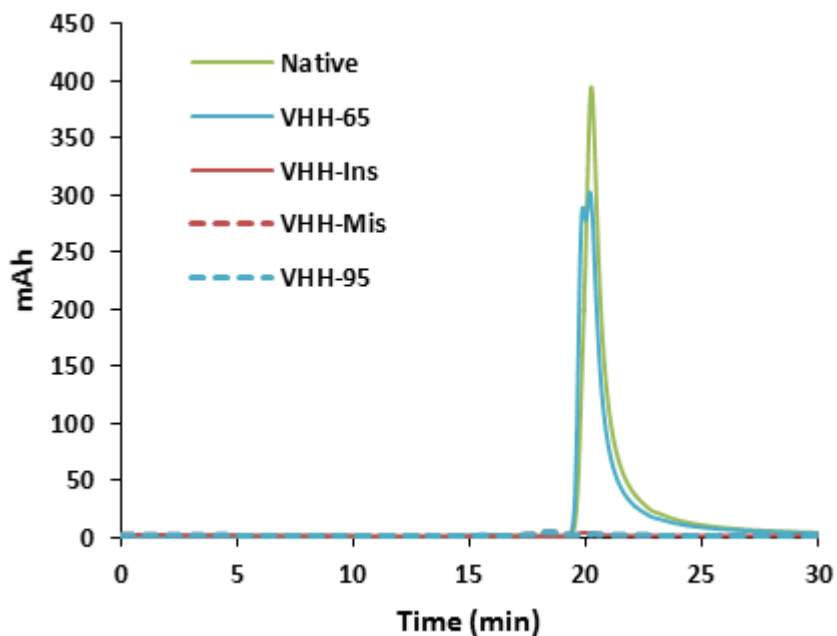


Figure 2.14. HP-SEC analysis of the oligomerization state. HP-SEC was performed to analyze the monomer and small oligomers that are present in the V_{HH} formulations. All of the five V_{HH} formulations were centrifuged at 20000 xg for 20 minutes and the supernatant concentration was measured by Nanodrop. Finally, 20 μL of the supernatant sample was used for HP-SEC analysis using PBS (pH 7.4) as a mobile solution and a flow rate of 0.5 mL/min. Protein elution was detected by a fluorescence detector (RF-20A, SHIMADZU CORP, Japan) using an excitation wavelength of 295 nm and an emission wavelength of 345 nm, specific for tryptophan residue. Line symbols are explained in the panel. Note that after centrifugation the supernatant concentrations of V_{HH} -Ins, V_{HH} -Mis and V_{HH} -95 were too low to obtain a HP-SEC signal.

Table 2.1. Secondary structure content by BeStSel

Sample	pH	α -helix (%)	anti-parallel (%)	parallel (%)	turn (%)	others (%)
Native	4.7	1.3	41.9	0.0	11.1	45.7
	7.4	1.3	41.4	0.0	11.2	46.1
V _{HH} -Ins	4.7	5.3	9.7	11.2	12.9	60.8
	7.4	NS*	NS*	NS*	NS*	NS*
V _{HH} -Mis	4.7	5.3	17.7	9.0	11.4	56.6
	7.4	NS*	NS*	NS*	NS*	NS*
V _{HH} -65	4.7	NM**	NM**	NM**	NM**	NM**
	7.4	0.0	38.9	3.9	12.4	44.8
V _{HH} -95	4.7	NM**	NM**	NM**	NM**	NM**
	7.4	NS*	NS*	NS*	NS*	NS*

*NS= No Signal due to the formation of large aggregates

**NM= Not Measured as this pH was not used for this formulation

Table 2.2. Tryptophan and ANS fluorescence intensities

Sample	Trp fluorescence (a.u) at 345 nm			ANS fluorescence (a.u) at 480 nm	
	pH 4.7	pH 7.4	Fluorescence shift (nm)	pH 4.7	pH 7.4
Native	3102 \pm 35	3140 \pm 53	0	9 \pm 3	7 \pm 2
V _{HH} -Ins	1676 \pm 80	1372 \pm 187	4 **	834 \pm 50	459 \pm 27
V _{HH} -Mis	894 \pm 127	1025 \pm 46	4 **	587 \pm 84	438 \pm 80
V _{HH} -65	NM*	2716 \pm 165	0	NM*	102 \pm 7
V _{HH} -95	NM*	894 \pm 170	4 **	NM*	298 \pm 24

*NM= Not measured ** correspond to blue-shift

Table 2.3. Aggregate's sizes by DLS and SLS

Sample	pH	DLS			SLS
		Zave (r.nm) *	PDI	Number mean (r.nm) **	Intensity (a.u)
Native	4.7	2.1 ± 0.5	0.24 ± 0.06	1.7 ± 0.1	8.9 ± 1.4
	7.4	3.5 ± 0.2	0.22 ± 0.07	2.1 ± 0.1	28.0 ± 0.5
V _{HH} -Ins	4.7	30.4 ± 1.0	0.36 ± 0.01	10.9 ± 1.5	239.0 ± 19.2
	7.4	1846.5 ± 409.4	0.27 ± 0.12	1166.4 ± 324.5	7877.5 ± 264.2
V _{HH} -Mis	4.7	20.0 ± 0.2	0.30 ± 0.01	8.1 ± 1.4	119.0 ± 2.0
	7.4	1951.7 ± 373.3	0.49 ± 0.08	1135.8 ± 269.0	6134.7 ± 84.6
V _{HH} -65	7.4	771.3 ± 26.3	0.15 ± 0.06	571.6 ± 25.0	2477.0 ± 115.0
V _{HH} -95	7.4	1722.3 ± 180.0	0.49 ± 0.09	1100.7 ± 258.1	8400.1 ± 454.1

*Mean Z-average hydrodynamic radius

** Hydrodynamic radius (R_h) calculated from the number mean. Errors indicate the standard deviations calculated over three measurements

Chapter-3

Immune response with long-term memory triggered by amorphous aggregates of misfolded anti-EGFR V_{HH}-7D12 is directed against the native V_{HH}-7D12 as well as the framework of the analogous V_{HH}-9G8

3.1.1 Introduction

Breakage of the immune tolerance and the consequent production of anti-drug antibodies (ADAs) is becoming a major concern in protein drug's safety and usage [88, 129]. Clinical observations indicate that ADAs can reduce the hemostatic efficiency of factor VIII by approximately 30% in haemophilia A patients [2, 130]. Likewise, antibodies developed against recombinant human acid-alpha glucosidase (rhGAA) can adversely impact their efficacy in the treatment of Pompe disease [131]. Protein aggregation has long been suspected of provoking accidental immunogenicity of protein drugs, resulting in ADAs [12, 23, 116]. Besides clinical observations, where protein aggregates are rarely monitored and characterized, several experimental studies using human interferon-beta (INF- β) [92], factor VIII [132], growth hormones [133], and monoclonal antibodies (mAbs) [94, 134] have shown that aggregates may indeed generate ADAs.

The increased immunogenicity of protein aggregates is not fully understood, but it is speculated that their multiple repetitive epitopes act like a pathogen-associated molecular pattern (PAMP), which are recognized by pattern recognition receptors (toll-like receptors, TLRs) residing on antigen-presenting cells (APCs) [116] and increase the expression of peptide associated MHC-II molecules [94, 135]. In another hypothesis, aggregated proteins, particularly monoclonal antibody aggregates, can act like an 'immune complex', thereby enhancing the Fc γ R mediated APCs internalization and processing [76]. From a protein conformational standpoint, it has been shown that aggregated protein potentially enhanced the expression of new B-cell epitopes and facilitating the IgG generation [135]. The aggregated proteins may be natively folded, misfolded, partially unfolded, or completely unfolded [59], which will presumably expose different epitopes and generate ADAs with different specificities [95].

Engineered antibody and antibody fragments are a fast-growing class of therapeutic proteins [8, 136-138]. Single domain antibody (V_{HH}) is a unique class of antibody, and unlike full-length antibody, it consists of a single variable heavy domain containing three complementarity determining regions (CDRs) [83]. V_{HH} adopts an Ig fold, and its framework regions have high sequence and structure similarities, but the sequence and conformation of CDRs are distinctive for each V_{HH} . The CDRs are critical for antigen-specific recognition;

they adopt a loop structure that increases their ability to fit the antigen surface resulting in a strong binding with the corresponding antigen [139]. ADAs targeting the CDRs are expected to inhibit V_{HH} 's ability to bind to the antigen and thus correspond to neutralizing ADAs, which are the most critical ones from a clinical perspective. ADAs that bind to the framework regions of the V_{HH} are anticipated to be non-neutralizing, but they are susceptible to show cross-immune reactivity with analogous V_{HHS} . Since the framework regions' sequences and structures of the V_{HHS} are very similar to each other, it is worth exploring the nature of ADAs specificity and their relationship with long-term immunogenicity risk.

3.1.2 Aim and objective

In our previous study, we reported the immunogenicity of an anti-EGFR V_{HH} -7D12 that increased by the formation of amorphous aggregates generated by miss-shuffling of its SS bonds (V_{HH} -Mis) [140]. Here, we sought to investigate further the nature of the immune response generated by V_{HH} -Mis by assessing its specificity against the CDRs/framework regions. To this end, we immunized the mice with V_{HH} -Mis and examined its effect on the immune response against its native self (native V_{HH} -7D12) and an analog (native anti-EGFR V_{HH} -9G8), whose framework region is virtually identical to that of V_{HH} -7D12, but the CDRs are different [141]. Furthermore, we assessed the generation of T-cell immunological memory by analyzing the cell surface CD (cluster of differentiations) marker. Our findings provide a deeper understanding of the specificity of the immune response and long-term immunogenicity generated by aggregates and misfolded proteins.

3.2 Materials and Methods

3.2.1 Protein expression and purification

A pAED4 vector [107] containing a synthetic gene that encodes anti-EGFR V_{HH}-7D12 or V_{HH}-9G8 was transformed into *E. coli* BL21 (DE3) pLysS cell lines and grown in Luria Bertani (LB) medium at 37 °C. Protein expression was induced with 1 mM isopropyl β-d-1-thiogalactopyranoside (IPTG) when the optical density (OD) of the culture reached 0.6 at 590 nm. Six hours after induction of protein expression, the cells were harvested by mild centrifugation (8000 rpm for 20 min at 4 °C). After sonication, the protein was purified by Ni-NTA (Qiagen, Germany), followed by ion-exchange chromatography (Gigacap-s-650 M, Tosoh Bioscience, Tokyo, Japan) according to our previously reported protocol [140]. Protein identities were then confirmed by MALDI-TOF mass spectrometry (autoflex speed TOF/TOF, US) (**Figure 3.1**), and the purified proteins dissolved in Milli-Q (MQ) water was kept at -30 °C as a stock protein solution.

3.2.2 Generation of misfolded V_{HH}-7D12 aggregates (V_{HH}-Mis)

Misfolded anti-EGFR V_{HH}-7D12 (V_{HH}-Mis) was generated according to our reported protocol [140]. In short, the native V_{HH}-7D12 protein was first dissolved in 6 M guanidine hydrochloride and 10 mM Tris-HCl (pH 8.5), **buffer A**, and reduced with 0.5 M dithiothreitol (DTT) by a 2-hour incubation at room temperature. The sample was dialyzed overnight against MQ water at 4 °C and centrifuged. The precipitate was collected and dissolved in **buffer A** and oxidized for 15 hours at 25 °C. The guanidine hydrochloride was removed by again overnight dialysis against 10 mM Tris-HCl (pH 8.5). The precipitate collected by centrifugation was again dissolved in **buffer A** and underwent a second iteration of dialysis and centrifugation. Similarly, after a third iteration, the resulting precipitate was dissolved in 6 M guanidine hydrochloride with 10% acetic acid solution and dialyzed overnight against MQ water at 4 °C. Finally, the supernatant containing misfolded V_{HH}-7D12 was stored at -30 °C as a V_{HH}-Mis stock solution. The V_{HH}-Mis sample was freshly prepared just before each set of experiments by adding the required amount of MQ-water and 5X PBS buffer to the V_{HH}-Mis stock solution to a final buffer condition of 1X PBS. A graphical representation of V_{HH}-Mis purification is available in the **chapter 2**.

3.2.3 Circular dichroism (cd)

Far-UV circular dichroism (cd) spectroscopy measurements were performed at a protein concentration of 0.3 mg/mL (20 μ M) in PBS (pH 7.4) using a JASCO J-820 spectropolarimeter (JASCO, Tokyo, Japan) at 37 °C. 300 μ L of the protein solution was placed in a 1 mm path-length quartz cuvette, and the spectra were collected in a continuous scanning mode from 260 to 200 nm wavelength. For each measurement, three accumulations were considered, and the final spectrum was obtained by subtracting the corresponding buffer spectrum.

3.2.4 Dynamic light scattering (DLS)

Dynamic light scattering (DLS) properties of both native and misfolded V_{HHs} were measured at 37 °C with a Zetasizer Nano-S system (Malvern, UK) in PBS (pH 7.4) at a final protein concentration of 0.3 mg/mL using a 100 μ L-polystyrene cuvette. The reported hydrodynamic radii (R_h) are the average of three or more individual readings.

3.2.5 Mice immunization

4-week old female mice (Jcl: ICR; CLEA, Japan) were immunized by subcutaneous injection of the samples according to the following protocol (**Figure 3.2B**). 100 μ L of V_{HH} -Mis at a concentration of 0.3 mg/mL in PBS (pH 7.4) were injected weekly for six weeks. Three control mice were treated with PBS only. Tail-bleed (TB) samples were collected three days after injection. After the six weeks, the mice were kept untreated for seventeen weeks and re-immunized with two boost shots of native V_{HH} -7D12 or V_{HH} -9G8. The mice were then sacrificed, the heart bleed was collected, and the spleen was gathered for flowcytometric analysis. Before each round of injection, we monitored the aggregate's sizes by taking an aliquot of the injected sample and measuring the R_h using DLS. All experiments were performed in compliance with the Tokyo University of Agriculture and Technology (TUAT) and Japanese governmental regulations on animal experimentation.

3.2.6 Enzyme-linked immunosorbent assay (ELISA)

ELISA was performed as previously reported [121]. In short, 96-well microtiter plates (TPP Techno Plastic Product, Switzerland) were coated with 100 μ L of 2.5 μ g/mL native V_{HH}

protein in PBS (pH 7.4) and incubated at 25 °C overnight. After washing the unbound V_{HH} with PBS, the plates were blocked with 1% BSA at 37 °C for 45 min. Afterward, 150 μ L of 50 times diluted serum samples were added onto the 1st well followed by 3-fold serial dilution in subsequent 0.1% BSA-PBS containing wells and incubated at 37 °C for 2 hours. After washing the unbound serum antibodies, 1:3000 diluted anti-mouse IgG-HRP conjugate in 0.1% BSA-PBS-0.05% Tween-20 were added. After washing the plates with PBS-0.05% Tween-20, 100 μ L OPD (o-phenylenediamine dihydrochloride) solution was added, and the plates were incubated for 20 min for coloring. The coloring reaction was stopped by adding 1 N sulfuric acid, and the color intensity was measured at 492 nm using a microplate reader (SH-9000 Lab, Hitachi High-Tech Science, Japan). Data were analyzed by a power fitting of OD 492 nm versus the reciprocal dilution of the anti-sera and a cutoff OD value of 0.1, which is above the background value. A previously developed DEN3 ED3 (dengue 3 envelop protein 3) anti-sera was used as a positive control in all ELISA experiments.

3.2.7 Cell surface CD marker analysis by flow cytometry

Experimental samples were prepared according to our previously reported protocol [121]. In short, single-cell suspension of mice splenocyte was prepared in FACS buffer (PBS supplemented with 2% FBS, 1 mM EDTA, and 0.1% sodium azide). Afterward, 1X red blood cell (RBC) lysis buffer (0.15 M ammonium chloride, 10 mM potassium bicarbonate, 0.1 mM EDTA) was used to lysis the RBCs. Further, 1 million splenocyte cells in 100 μ L of pre-cooled FACS buffer were surface stained with fluorescence level antibodies according to the manufacture guidelines. To study the CD4 T-lymphocytes, cells were stained with anti-CD3-Pcy5, CD4-Pcy7, CD44-FITC, and CD62LPE-conjugated antibodies in one tube, and CD8 T-lymphocytes cells were stained with anti-CD3-Pcy5, CD8-Pcy7, CD44-FITC, and CD62LPE-conjugated antibodies in another tube (0.2 μ g of antibodies/100 μ L) for 30 min in the dark. Unbound conjugated antibodies were removed by centrifugation. Finally, cells were resuspended in a 500 μ L of FACS buffer, and the data were collected using CytoFlex (Beckman Coulter, US).

3.3 Results

3.3.1 Structural and biophysical assessment

The secondary structure content of V_{HH}-7D12 and V_{HH}-9G8 at pH 7.4 in PBS was assessed by circular dichroism (far UV-cd, 200-260 nm). Both V_{HHS} showed a spectrum typical of a β -sheeted protein (**Figure 3.3A**). The misfolded V_{HH}-7D12 (V_{HH}-Mis) precipitated in PBS, and no spectroscopic measurement was possible in this buffer, but in Na-acetate buffer (pH 4.7), where it was soluble and showed CD spectra distinct from the native one (**chapter 2, Figure 2.3A**). V_{HH}-7D12 and V_{HH}-9G8 appeared to be monomeric as suggested by a hydrodynamic radius (R_h) of around 2 nm as measured by DLS, whereas V_{HH}-Mis exhibited a larger R_h value, indicating its aggregated state (**Figure 3.4A and Table 3.1**). These results were corroborated by static light scattering (SLS) (**Figure 3.4B and Table 3.1**).

3.3.2 A strong immune response generated by the aggregated V_{HH}-Mis

The mice were immunized weekly once for six times with the misfolded V_{HH}-7D12 (V_{HH}-Mis). The serum IgG response against the native V_{HH}-7D12 and V_{HH}-9G8 was monitored for 26 weeks by measuring the IgG titer using ELISA with plates coated with native V_{HH}-7D12 or V_{HH}-9G8. As a control, we immunized two groups of mice with the native monomeric V_{HH}-7D12 and V_{HH}-9G8. First, we examined the anti-sera just after completing the primary immunization (TB-6, Scheme: 1). Both native V_{HHS} were barely immunogenic (**Figure 3.5A**), as expected for small proteins, and in line with our previous report [142]. In contrast, mice immunized with aggregated V_{HH}-Mis, which had altered secondary and tertiary structures (**Figure 3.3A and B**), showed a strong IgG titer against the native V_{HH}-7D12. The results are in line with our previous report, where we showed that amorphous aggregates of misfolded V_{HH}-7D12 increased the immune response against the native V_{HH}-7D12 in mice; but denatured aggregates induced by heat stress did not, even though the aggregates' sizes were almost identical. We thus concluded that the biophysical and biochemical nature of the misfolded aggregates are critical in generating ADAs against the native V_{HH}-7D12 [140]. Indeed, the IgG titers against the native V_{HH}-7D12 were stronger in twelve mice out of the thirteen immunized with V_{HH}-Mis than in mice immunized with the native V_{HHS} (**Figure 3.5A**).

Furthermore, the anti-sera raised against V_{HH}-Mis, during the primary round of immunization, were analyzed by ELISA by using both the native V_{HH}-7D12 and V_{HH}-9G8 as coating antigens. This is because we anticipated seeing cross-reaction because of their nearly identical frameworks (**Figure 3.2A**). 60% of mice (8 out of 13) immunized with V_{HH}-Mis exhibited a serum IgG response against native V_{HH}-7D12 that was much stronger than against native V_{HH}-9G8 (**Figure 3.6** and **Table 3.2**). The remaining mice (5 out of 13 or 40%) exhibited a nearly identical IgG response against the native V_{HH}-7D12 and V_{HH}-9G8. According to IgG specificity, we divided the V_{HH}-Mis immunized mice ($n=13$) into two groups: **Group-1**, which included the mice showing a strong IgG titer against the native V_{HH}-7D12 but a weak one if any against the native V_{HH}-9G8 ($n=8$); **Group-2**, which included the mice showing very similar IgG titer against native V_{HH}-7D12 and V_{HH}-9G8 ($n=5$) (**Table 3.2**). In the next section, we analyze the extent of the breakage of the immune tolerance generated by the misfolded V_{HH}-7D12 (V_{HH}-Mis).

3.3.3 Nature of the long term immune response against the native V_{HH}S

We thus asked whether V_{HH}-Mis would generate a long-lasting immune memory against the native V_{HH}-9G8, whose framework region is very similar to that of V_{HH}-7D12 but has distinct CDRs (**Figure 3.2A**). After 17 weeks of without injection, the mice were re-immunized (boost injection) using either native V_{HH}-7D12 or native V_{HH}-9G8. Three mice of **Group-1** (M1, M3, and M9) were re-immunized with native V_{HH}-9G8 (**Figure 3.7**), and two mice (M10 and M11) were re-immunized with native V_{HH}-7D12 (**Figure 3.8**). By re-immunizing with native V_{HH}-7D12, the serum IgG titer substantially increased after two injections, suggesting the presence of immunological memory against native V_{HH}-7D12 (**Figure 3.8**). Oppositely, re-immunization with V_{HH}-9G8 did not increase the titer against V_{HH}-7D12 or even against V_{HH}-9G8 (**Figure 3.7**). This suggested that the immune memory in **Group-1** mice was generated against regions of V_{HH} that are specific to V_{HH}-7D12, i.e., the CDRs. Next, **Group-2** mice (M12 and M13) re-immunized with native V_{HH}-7D12 increased their anti-V_{HH}-7D12 IgG titer sharply, even much higher than primary immunization with V_{HH}-Mis (except M13), but not against V_{HH}-9G8 (**Figure 3.10**). The remaining **Group-2** mice (M2, M4, and M7) were re-immunized with native V_{HH}-9G8, but we observed a slower and moderate immune response,

as the increase needed one more week to appear (TB-26) than when the mice were re-immunized with native V_{HH} -7D12 (**Figure 3.9**).

3.3.4 Immunization with V_{HH} -Mis established T-cell effector and central memory

The generation of immunological memory was further analyzed by cell surface CD markers in mice that responded strongly to re-immunization with native V_{HH} -7D12. The mice were sacrificed 26 weeks after the first immunization and their spleen collected for CD analysis. The mice primarily immunized with native V_{HH} -7D12 (as a control) had a low number of CD44⁺ and high CD62L⁺ CD4 (T-helper) (**Figure 3.11**) and CD8 (T-cytolytic) cells (**Figure 3.12**). Moreover, a higher number of CD44-CD62L⁺ co-expressing T-helper (77%) and T-cytolytic (74%) cells was observed, indicating their naïve immunological status (**Figure 3.13**).

On the other hand, the V_{HH} -Mis immunized mice showed a high number of CD44⁺ and low CD62L⁺ (both CD4 and CD8 cells) population (**Figure 3.11** and **3.12**). Additionally, a lower percentage of CD44-CD62L⁺ cells, and a higher percentage of CD44⁺CD62L⁺ and CD44⁺CD62L⁻ co-expressing T-helper and T-cytolytic cells were observed (**Figure 3.13**), indicating that the misfolded V_{HH} -7D12 (V_{HH} -Mis) generated central and effector T-cell memory.

3.4 Discussion

Therapeutic proteins, the largest and fastest-growing class of biopharmaceutical product, can provoke ADAs [143-145]. Aggregation is a critical factor causing the undesired immune response affecting the protein's therapeutic properties [57, 129], and clinical observations relating ADAs with aggregates have been reported for human growth hormone (hGH) [21, 22]. However, amorphous aggregates of different sizes [35, 37, 40, 146] and distinct biophysical and biochemical attributes are formed depending on how they are generated [147-150], which may result in ADAs having distinct properties [33, 39, 132]. For instance, ADAs may bind near the active site or apart from the active site (so-called neutralizing or non-neutralizing, respectively) [7, 151], however, in any case, ADAs can alter a protein's therapeutic efficiency by accelerating its clearance from the organs and the body, as clinically shown for adalimumab [152]. Alternatively, ADAs may recognize a host endogenous protein, which could induce serious side effects, as seen with recombinant erythropoietin [5].

The misfolded $V_{HH-7D12}$ (V_{HH-Mis}), which were functionally inactive (**Figure 3.15**), induced an IgG response in 60% mice (**Group-1**), hypothesized as being directed against $V_{HH-7D12}$'s CDRs, because the anti- $V_{HH-7D12}$ IgG titer was much stronger than the anti- V_{HH-9G8} titer. The rationale for the CDRs specificity is unclear from a protein structural viewpoint since the CDR's conformation in the misfolded $V_{HH-7D12}$ is expected to be different from that in the native $V_{HH-7D12}$. Re-immunizing these mice with native $V_{HH-7D12}$ sharply increased the immune response against the native $V_{HH-7D12}$ (**Figure 3.8**), however, no mice showed such a response by re-immunizing with native V_{HH-9G8} (**Figure 3.7**), suggesting an immunological memory against the CDRs of native $V_{HH-7D12}$ was established. We thus speculate that the CDRs of misfolded $V_{HH-7D12}$ have a structure similar to that in the native $V_{HH-7D12}$, which are constrained but flexible loops (**Figure 3.2A**). Our observation is essentially in line with a previous report showing that rhIFN β -1a aggregates generate neutralizing ADAs targeting the native rhIFN β -1a [128]. Noteworthy, a similar phenomenon was also observed by re-immunizing the Group-1 mice with the misfolded $V_{HH-7D12}$ (V_{HH-Mis}).

Cross-reactive and pre-existing antibodies create much concern as they may reduce the related drug's therapeutic efficacy [151]. For example, ADAs generated against CT-P13, which is

biosimilar to infliximab, recognize both CT-P13 and infliximab and neutralize their function [153]. In our experiment, cross-reaction was observed in **group-2** mice (40%), where the immune response against V_{HH}-7D12 and V_{HH}-9G8 were of similar strength. Furthermore, **Group-2** mice re-immunized with the native V_{HH}-7D12 produced anti-sera recognizing the native V_{HH}-7D12 more strongly than the native V_{HH}-9G8, suggesting the presence of IgG antibodies targeting the V_{HH}-7D12's CDRs (**Figure 3.10**). We initially expected **Group-2** mice would respond upon re-immunization with native V_{HH}-9G8 as strongly as observed with V_{HH}-7D12, but we observed a relatively slower and moderate immune response (**Figure 3.9**). Moreover, their specificity was essentially unchanged (**Figure 3.9**), unlike the immune response that we observed by re-immunizing the mice with native V_{HH}-7D12. These results suggest that the risks of ADAs generation by subsequent injections are high when the same protein, even natively folded, is used, but they remain low-to-moderate when a biosimilar analog is used.

Immune responses against aggregated proteins can occur through a T-cell dependent (TD) pathway or a T-cell independent (TI) pathway [24, 154]. In a TD pathway, the recognition of antigenic epitopes by B-cell receptors (BCRs) provides the first signal for B-cells activation and the second signal comes from the T-cells, which are activated by antigen-presenting cells (APCs), primed with the same antigen [24]. B-cell Ig isotype switching and immunological memory are generated by the TD pathway, resulting in a long-lasting immunogenic response. Here, we found that V_{HH}-Mis immunized mice had a higher CD44⁺ cell population. Furthermore, both CD4⁺ (T-helper cell) and CD8⁺ (T-cytolytic) showed an increased number of CD44⁺CD62L⁺ and CD44⁺CD62L⁻ co-expressed cell population, which strongly indicates the generation of central and effector memory T-cells [155]. Moreover, V_{HH}-Mis induced a long-lasting anti-V_{HH} serum IgG response, particularly the IgG1 response (**Figure 3.14**), which are indicative of Th2 skewed immune response [38]. Such long-lasting ADAs response was observed in a clinical study with INF- β [156] and other therapeutic mAbs [157]. According to the ADAs model, the persistent generation of serum IgG will affect the drug's efficacy, especially those that bind near the active site [158].

3.5 Conclusion

Amorphous aggregation of therapeutic antibodies and antibody fragments is the focus of much attention as it may decline drug safety and cause severe side effects in the form of ADAs. Previously, we showed how aggregate's biophysical and biochemical properties of V_{HH} antibody influenced the immunogenic response [140]. Our current observations indicate that the immunological memory developed by amorphous aggregates made of misfolded V_{HH} can induce substantial and long-lasting ADAs against its native self. However, the response against an analogous V_{HH} having an almost identical framework region but different CDRs was less severe (60% in our experimental setting). This observation indeed suggests that by determining the ADAs specificity one might avoid ADAs' appearance by switching the therapeutic antibody to an analogous one that targets the same EGFR and would thus allow keeping the same therapeutic strategy. We hope that such a conclusion will remain valid for therapeutic V_{HHS} and other antibody drugs since they hold similar structural properties with common framework regions and variable CDRs.

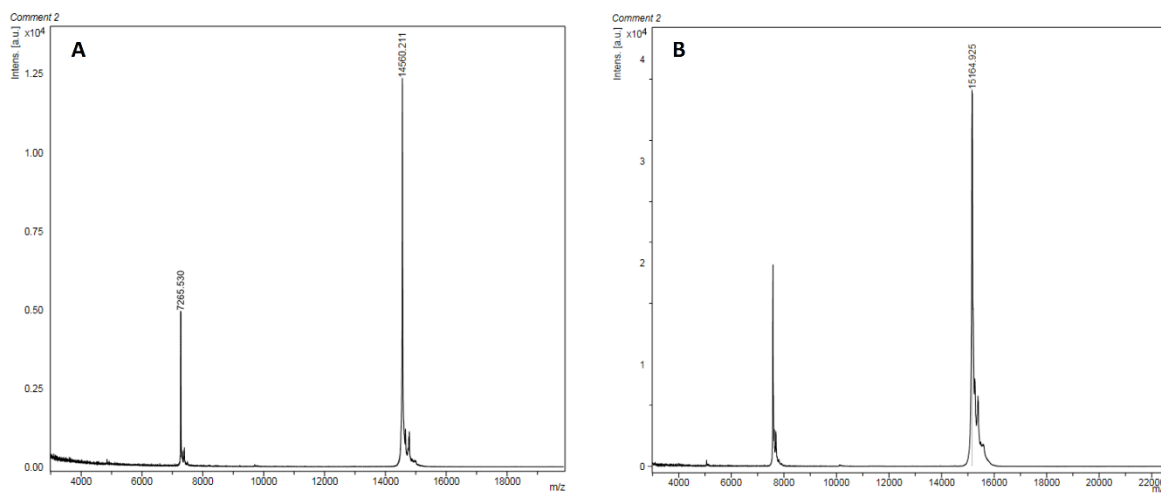


Figure 3.1. Determination of molecular weight of purified V_{HH}S. Purified V_{HH} protein identities were analyzed by MALDI-TOF mass spectroscopy (autoflex speed TOF/TOF, US) **(A)** Native V_{HH}-7D12 (Mw: 14560.21 Da) and **(B)** Native V_{HH}-9G8 (Mw: 15164.92 Da). The theoretical molecular weight of V_{HH}-7D12 and V_{HH}-9G8 calculated from ExPASy ProtParam was 14559.95 Da and 15169.69, respectively, which is almost identical to our measured molecular weight, ensuring V_{HH}S protein identities.

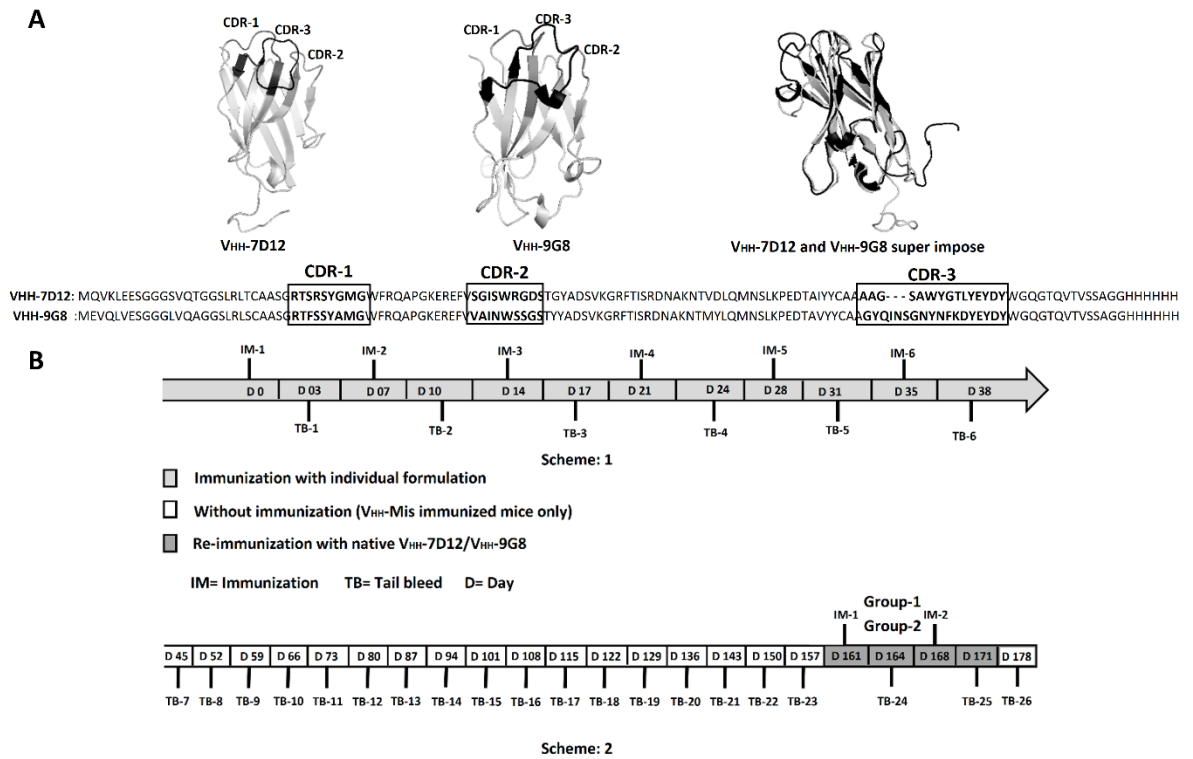


Figure 3.2. Structure of anti-EGFR V_{HH}-7D12 and V_{HH}-9G8 antibodies and schematic representation of immunization. (A) Surface model representation of the V_{HH}-7D12, V_{HH}-9G8, and their superimpose image generated using Pymol (PDB ID 4KRL and 4KRP, respectively); and their sequence alignment. They have 89% framework and 77% overall sequence similarities. Gray, deep gray and black indicate the complementarity determining region 1 (CDR1), CDR2, and CDR3, respectively. (B) The schematic of immunization. In **Scheme 1**, each group of mice was immunized (IM) with individual V_{HH} formulation once a week (up to six weeks), and tail bleed (TB) samples were collected three days after each round of immunization and performed ELISA. In **Scheme 2**, V_{HH}-Mis immunized mice were kept untreated for 17 weeks. Only the serum IgG level was monitored by ELISA using tail bleed samples from TB-7 to TB-23 (white box). Afterward, mice were re-immunized with native V_{HH}-7D12, native V_{HH}-9G8, or V_{HH}-Mis and performed TB-24 and TB-25 (deep gray box). TB-26 was performed without immunization.

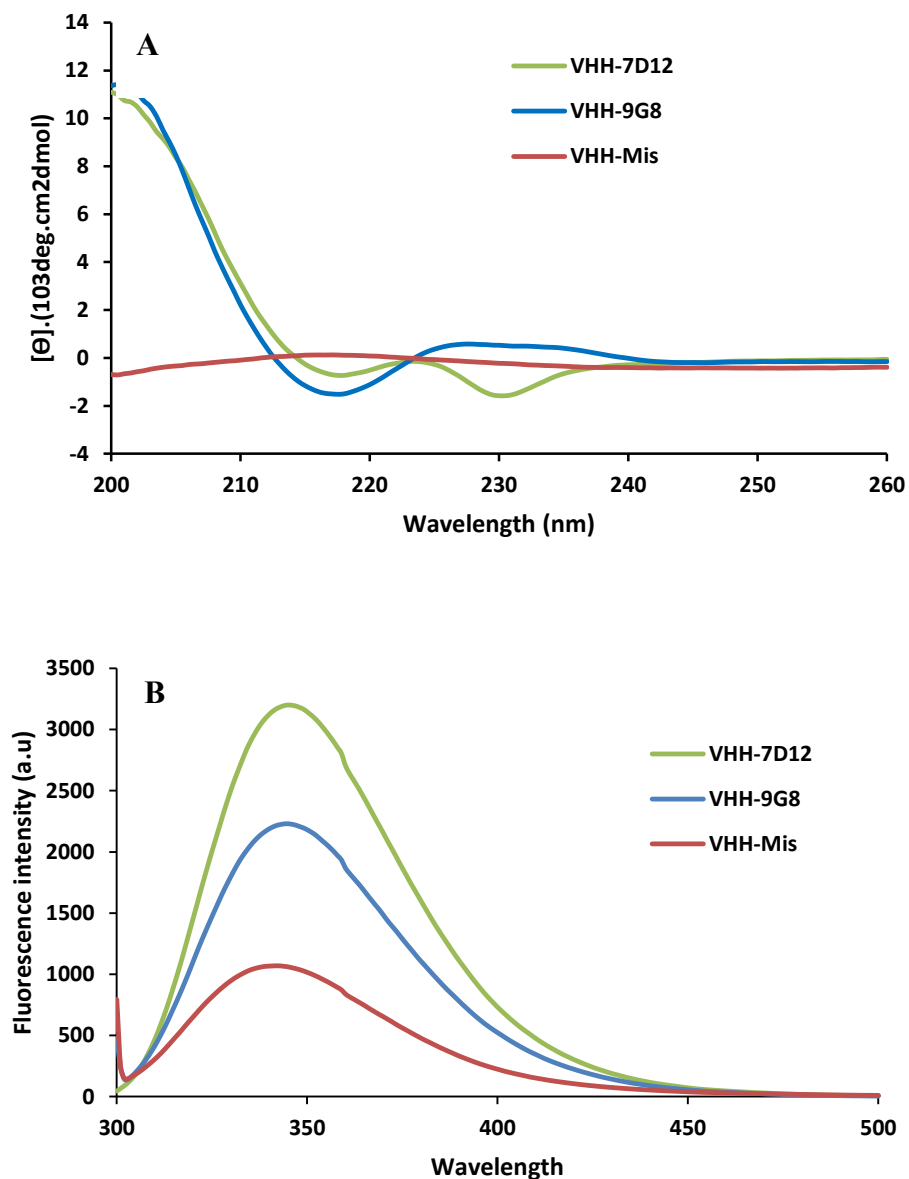


Figure 3.3. Secondary and tertiary structural properties of anti-EGFR V_{HH}: (A) Circular dichroism (cd) spectra at 37 °C and (B) Tryptophan fluorescence spectra at 37 °C. All protein samples were formulated in PBS, pH 7.4, at a concentration of 0.3 mg/mL. Three accumulations were taken for each measurements. Line symbols are explained within the panels.

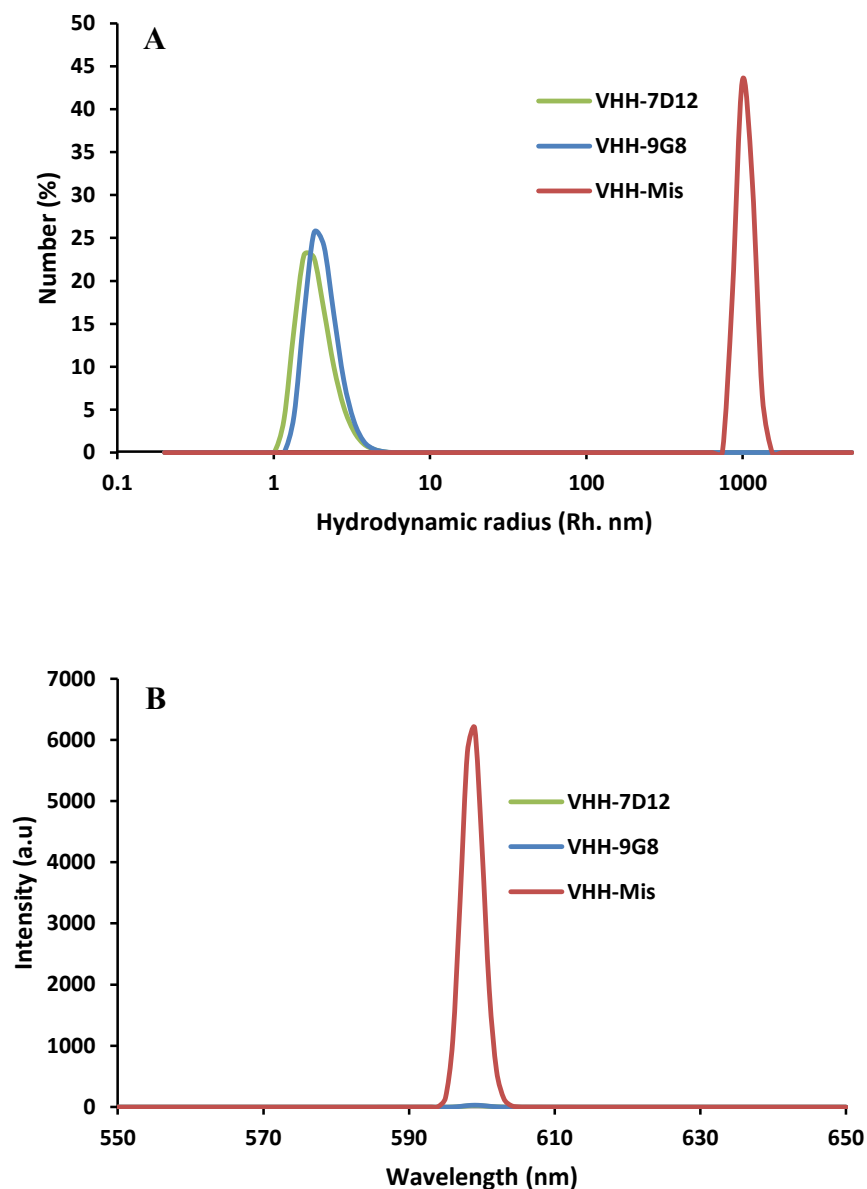


Figure 3.4. Aggregates size measurement by DLS and SLS: All protein samples were formulated in PBS, pH 7.4, at a concentration of 0.3 mg/mL **(A)** Aggregate's size of V_{HHS} measured by dynamic light scattering (DLS): spectra of size distribution in number (%) at 37 °C. **(B)** Aggregation intensities of V_{HHS} at 37 °C measured by SLS at a wavelength of 600 nm. The misfolded $V_{HH-7D12}$ (V_{HH-Mis}) showed higher scattering intensity, indicating its aggregated state, whereas native $V_{HH-7D12}$ and V_{HH-9G8} showed a minimum scattering intensity. Line symbols are explained within the panel.

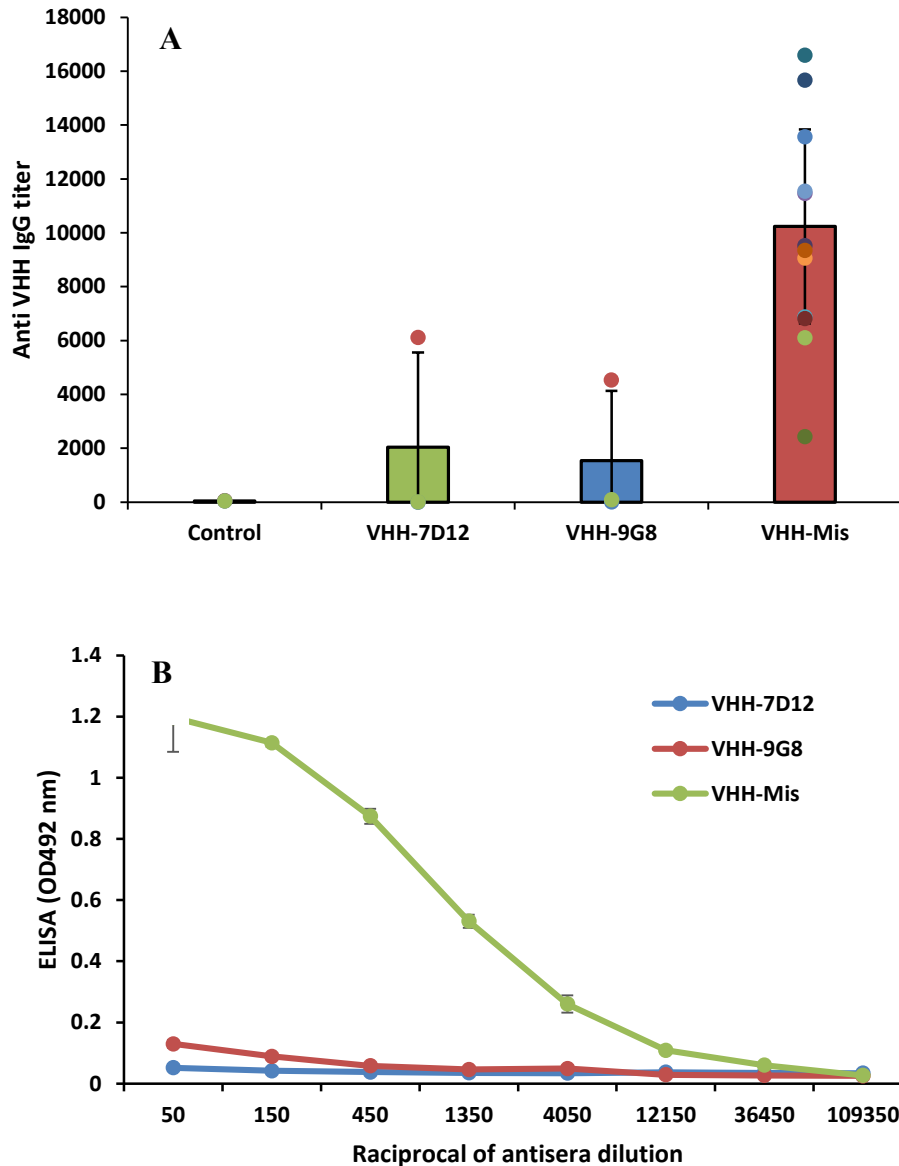


Figure 3.5: Anti-V_{HH} IgG titer by ELISA. ELISA was performed using tail bleed serum samples after six doses of subcutaneous immunization (TB-6). **(A)** anti-V_{HH} IgG titer of different V_{HH}S formulations. ELISA plates were coated with native V_{HH}-7D12 or native V_{HH}-9G8 to measure the serum IgG titer of their respective formulations. Each circle indicates the individual's mice titer, and bars show the average titer. The total number of mice in each group and the number of mice accounting for average titer calculation are shown in parentheses. **(B)** Absorbance at 492 nm versus the reciprocal dilution of anti-sera develops against V_{HH}S.

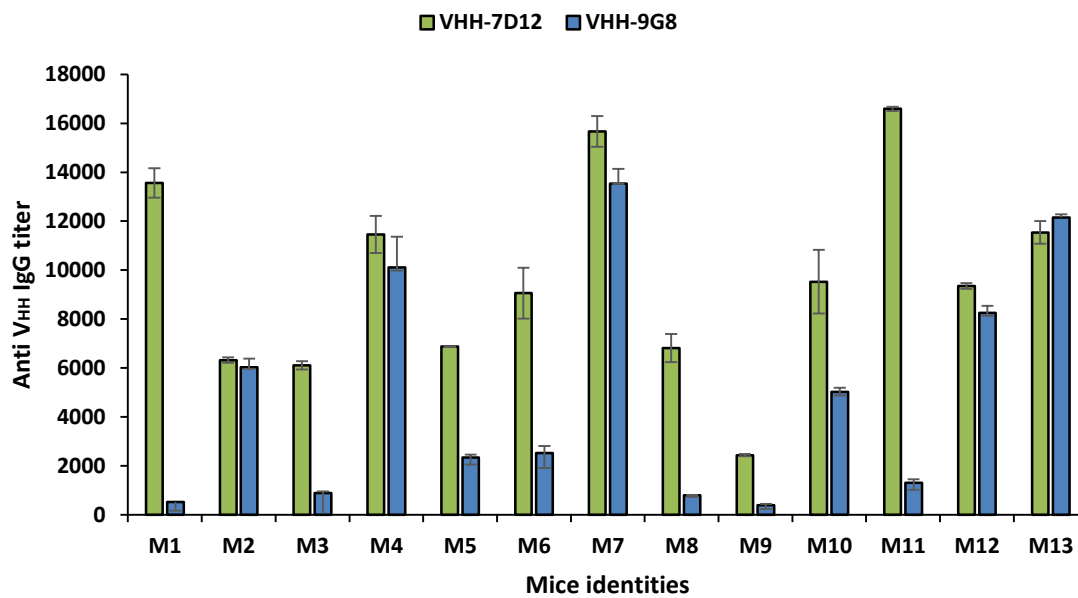


Figure 3.6: Specificity of V_{HH} -Mis anti-sera against native V_{HH} -7D12 and V_{HH} -9G8 assayed by ELISA: ELISA plate were coated with native V_{HH} -7D12 and native V_{HH} -9G8. 'M' indicates the mice's identity, and line symbols are explained within the panels.

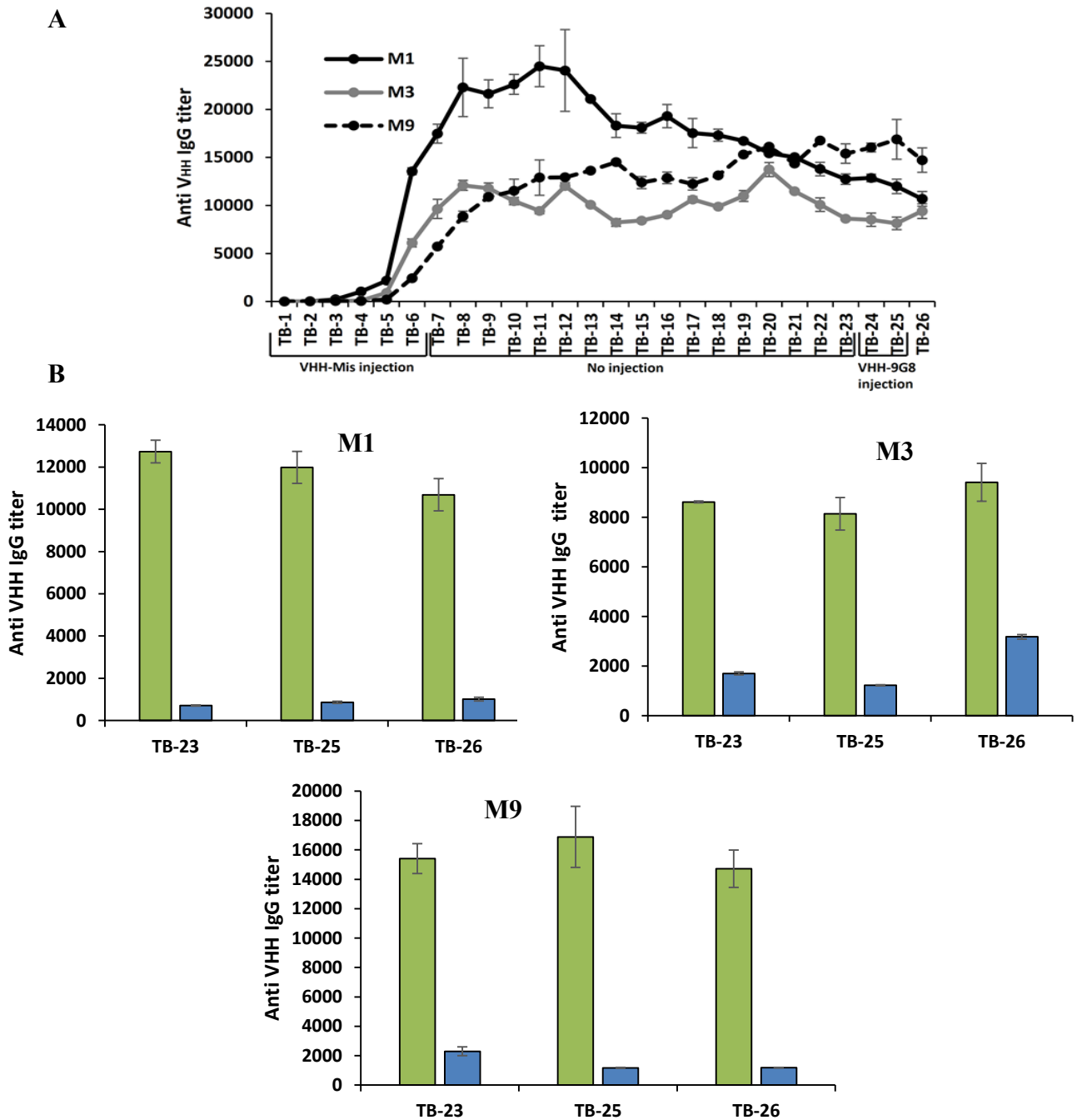


Figure 3.7: Re-immunization of Group-1 mice with native V_{HH}-9G8 (Scheme-2). (A) Long-term anti-V_{HH}-7D12 IgG titers of mice M1, M3 and M9, and the IgG titers after re-immunization with two boost shots of native V_{HH}-9G8 (TB-24 and TB-25). TB-26 was performed without immunization. (B) Specificity against native V_{HH}-7D12 and native V_{HH}-9G8 just before (TB-23) and after re-immunization with V_{HH}-9G8 (TB-25 and TB-26).

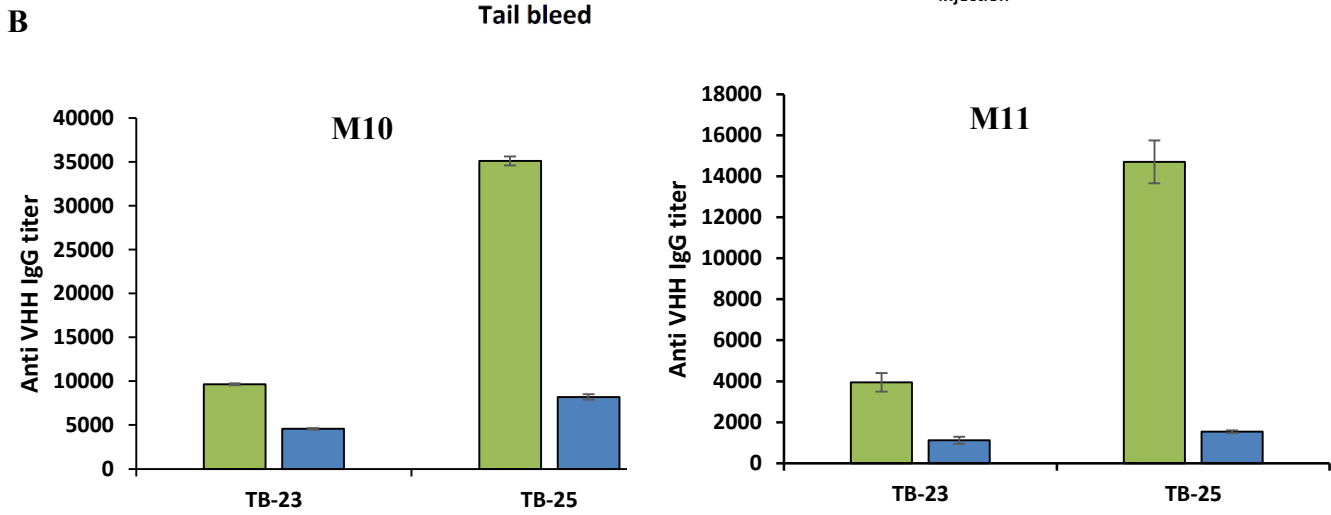
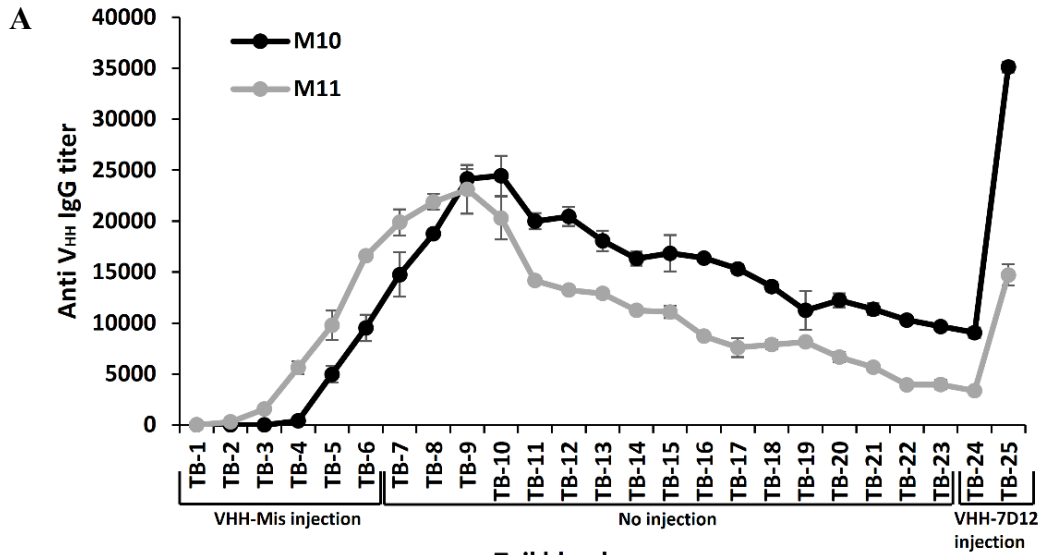


Figure 3.8: Re-immunization of Group-1 mice with native V_{HH}-7D12 (Scheme-2). (A) Long-term anti-V_{HH}-7D12 IgG titers of mice M10 and M11, and the IgG titers after re-immunization with two boost shots of native V_{HH}-9G8 (TB-24 and TB-25). (B) Specificity against native V_{HH}-7D12 and native V_{HH}-9G8 just before (TB-23) and after re-immunization with native V_{HH}-7D12 (TB-25).

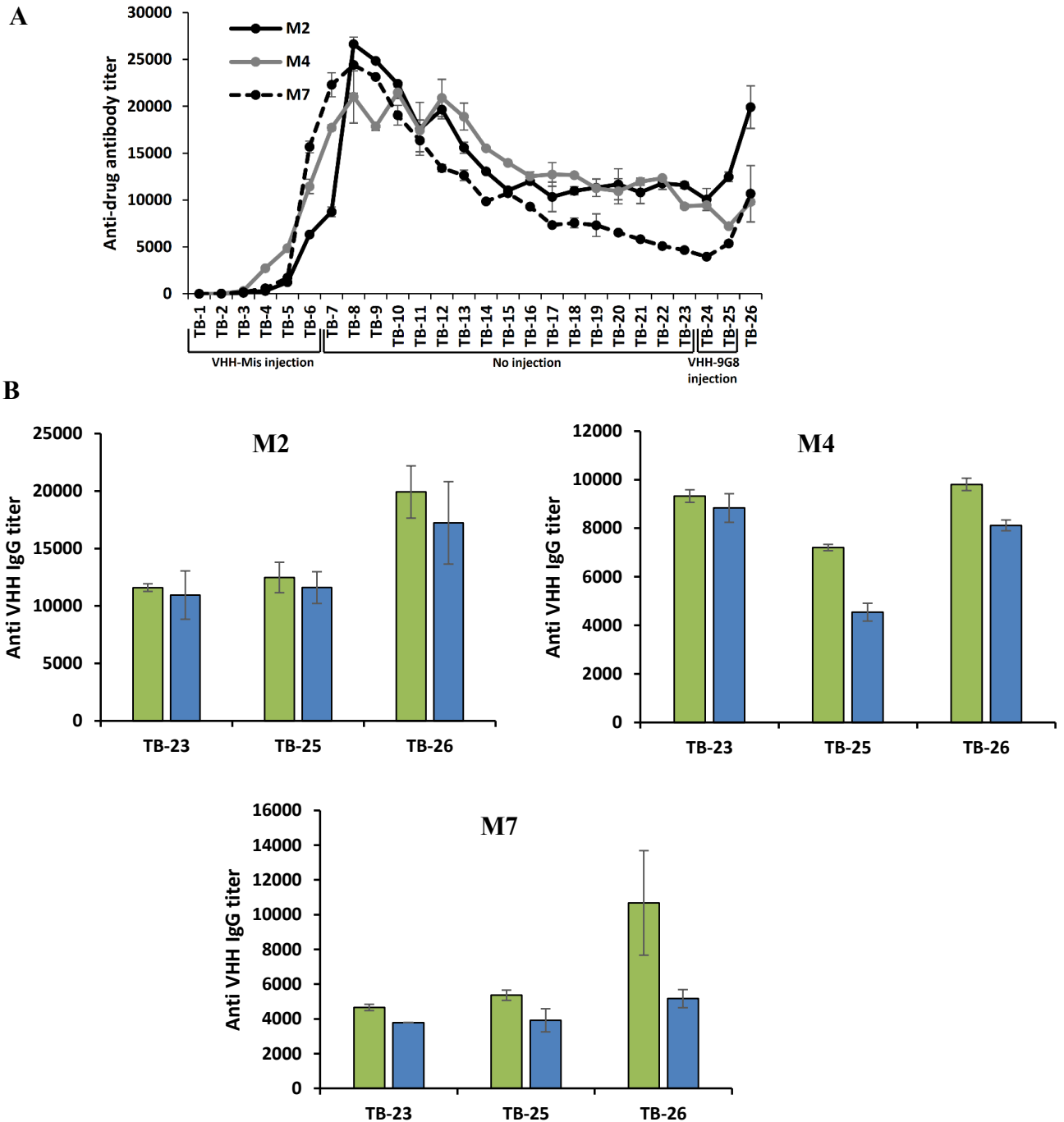


Figure 3.9: Re-immunization of Group-2 mice with native V_{HH}-9G8 (Scheme-2). (A) Long-term anti-V_{HH}-7D12 IgG titers of mice M2, M4 and M7, and the IgG titers after re-immunization with two boost shots of native V_{HH}-9G8 (TB-24 and TB-25). TB-26 was performed without immunization. (B) Specificity against native V_{HH}-7D12 and native V_{HH}-9G8 just before (TB-23) and after re-immunization with V_{HH}-9G8 (TB-25 and TB-26).

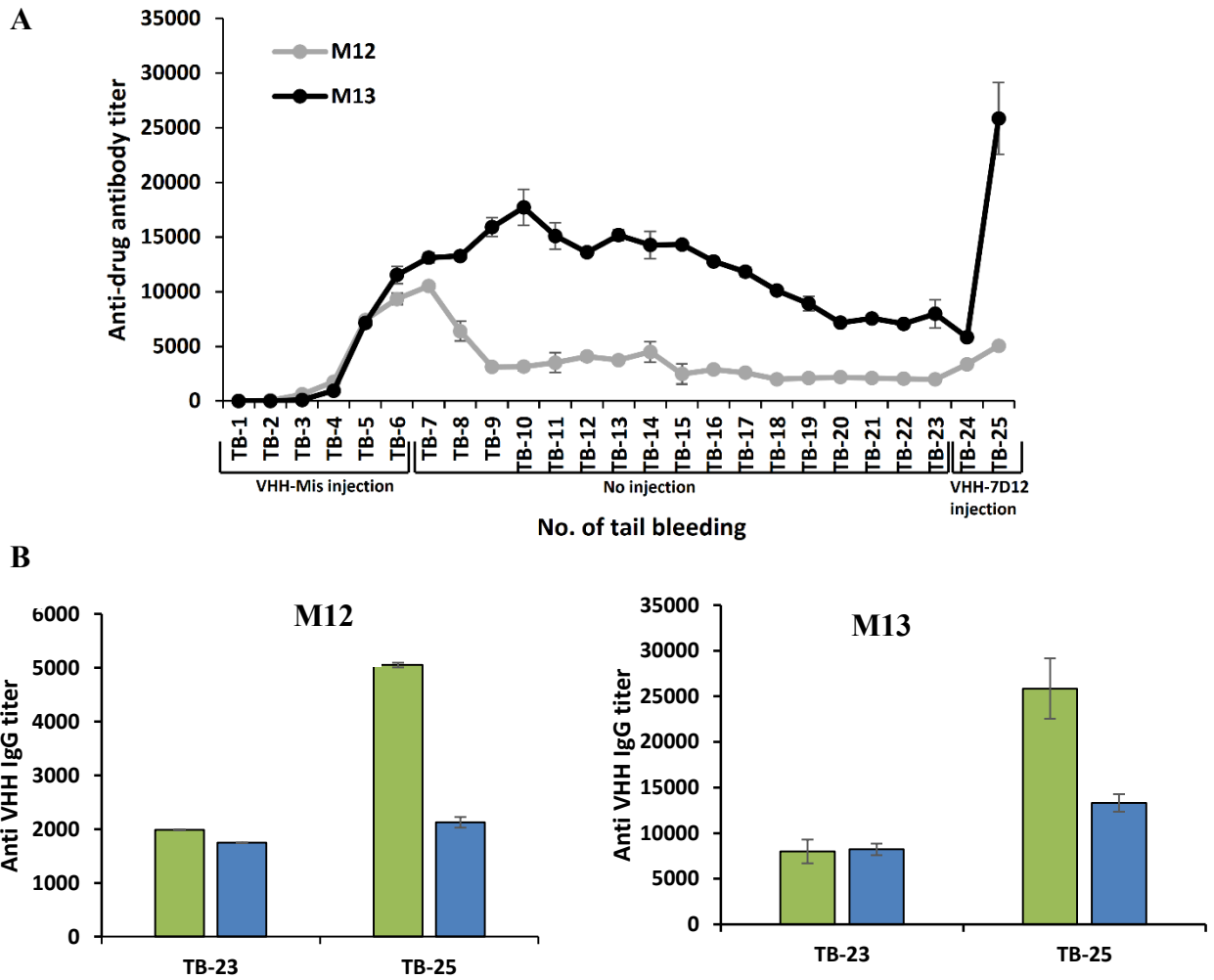


Figure 3.10: Re-immunization of Group-2 mice with native V_{HH}-7D12 (Scheme-2). (A) Long-term anti-V_{HH}-7D12 IgG titers of mice M12 and M13, and the IgG titers after re-immunization with two boost shots of native V_{HH}-9G8 (TB-24 and TB-25). (B) Specificity against native V_{HH}-7D12 and native V_{HH}-9G8 just before (TB-23) and after re-immunization with native V_{HH}-7D12 (TB-25).

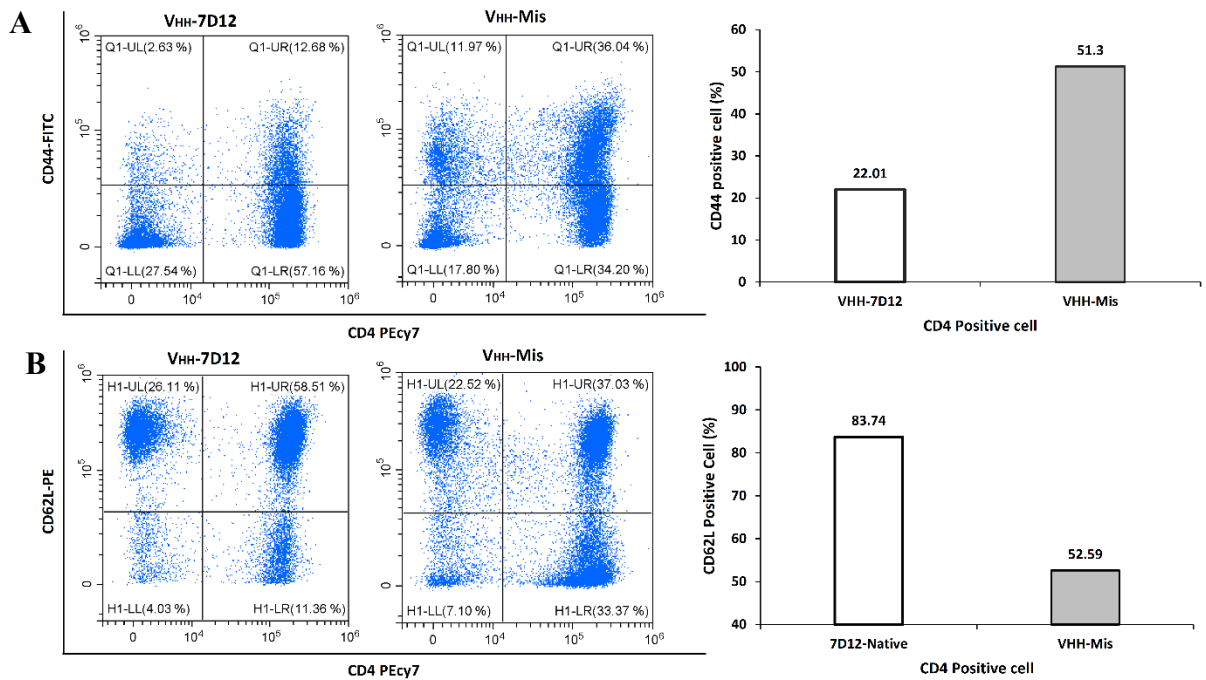


Figure 3.11. Flow-cytometry analysis of cell surface CD (cluster of differentiation) markers (T-helper cells). A single-cell suspension of mice splenocytes in FACS buffer was used for flow-cytometry analysis. Differential expressions of cell surface (A) CD44 and (B) CD 62L markers induced by native and aggregated misfolded V_{HH}-7D12 (V_{HH}-Mis) on T-helper cell (CD4⁺). V_{HH}-Mis immunized mice had a very high population of CD44⁺ Th-cell than that of native V_{HH}-7D12 immunized mice.

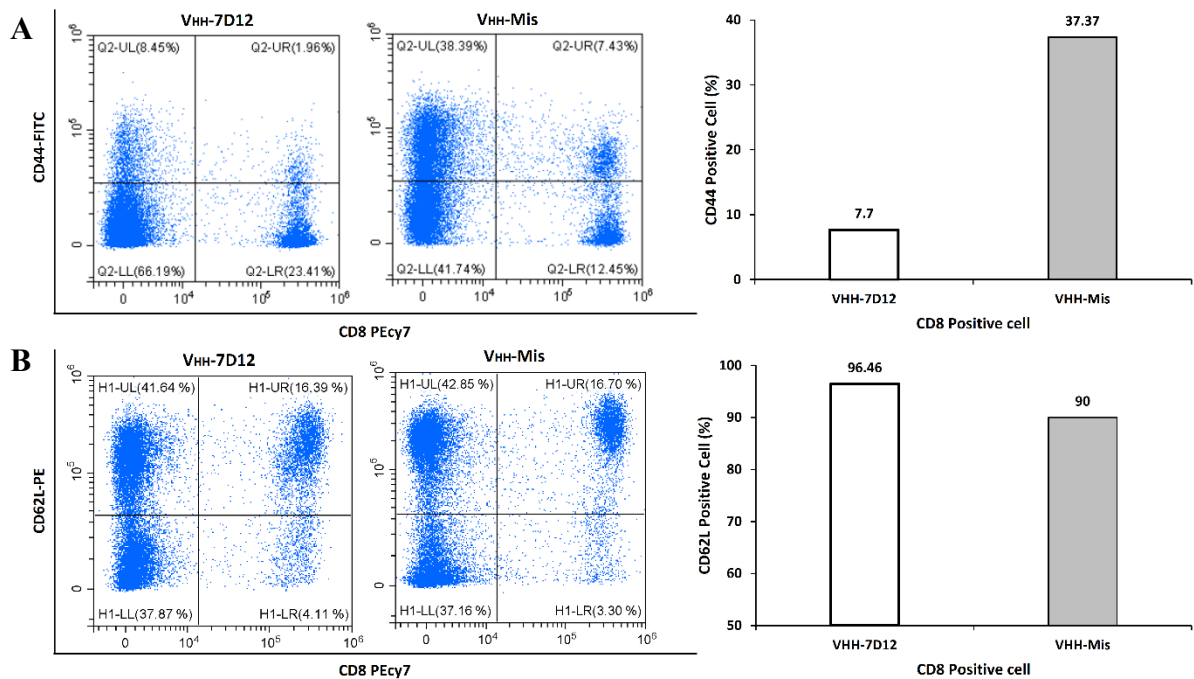


Figure 3.12. Flow-cytometry analysis of cell surface CD (cluster of differentiation) markers (T-cytolytic cells). A single-cell suspension of mice splenocytes in FACS buffer was used for flow-cytometry analysis. Differential expressions of cell surface **(A)** CD44 and **(B)** CD62L markers induced by native and aggregated misfolded V_{HH}-7D12 (V_{HH}-Mis) on T-cytolytic cell (CD8⁺). V_{HH}-Mis immunized mice had a very high population of CD44⁺ Tc-cell than that of native V_{HH}-7D12 immunized mice.

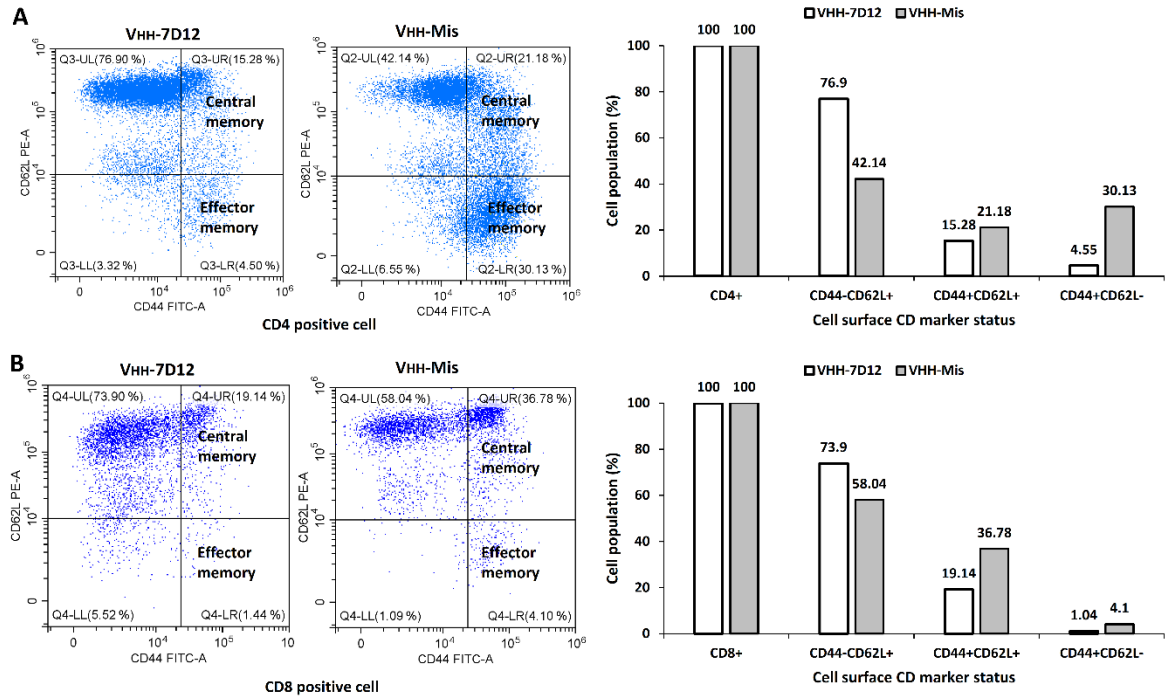


Figure 3.13. Characterization of effector and central T-cell memory by flow cytometry. A single-cell suspension of mice splenocytes in FACS buffer was used for flow-cytometry analysis. Co-expression patterns of CD44 and CD62L on Th-cell (CD4 positive cell) and Tc-cell (CD8 positive cell) are shown in panels (A) and (B), respectively. V_{HH}-Mis induced a higher proportion of CD44+CD62L+ and CD44+CD62L- expressed Th and Tc cell than that of native V_{HH}-7D12, ensuring the presence of effector and central T-cell memory.

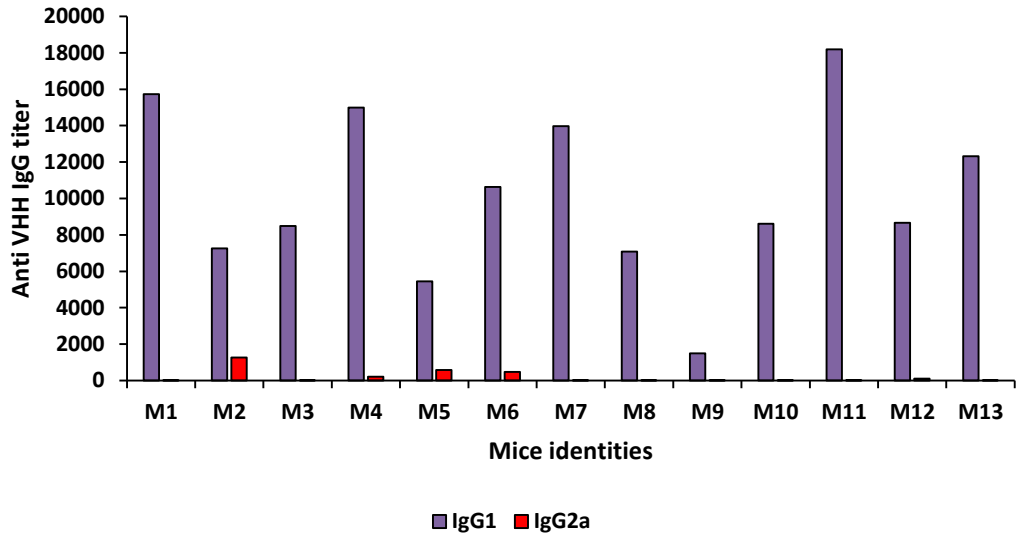


Figure 3.14. Determination of IgG sub-class by ELISA. ELISA experiment was performed following the method explained in the main text. Tail bleed 6 (TB-6) serum sample was used for ELISA experiment.

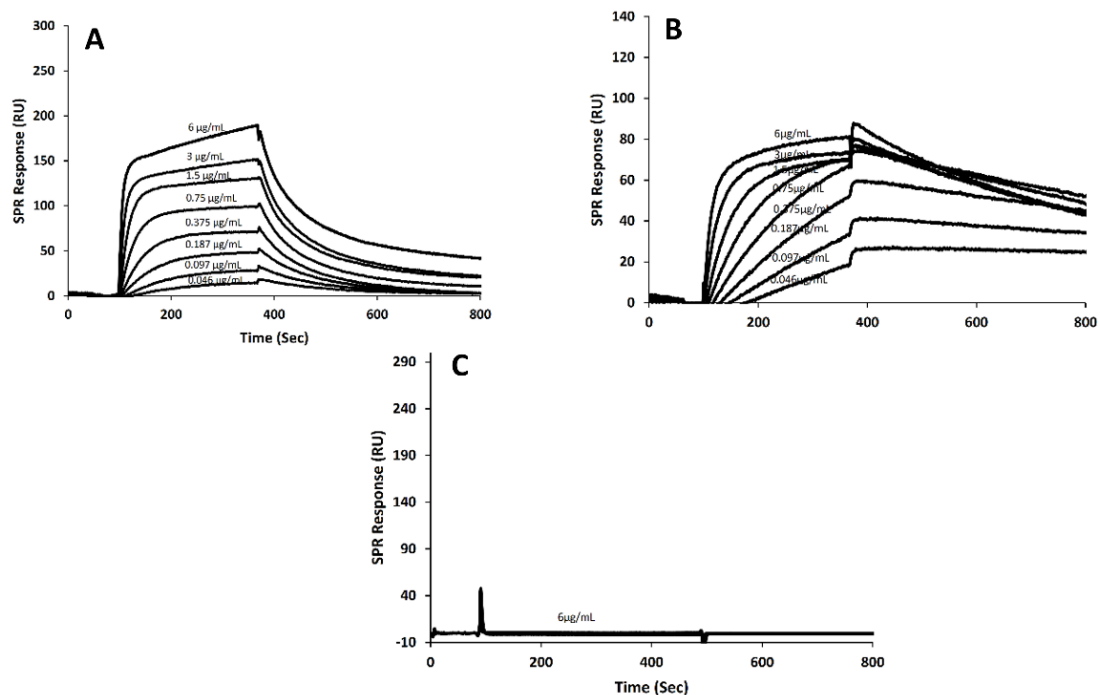


Figure 3.15. Binding activity measurement by surface plasmon resonance (SPR): The binding affinity of the anti-EGFR V_{HHs} to the extracellular domain of human EGFR (Abcam, UK) was carried out by SPR. In short, the EGFR extracellular domain was first immobilized onto the CM5 sensor chip (Biacore 2000, GE Healthcare, USA) according to the manufacturer's guidance. SPR was measured at concentrations between 6.0 and 0.046 $\mu\text{g}/\text{mL}$ at 20 $^{\circ}\text{C}$ and at a flow rate of 30 $\mu\text{L}/\text{min}$ in 10 mM HBS-EP buffer, pH 7.4, (10 mM HEPES, 150 mM NaCl, 3 mM EDTA, and 0.005% surfactant P20). SPR sonogram of (A) $V_{HH-7D12}$ (B) V_{HH-9G8} and (C) V_{HH-Mis} .

Table 3.1. Aggregate's size by DLS and SLS

V _{HH} S formulation	Hydrodynamic radius (<i>R_h</i>) by	Light scattering intensity by
	DLS	SLS
V _{HH} -7D12	1.9 ± 0.10	18.70±1.29
V _{HH} -9G8	1.98 ± 0.11	23.01±0.50
V _{HH} -Mis	1115.81 ± 312.50	6194.57±84.64

All proteins were formulated at a final concentration of 0.3 mg/mL in PBS. The values are the average of three or more independent measurements and the error are standard deviation (SD).

Table 3.2. Serum IgG titer of V_{HH}-Mis immunized mice against native V_{HH}-7D12 and V_{HH}-9G8

Group-1		
Mice ID	TB-6	
	V_{HH}-7D12	V_{HH}-9G8
M1	13565±605	513±21
M3	6099±170	889±60
M5	6873±21	2331±127
M6	9056±1045	2515±287
M8	6814±575	788±11
M9	2433±50	388±56
M10	9525±1299	5022±162
M11	16595±83	1367±151
Group-2		
M2	6318±109	6024±350
M4	11455±762	10109±1262
M7	15669±625	13537±605
M12	9344±116	8253±280
M13	11540±466	12154±121

TB: Tail bleed; M: Mouse identities

ELISA plates were coated with native V_{HH}-7D12 and native V_{HH}-9G8. The titer values are the average of two independent measurements and the errors are standard deviations (SD)

Chapter-4
Conclusions

Engineered antibody and antibody fragments are a fast-growing class of biotherapeutic protein. The generation of anti-drug antibodies (ADAs) is one of the major concerns in biotherapeutic drug development. Even though many of the intrinsic and extrinsic factors influence the anti-drug antibodies generation, protein amorphous aggregation identifies as a critical one. So far, many of the experimental studies have focused on examining the sizes of amorphous aggregates that generate ADAs, but counter-examples have led to some controversy, and it now appears that amorphous aggregates can possess unique biophysical attributes other than their sizes. In this dissertation, I systematically showed that amorphous aggregates with very similar size but distinct biochemical and biophysical nature can generate different immunogenicity. Two misfolded (V_{HH} -Ins and V_{HH} -Mis) and two heat-induced aggregates (V_{HH} -95 and V_{HH} -65) were generated from an anti-EGFR V_{HH} antibody (V_{HH} -7D12), a potential anti-cancer drug. Both of the misfolded V_{HHS} and V_{HH} -95 (complete denatured) formed aggregates with hydrodynamic radii of $\sim 2 \mu\text{m}$ according to DLS measurements, but distinct with their biochemical (intermolecular SS bonds) and biophysical properties (folded/unfolded). As such, the misfolded V_{HHS} (V_{HH} -Mis and V_{HH} -Ins) showed higher immunogenicity in mice model than heat-induced V_{HH} -95 aggregates, which formed through complete denaturation. This study shows that the biophysical and biochemical nature of aggregates play a vital role in generating ADAs, rather than the size of the aggregates, as we imagined so far, and expected to pave the way toward a deeper understanding of the immunogenic mechanism associated with aggregated therapeutic protein. Moreover, in a follow-up study with misfolded V_{HH} -7D12 (V_{HH} -Mis) aggregates we investigated the immunological memory and long-term ADAs generation risk, which rarely monitored any of the previous studies. We observed that misfolded V_{HH} aggregates can generate IgG and

immunological memory recognizing the natively folded V_{HH}-7D12's CDRs (60% mice). Such IgG and immunological memory can not recognize the analogous V_{HH} antibody-drug (V_{HH}-9G8 in our study), having similar antibody frameworks but distinct CDRs and thus safer for replacing the analogous V_{HH} antibody drugs for treatment. This observation indeed suggests that by determining the ADAs specificity one might avoid ADAs' appearance by switching the therapeutic antibody to an analogous one that targets the same EGFR and would thus allow keeping the same therapeutic strategy. The remaining 40% of the mice generated IgG and long-term immunological memory that recognizing both of the V_{HH}s (V_{HH}-7D12 and V_{HH}-9G8), indicating that the immunological response is generated against the framework regions that are common for both V_{HH}s. Such immune responses carry the long-term ADAs generation risk not only for the self V_{HH} (against immune response are generated, in this study V_{HH}-7D12) but also for analogous V_{HH} antibody (hold similar framework but different CRDs, thus functioning differently, in this study V_{HH}-9G8). As such, this study is expected to pave the way toward a deeper understanding of the long-term and cross responsive immune response against related drug molecules, particularly for the therapeutic monoclonal antibodies (mAbs) that hold similar antibody framework regions but distinct CDRs, functional region of the mAbs.

Chapter-5

References

References

1. Baker, M.P. and T.D. Jones, *Identification and removal of immunogenicity in therapeutic proteins*. *Curr Opin Drug Discov Devel*, 2007. **10**(2): p. 219-27.
2. Jacquemin, M.G. and J.M. Saint-Remy, *Factor VIII immunogenicity*. *Haemophilia*, 1998. **4**(4): p. 552-7.
3. Farrell, R.A., et al., *Development of resistance to biologic therapies with reference to IFN- β* . *Rheumatology*, 2012. **51**(4): p. 590-9.
4. Bennett, C.L., et al., *Pure red-cell aplasia and epoetin therapy*. *N Engl J Med*, 2004. **351**(14): p. 1403-8.
5. Casadevall, N., et al., *Pure red-cell aplasia and antierythropoietin antibodies in patients treated with recombinant erythropoietin*. *N Engl J Med*, 2002. **346**(7): p. 469-75.
6. Li, J., et al., *Thrombocytopenia caused by the development of antibodies to thrombopoietin*. *Blood*, 2001. **98**(12): p. 3241-8.
7. Gunn, G.R., 3rd, et al., *From the bench to clinical practice: understanding the challenges and uncertainties in immunogenicity testing for biopharmaceuticals*. *Clin Exp Immunol*, 2016. **184**(2): p. 137-46.
8. Brekke, O.H. and I. Sandlie, *Therapeutic antibodies for human diseases at the dawn of the twenty-first century*. *Nat Rev Drug Discov*, 2003. **2**(1): p. 52-62.
9. Norman, D.J., et al., *Consensus statement regarding OKT3-induced cytokine-release syndrome and human antimouse antibodies*. *Transplant Proc*, 1993. **25**(2 Suppl 1): p. 89-92.
10. Frödin, J.E., A.K. Lefvert, and H. Mellstedt, *The clinical significance of HAMA in patients treated with mouse monoclonal antibodies*. *Cell Biophys*, 1992. **21**(1-3): p. 153-65.
11. Harding, F.A., et al., *The immunogenicity of humanized and fully human antibodies: residual immunogenicity resides in the CDR regions*. *MAbs*, 2010. **2**(3): p. 256-65.
12. Ratanji, K.D., et al., *Immunogenicity of therapeutic proteins: influence of aggregation*. *J Immunotoxicol*, 2014. **11**(2): p. 99-109.
13. Ross, C., et al., *Immunogenicity of interferon-beta in multiple sclerosis patients: influence of preparation, dosage, dose frequency, and route of administration*. *Danish Multiple Sclerosis Study Group*. *Ann Neurol*, 2000. **48**(5): p. 706-12.
14. Fathallah, A.M., R.B. Bankert, and S.V. Balu-Iyer, *Immunogenicity of subcutaneously administered therapeutic proteins--a mechanistic perspective*. *The AAPS journal*, 2013. **15**(4): p. 897-900.
15. Jarvi, N.L. and S.V. Balu-Iyer, *Immunogenicity challenges associated with subcutaneous delivery of therapeutic proteins*. *BioDrugs*, 2021. **35**(2): p. 125-146.
16. Fakharzadeh, S.S. and H.H. Kazazian, Jr., *Correlation between factor VIII genotype and inhibitor development in hemophilia A*. *Semin Thromb Hemost*, 2000. **26**(2): p. 167-71.
17. Schwaab, R., et al., *Haemophilia A: mutation type determines risk of inhibitor formation*. *Thromb Haemost*, 1995. **74**(6): p. 1402-6.
18. Scharrer, I., G.L. Bray, and O. Neutzling, *Incidence of inhibitors in haemophilia A patients--a review of recent studies of recombinant and plasma-derived factor VIII concentrates*. *Haemophilia*, 1999. **5**(3): p. 145-54.

19. Hermeling, S., et al., *Structural characterization and immunogenicity in wild-type and immune tolerant mice of degraded recombinant human interferon alpha2b*. Pharm Res, 2005. **22**(12): p. 1997-2006.
20. Verthelyi, D. and V. Wang, *Trace levels of innate immune response modulating impurities (IIRMI)s synergize to break tolerance to therapeutic proteins*. PLoS One, 2010. **5**(12): p. 0015252.
21. Moore, W.V., *The role of aggregated hGH in therapy of hGH-deficient children*. J Clin Endocrinol Metab, 1978. **46**(1): p. 20-7.
22. Moore, W.V. and P. Leppert, *Role of aggregated human growth hormone (hGH) in development of antibodies to hGH*. J Clin Endocrinol Metab, 1980. **51**(4): p. 691-7.
23. Rosenberg, A.S., *Effects of protein aggregates: an immunologic perspective*. Aaps J, 2006. **8**(3).
24. Sauerborn, M., et al., *Immunological mechanism underlying the immune response to recombinant human protein therapeutics*. Trends Pharmacol Sci, 2010. **31**(2): p. 53-9.
25. Christian, C., *Studies of Aggregated γ -Globulin II. effect in vivo*. Journal of Immunology, 1960. **84**: p. 117-121.
26. Christian, C.L., *Studies of aggregated gamma-globulin. I. Sedimentation, electrophoretic and anticomplementary properties*. J Immunol, 1960. **84**: p. 112-6.
27. Ellis, E.F. and C.S. Henney, *Adverse reactions following administration of human gamma globulin*. J Allergy, 1969. **43**(1): p. 45-54.
28. Bachmann, M.F., et al., *Correlation of tolerogenicity of a viral antigen with its immunogenicity*. The Journal of Immunology, 1997. **158**(11): p. 5106-5111.
29. Dintzis, R.Z., M.H. Middleton, and H.M. Dintzis, *Studies on the immunogenicity and tolerogenicity of T-independent antigens*. J Immunol, 1983. **131**(5): p. 2196-203.
30. Carpenter, J.F., et al., *Overlooking subvisible particles in therapeutic protein products: gaps that may compromise product quality*. Journal of pharmaceutical sciences, 2009. **98**(4): p. 1201-5.
31. Hermeling, S., et al., *Antibody response to aggregated human interferon alpha2b in wild-type and transgenic immune tolerant mice depends on type and level of aggregation*. Journal of pharmaceutical sciences, 2006. **95**(5): p. 1084-96.
32. Grillo, A.O., et al., *Conformational origin of the aggregation of recombinant human factor VIII*. Biochemistry, 2001. **40**(2): p. 586-595.
33. Purohit, V.S., C.R. Middaugh, and S.V. Balasubramanian, *Influence of aggregation on immunogenicity of recombinant human Factor VIII in hemophilia A mice*. Journal of pharmaceutical sciences, 2006. **95**(2): p. 358-371.
34. Ramani, K., et al., *Aggregation kinetics of recombinant human FVIII (rFVIII)*. Journal of pharmaceutical sciences, 2005. **94**(9): p. 2023-2029.
35. Fathallah, A.M., et al., *The Effect of small oligomeric protein aggregates on the immunogenicity of intravenous and subcutaneous administered antibodies*. J Pharm Sci, 2015. **104**(11): p. 3691-3702.
36. Fradkin, A.H., J.F. Carpenter, and T.W. Randolph, *Glass particles as an adjuvant: a model for adverse immunogenicity of therapeutic proteins*. Journal of pharmaceutical sciences, 2011. **100**(11): p. 4953-64.

37. Kijanka, G., et al., *Submicron size particles of a murine monoclonal antibody are more immunogenic than soluble oligomers or micron size particles upon subcutaneous administration in mice*. J Pharm Sci, 2018. **107**(11): p. 2847-2859.
38. Ratanji, K.D., et al., *Editor's Highlight: Subvisible aggregates of immunogenic proteins promote a Th1-type response*. Toxicological sciences : an official journal of the Society of Toxicology, 2016. **153**(2): p. 258-270.
39. Boll, B., et al., *Extensive chemical modifications in the primary protein structure of IgG1 subvisible particles are necessary for breaking immune tolerance*. Molecular Pharmaceutics, 2017. **14**(4): p. 1292-1299.
40. Rahman, N., et al., *Nanometer-sized aggregates generated using short solubility controlling peptide tags do increase the in vivo immunogenicity of a nonimmunogenic protein*. Mol Pharm, 2020. **17**(5): p. 1629-1637.
41. Cromwell, M.E.M., E. Hilario, and F. Jacobson, *Protein aggregation and bioprocessing*. The AAPS journal, 2006. **8**(3): p. E572-E579.
42. Wang, W., S. Nema, and D. Teagarden, *Protein aggregation--pathways and influencing factors*. Int J Pharm, 2010. **390**(2): p. 89-99.
43. Cordoba-Rodriguez, R., *Aggregates in MABs and recombinant therapeutic Proteins : a regulatory perspective*. Biopharm International, 2008. **21**.
44. Borgia, M.B., et al., *A mechanistic model for amorphous protein aggregation of immunoglobulin-like domains*. Journal of the American Chemical Society, 2013. **135**(17): p. 6456-6464.
45. Inyang, U.E. and A.O. Iduh, *Influence of pH and salt concentration on protein solubility, emulsifying and foaming properties of sesame protein concentrate*. Journal of the American Oil Chemists' Society, 1996. **73**(12): p. 1663-1667.
46. Li, Y., B.A. Ogunnaiké, and C.J. Roberts, *Multi-variate approach to global protein aggregation behavior and kinetics: effects of pH, NaCl, and temperature for alpha-chymotrypsinogen A*. Journal of pharmaceutical sciences, 2010. **99**(2): p. 645-62.
47. Schein, C.H., *Solubility as a function of protein structure and solvent components*. Bio/Technology, 1990. **8**(4): p. 308-317.
48. Niwa, T., et al., *Bimodal protein solubility distribution revealed by an aggregation analysis of the entire ensemble of Escherichia coli proteins*. Proc Natl Acad Sci U S A, 2009. **106**(11): p. 4201-6.
49. Mahler, H.C., et al., *Protein aggregation: pathways, induction factors and analysis*. J Pharm Sci, 2009. **98**(9): p. 2909-34.
50. Zhang, Z., H. Pan, and X. Chen, *Mass spectrometry for structural characterization of therapeutic antibodies*. Mass Spectrom Rev, 2009. **28**(1): p. 147-76.
51. Finley, E.L., et al., *Identification of tryptophan oxidation products in bovine alpha-crystallin*. Protein Sci, 1998. **7**(11): p. 2391-7.
52. Pan, H., et al., *Methionine oxidation in human IgG2 Fc decreases binding affinities to protein A and FcRn*. Protein Sci, 2009. **18**(2): p. 424-33.
53. Schöneich, C., *Mechanisms of metal-catalyzed oxidation of histidine to 2-oxo-histidine in peptides and proteins*. J Pharm Biomed Anal, 2000. **21**(6): p. 1093-7.
54. Luo, Q., et al., *Chemical modifications in therapeutic protein aggregates generated under different stress conditions*. J Biol Chem, 2011. **286**(28): p. 25134-44.
55. Huang, L., et al., *In vivo deamidation characterization of monoclonal antibody by LC/MS/MS*. Anal Chem, 2005. **77**(5): p. 1432-9.

56. Connolly, B.D., et al., *Weak interactions govern the viscosity of concentrated antibody solutions: high-throughput analysis using the diffusion interaction parameter.* Biophys J, 2012. **103**(1): p. 69-78.
57. Wang, W., et al., *Immunogenicity of protein aggregates--concerns and realities.* Int J Pharm, 2012. **431**(1-2): p. 1-11.
58. Frokjaer, S. and D.E. Otzen, *Protein drug stability: a formulation challenge.* Nat Rev Drug Discov, 2005. **4**(4): p. 298-306.
59. Fink, A.L., *Protein aggregation: folding aggregates, inclusion bodies and amyloid.* Folding and Design, 1998. **3**(1): p. R9-R23.
60. Rambaran, R.N. and L.C. Serpell, *Amyloid fibrils: abnormal protein assembly.* Prion, 2008. **2**(3): p. 112-117.
61. Karshikoff, A., *Non-covalent interactions in proteins.* 2006, London; Hackensack, NJ: Imperial College Press ; Distributed by World Scientific Pub. Co. Pte. Ltd.
62. Narhi, L.O., et al., *Classification of protein aggregates.* J Pharm Sci, 2012. **101**(2): p. 493-8.
63. Currais, A., et al., *Intraneuronal protein aggregation as a trigger for inflammation and neurodegeneration in the aging brain.* The FASEB Journal, 2017. **31**(1): p. 5-10.
64. Fathallah, A.M., R.B. Bankert, and S.V. Balu-Iyer, *Immunogenicity of subcutaneously administered therapeutic proteins--a mechanistic perspective.* Aaps J, 2013. **15**(4): p. 897-900.
65. Haile, L.A., et al., *In vivo effect of innate immune response modulating impurities on the skin milieu using a macaque model: impact on product immunogenicity.* Journal of pharmaceutical sciences, 2017. **106**(3): p. 751-760.
66. Udan, M.L., et al., *Toll-like receptors 2 and 4 mediate Abeta(1-42) activation of the innate immune response in a human monocytic cell line.* J Neurochem, 2008. **104**(2): p. 524-33.
67. Aderem, A. and R.J. Ulevitch, *Toll-like receptors in the induction of the innate immune response.* Nature, 2000. **406**(6797): p. 782-7.
68. Hoffmann, J.A., et al., *Phylogenetic perspectives in innate immunity.* Science, 1999. **284**(5418): p. 1313-8.
69. Boehme, K.W. and T. Compton, *Innate sensing of viruses by toll-like receptors.* J Virol, 2004. **78**(15): p. 7867-73.
70. Joubert, M.K., et al., *Highly aggregated antibody therapeutics can enhance the in vitro innate and late-stage T-cell immune responses.* J Biol Chem, 2012. **287**(30): p. 25266-79.
71. Luo, Y., et al., *Dimers and multimers of monoclonal IgG1 exhibit higher in vitro binding affinities to Fc gamma receptors.* mAbs, 2009. **1**(5): p. 491-504.
72. Sarma, J.V. and P.A. Ward, *The complement system.* Cell Tissue Res, 2011. **343**(1): p. 227-35.
73. Doekes, G., L.A. Vanes, and M.R. Daha, *Influence of aggregate size on the binding and activation of the first component of human complement by soluble IgG aggregates.* Immunology, 1982. **45**(4): p. 705-713.
74. García, M., et al., *Effect of preservatives on IgG aggregation, complement-activating effect and hypotensive activity of horse polyvalent antivenom used in snakebite envenomation.* Biologicals, 2002. **30**(2): p. 143-51.

75. Merad, M. and M.G. Manz, *Dendritic cell homeostasis*. Blood, 2009. **113**(15): p. 3418-27.
76. Bessa, J., et al., *The immunogenicity of antibody aggregates in a novel transgenic mouse model*. Pharm Res, 2015. **32**(7): p. 2344-59.
77. Martín-Fontecha, A., A. Lanzavecchia, and F. Sallusto, *Dendritic cell migration to peripheral lymph nodes*. Handb Exp Pharmacol, 2009. **188**: p. 31-49.
78. Dintzis, H.M., R.Z. Dintzis, and B. Vogelstein, *Molecular determinants of immunogenicity: the immunon model of immune response*. Proc Natl Acad Sci U S A, 1976. **73**(10): p. 3671-5.
79. Bachmann, M.F., et al., *The influence of antigen organization on B cell responsiveness*. Science, 1993. **262**(5138): p. 1448-51.
80. Ceresa, B.P. and J.L. Peterson, *Chapter Five - Cell and molecular biology of epidermal growth factor receptor*, in *international review of cell and molecular biology*, K.W. Jeon, Editor. 2014, Academic Press. p. 145-178.
81. Keating, G.M., *Panitumumab*. Drugs, 2010. **70**(8): p. 1059-1078.
82. Li, S., et al., *Structural basis for inhibition of the epidermal growth factor receptor by cetuximab*. Cancer Cell, 2005. **7**(4): p. 301-311.
83. Holliger, P. and P.J. Hudson, *Engineered antibody fragments and the rise of single domains*. Nature Biotechnology, 2005. **23**(9): p. 1126-1136.
84. Conrath, K.E., et al., *β -lactamase inhibitors derived from single-domain antibody fragments elicited in the Camelidae*. Antimicrobial Agents and Chemotherapy, 2001. **45**(10): p. 2807-2812.
85. Desmyter, A., et al., *Crystal structure of a camel single-domain VH antibody fragment in complex with lysozyme*. Nature Structural Biology, 1996. **3**(9): p. 803-811.
86. Rasmussen, S.G.F., et al., *Structure of a nanobody-stabilized active state of the β 2 adrenoceptor*. Nature, 2011. **469**(7329): p. 175-180.
87. Leader, B., Q.J. Baca, and D.E. Golan, *Protein therapeutics: a summary and pharmacological classification*. Nature Reviews Drug Discovery, 2008. **7**: p. 21.
88. Schellekens, H., *Immunogenicity of therapeutic proteins: clinical implications and future prospects*. Clin Ther, 2002. **24**(11): p. 1720-40.
89. Shankar, G., et al., *Assessment and reporting of the clinical immunogenicity of therapeutic proteins and peptides-harmonized terminology and tactical recommendations*. Aaps J, 2014. **16**(4): p. 658-73.
90. Henney, C.S. and E.F. Ellis, *Antibody production to aggregated human gamma-G globulin in acquired hypogammaglobulinemia*. N Engl J Med, 1968. **278**(21): p. 1144-6.
91. Ryff, J.C., *Clinical investigation of the immunogenicity of interferon-alpha 2a*. J Interferon Cytokine Res, 1997. **17**(1): p. S29-33.
92. van Beers, M.M., et al., *Oxidized and aggregated recombinant human interferon beta is immunogenic in human interferon beta transgenic mice*. Pharm Res, 2011. **28**(10): p. 2393-402.
93. Pisal, D.S., et al., *Native-like aggregates of factor VIII are immunogenic in von Willebrand factor deficient and hemophilia a mice*. J Pharm Sci, 2012. **101**(6): p. 2055-65.

94. Rombach-Riegraf, V., et al., *Aggregation of human recombinant monoclonal antibodies influences the capacity of dendritic cells to stimulate adaptive T-cell responses in vitro*. PLoS One, 2014. **9**(1).
95. Purohit, V.S., C.R. Middaugh, and S.V. Balasubramanian, *Influence of aggregation on immunogenicity of recombinant human Factor VIII in hemophilia A mice*. J Pharm Sci, 2006. **95**(2): p. 358-71.
96. Filipe, V., et al., *Immunogenicity of different stressed IgG monoclonal antibody formulations in immune tolerant transgenic mice*. MAbs, 2012. **4**(6): p. 740-52.
97. Bi, V., et al., *Development of a human antibody tolerant mouse model to assess the immunogenicity risk due to aggregated biotherapeutics*. Journal of Pharmaceutical Sciences, 2013. **102**(10): p. 3545-3555.
98. Yoshimura, Y., et al., *Distinguishing crystal-like amyloid fibrils and glass-like amorphous aggregates from their kinetics of formation*. Proc Natl Acad Sci U S A, 2012. **109**(36): p. 14446-51.
99. Roberts, C.J., *Non-native protein aggregation kinetics*. Biotechnol Bioeng, 2007. **98**(5): p. 927-38.
100. Uchiyama, S., *Liquid formulation for antibody drugs*: Biochim Biophys Acta. 2014 Nov;1844(11):2041-2052. doi: 10.1016/j.bbapap.2014.07.016. Epub 2014 Aug 13.
101. Vazquez-Rey, M. and D.A. Lang, *Aggregates in monoclonal antibody manufacturing processes*. Biotechnol Bioeng, 2011. **108**(7): p. 1494-508.
102. Roovers, R.C., et al., *A biparatopic anti-EGFR nanobody efficiently inhibits solid tumour growth*. Int J Cancer, 2011. **129**(8): p. 2013-24.
103. Ceresa, B.P. and J.L. Peterson, *Cell and molecular biology of epidermal growth factor receptor*. Int Rev Cell Mol Biol, 2014. **313**: p. 145-78.
104. Martinelli, E., et al., *Anti-epidermal growth factor receptor monoclonal antibodies in cancer therapy*. Clinical and experimental immunology, 2009. **158**(1): p. 1-9.
105. Holliger, P. and P.J. Hudson, *Engineered antibody fragments and the rise of single domains*. Nat Biotechnol, 2005. **23**(9): p. 1126-36.
106. Kuriakose, A., N. Chirmule, and P. Nair, *Immunogenicity of biotherapeutics: Causes and association with posttranslational modifications*. J Immunol Res, 2016. **1298473**(10): p. 29.
107. Doering, D.S. and P. Matsudaira, *Cysteine scanning mutagenesis at 40 of 76 positions in villin headpiece maps the F-actin binding site and structural features of the domain*. Biochemistry, 1996. **35**(39): p. 12677-85.
108. Akazawa-Ogawa, Y., H. Nagai, and Y. Hagihara, *Heat denaturation of the antibody, a multi-domain protein*. Biophys Rev, 2018. **10**(2): p. 255-258.
109. Micsonai, A., et al., *BeStSel: a web server for accurate protein secondary structure prediction and fold recognition from the circular dichroism spectra*. Nucleic Acids Res, 2018. **46**(W1): p. W315-W322.
110. Fink, A.L., et al., *Classification of acid denaturation of proteins: intermediates and unfolded states*. Biochemistry, 1994. **33**(41): p. 12504-11.
111. Hawe, A., M. Sutter, and W. Jiskoot, *Extrinsic fluorescent dyes as tools for protein characterization*. Pharmaceutical research, 2008. **25**(7): p. 1487-1499.
112. Akazawa-Ogawa, Y., et al., *Heat-induced irreversible denaturation of the camelid single domain VHH antibody is governed by chemical modifications*. J Biol Chem, 2014. **289**(22): p. 15666-79.

113. Nautiyal, K., et al., *Design and assessment of an active anti-epidermal growth factor receptor (EGFR) single chain variable fragment (ScFv) with improved solubility*. Biochem Biophys Res Commun, 2019. **508**(4): p. 1043-1049.
114. Kuroda, Y., S. Endo, and H. Nakamura, *How a novel scientific concept was coined the "Molten Globule State"*. Biomolecules, 2020. **10**(2): p. 269.
115. Rarity, J.G., et al., *Light-scattering studies of aggregation*. Proceedings of the Royal Society of London. Series A, Mathematical and Physical Sciences, 1989. **423**(1864): p. 89-102.
116. Moussa, E.M., et al., *Immunogenicity of therapeutic protein aggregates*. J Pharm Sci, 2016. **105**(2): p. 417-430.
117. Schellekens, H., *Bioequivalence and the immunogenicity of biopharmaceuticals*. Nat Rev Drug Discov, 2002. **1**(6): p. 457-62.
118. Jiskoot, W., et al., *Mouse models for assessing protein immunogenicity: Lessons and challenges*. J Pharm Sci, 2016. **105**(5): p. 1567-1575.
119. Ghisaidoobe, A.B.T. and S.J. Chung, *Intrinsic tryptophan fluorescence in the detection and analysis of proteins: a focus on Förster resonance energy transfer techniques*. International journal of molecular sciences, 2014. **15**(12): p. 22518-22538.
120. Fradkin, A.H., et al., *UV photodegradation of murine growth hormone: Chemical analysis and immunogenicity consequences*. European Journal of Pharmaceutics and Biopharmaceutics, 2014. **87**(2): p. 395-402.
121. Islam, M.M., et al., *Anti-dengue ED3 long-term immune response with T-cell memory generated using solubility controlling peptide tags*. Frontiers in immunology, 2020. **11**: p. 333-333.
122. Fink, A.L., *Protein aggregation: folding aggregates, inclusion bodies and amyloid*. Fold Des, 1998. **3**(1): p. 00002-9.
123. Mitraki, A. and J. King, *Protein folding intermediates and inclusion body formation*. Bio/Technology, 1989. **7**(7): p. 690-697.
124. Saotome, T., T. Yamazaki, and Y. Kuroda, *Misfolding of a single disulfide bonded globular protein into a low-solubility species conformationally and biophysically distinct from the native one*. Biomolecules, 2019. **9**(6).
125. Sen Mojumdar, S., et al., *Partially native intermediates mediate misfolding of SOD1 in single-molecule folding trajectories*. Nat Commun, 2017. **8**(1): p. 017-01996.
126. Groell, F., O. Jordan, and G. Borchard, *In vitro models for immunogenicity prediction of therapeutic proteins*. European Journal of Pharmaceutics and Biopharmaceutics, 2018. **130**: p. 128-142.
127. Sauerborn, M., et al., *Immunological mechanism underlying the immune response to recombinant human protein therapeutics*. Trends in Pharmacological Sciences, 2010. **31**(2): p. 53-59.
128. van Beers, M.M., et al., *Aggregated recombinant human interferon Beta induces antibodies but no memory in immune-tolerant transgenic mice*. Pharm Res, 2010. **27**(9): p. 1812-24.
129. Schellekens, H., *Bioequivalence and the immunogenicity of biopharmaceuticals*. Nature Reviews Drug Discovery, 2002. **1**(6): p. 457-462.
130. Tieu, P., A. Chan, and D. Martino, *Molecular mechanisms of inhibitor development in hemophilia*. Mediterr J Hematol Infect Dis, 2020. **12**(1).

131. Banugaria, S.G., et al., *The impact of antibodies on clinical outcomes in diseases treated with therapeutic protein: lessons learned from infantile Pompe disease*. Genet Med, 2011. **13**(8): p. 729-36.
132. Pisal, D.S., et al., *Native-like aggregates of factor VIII are immunogenic in von Willebrand factor deficient and hemophilia a mice*. Journal of Pharmaceutical Sciences, 2012. **101**(6): p. 2055-2065.
133. Fradkin, A.H., J.F. Carpenter, and T.W. Randolph, *Immunogenicity of aggregates of recombinant human growth hormone in mouse models*. J Pharm Sci, 2009. **98**(9): p. 3247-64.
134. Filipe, V., et al., *Immunogenicity of different stressed IgG monoclonal antibody formulations in immune tolerant transgenic mice*. mAbs, 2012. **4**(6): p. 740-752.
135. Eyes, T.J., et al., *Identification of B cell epitopes enhanced by protein unfolding and aggregation*. Molecular Immunology, 2019. **105**: p. 181-189.
136. Nelson, A.L., *Antibody fragments: hope and hype*. mAbs, 2010. **2**(1): p. 77-83.
137. Nelson, A.L. and J.M. Reichert, *Development trends for therapeutic antibody fragments*. Nature Biotechnology, 2009. **27**(4): p. 331-337.
138. Schrama, D., R.A. Reisfeld, and J.C. Becker, *Antibody targeted drugs as cancer therapeutics*. Nat Rev Drug Discov, 2006. **5**(2): p. 147-59.
139. Hoey, R.J., H. Eom, and J.R. Horn, *Structure and development of single domain antibodies as modules for therapeutics and diagnostics*. Experimental Biology and Medicine, 2019. **244**(17): p. 1568-1576.
140. Kibria, M.G., et al., *The immunogenicity of an anti-EGFR single domain antibody (V(HH)) is enhanced by misfolded amorphous aggregation but not by heat-induced aggregation*. Eur J Pharm Biopharm, 2020. **152**: p. 164-174.
141. Schmitz, K.R., et al., *Structural evaluation of EGFR inhibition mechanisms for nanobodies/VHH domains*. Structure, 2013. **21**(7): p. 1214-24.
142. Rahman, N., et al., *A systematic mutational analysis identifies a 5-residue proline tag that enhances the in vivo immunogenicity of a non-immunogenic model protein*. FEBS open bio, 2020. **10**(10): p. 1947-1956.
143. Holgate, R.G. and M.P. Baker, *Circumventing immunogenicity in the development of therapeutic antibodies*. IDrugs, 2009. **12**(4): p. 233-7.
144. Liu, M., et al., *Identification of HLA-DRB1 association to adalimumab immunogenicity*. PLoS One, 2018. **13**(4).
145. Ridker, P.M., et al., *Lipid-reduction variability and antidrug-antibody formation with bococizumab*. N Engl J Med, 2017. **376**(16): p. 1517-1526.
146. Ahmadi, M., et al., *Small amounts of sub-visible aggregates enhance the immunogenic potential of monoclonal antibody therapeutics*. Pharm Res, 2015. **32**(4): p. 1383-94.
147. Jozawa, H., et al., *Amorphous protein aggregation monitored using fluorescence self-quenching*: FEBS Lett. 2016 Oct;590(20):3501-3509. doi: 10.1002/1873-3468.12439. Epub 2016 Oct 18.
148. Khan, M.A., M.M. Islam, and Y. Kuroda, *Analysis of protein aggregation kinetics using short amino acid peptide tags*. Biochim Biophys Acta, 2013. **10**(15): p. 28.
149. Kuroda, Y., *Biophysical studies of protein solubility and amorphous aggregation by systematic mutational analysis and a helical polymerization model*. Biophys Rev, 2018. **10**(2): p. 473-480.

150. Nakamura, S., et al., *Reversible oligomerization and reverse hydrophobic effect induced by isoleucine tags attached at the C-terminus of a simplified BPTI variant*. *Biochemistry*, 2020. **59**(39): p. 3660-3668.
151. van Schie, K.A., G.J. Wolbink, and T. Rispens, *Cross-reactive and pre-existing antibodies to therapeutic antibodies--Effects on treatment and immunogenicity*. *mAbs*, 2015. **7**(4): p. 662-71.
152. Bartelds, G.M., et al., *Clinical response to adalimumab: relationship to anti-adalimumab antibodies and serum adalimumab concentrations in rheumatoid arthritis*. *Ann Rheum Dis*, 2007. **66**(7): p. 921-6.
153. Reinisch, W., et al., *Evaluation of the cross-reactivity of antidrug antibodies to CT-P13 and infliximab reference product (remicade): An analysis using immunoassays tagged with both agents*. *BioDrugs : clinical immunotherapeutics, biopharmaceuticals and gene therapy*, 2017. **31**(3): p. 223-237.
154. Groell, F., O. Jordan, and G. Borchard, *In vitro models for immunogenicity prediction of therapeutic proteins*. *Eur J Pharm Biopharm*, 2018. **130**: p. 128-142.
155. Roberts, A.D., K.H. Ely, and D.L. Woodland, *Differential contributions of central and effector memory T cells to recall responses*. *The Journal of experimental medicine*, 2005. **202**(1): p. 123-133.
156. Petersen, B., et al., *Persistence of neutralizing antibodies after discontinuation of IFNbeta therapy in patients with relapsing-remitting multiple sclerosis*. *Mult Scler*, 2006. **12**(3): p. 247-52.
157. Yoon, S., et al., *Current perspectives on therapeutic antibodies*. *Biotechnology and Bioprocess Engineering*, 2010. **15**(5): p. 709-715.
158. Sandborn, W.J., et al., *Effects of transient and persistent anti-drug antibodies to certolizumab pegol: Longitudinal data from a 7-year study in Crohn's Disease*. *Inflamm Bowel Dis*, 2017. **23**(7): p. 1047-1056.